VISIBLE LIGHT POSITIONING IN PRESENCE OF MALICIOUS LED TRANSMITTERS OR INTELLIGENT REFLECTING SURFACES

A DISSERTATION SUBMITTED TO

THE GRADUATE SCHOOL OF ENGINEERING AND SCIENCE

OF BILKENT UNIVERSITY

IN PARTIAL FULFILLMENT OF THE REQUIREMENTS FOR

THE DEGREE OF

DOCTOR OF PHILOSOPHY

IN

ELECTRICAL AND ELECTRONICS ENGINEERING

By

Furkan Kökdoğan

September 2023

VISIBLE LIGHT POSITIONING IN PRESENCE OF MALICIOUS LED TRANSMITTERS OR INTELLIGENT REFLECTING SURFACES

By Furkan Kökdoğan

September 2023

We certify that we have read this dissertation and that in our opinion it is fully adequate, in scope and in quality, as a dissertation for the degree of Doctor of Philosophy.

Sinan Gezici (Advisor)

Orhan Arıkan

Berkan Dülek

Tolga Mete Duman

Umut Orguner

Approved for the Graduate School of Engineering and Science:

Orhan Arıkan
Director of the Graduate School

ABSTRACT

VISIBLE LIGHT POSITIONING IN PRESENCE OF MALICIOUS LED TRANSMITTERS OR INTELLIGENT REFLECTING SURFACES

Furkan Kökdoğan
Ph.D. in Electrical and Electronics Engineering
Advisor: Sinan Gezici
September 2023

Visible light positioning (VLP) is a recent solution to the localization problem in indoor environments which involves the use of light emitting diodes (LEDs) as transmitters and photodetectors (PDs) as receivers. VLP systems have increasingly been popular as LEDs are employed for illumination purposes over conventional light bulbs nowadays due to their various advantages. In this thesis, we develop VLP algorithms for two main scenarios. In the first scenario, we assume that the system is not completely secure, meaning that the transmit power of some LEDs can be controlled by a third unknown party, i.e., hijacked, to degrade the positioning accuracy. In the second scenario, we assume the deployment of intelligent reflecting surfaces (IRSs) into the system to improve the positioning accuracy in the absence of line-of-sight (LOS) signals from of a subset of LED transmitters.

First, we consider a VLP system in which a receiver performs position estimation based on signals emitted from a number of LED transmitters. Each LED transmitter can be malicious and transmit at an unknown power level with a certain probability. A maximum likelihood (ML) position estimator is derived based on the knowledge of probabilities that LED transmitters can be malicious. In addition, in the presence of training measurements, decision rules are designed for detection of malicious LED transmitters, and based on detection results, various ML based location estimators are proposed. To evaluate the performance of the proposed estimators, Cramér-Rao lower bounds (CRLBs) are derived for position estimation in scenarios with and without a training phase. Moreover, an ML estimator is derived when the probabilities that the LED transmitters can be malicious are unknown. The performances of all the proposed estimators are evaluated via numerical examples and compared against the CRLBs.

Second, we formulate and analyze a received power based position estimation problem for VLP systems in the presence of IRSs. In the proposed problem formulation, a visible light communication (VLC) receiver collects signals from a number of LED transmitters via LOS paths and/or via reflections from IRSs. We derive the CRLB expression and the ML estimator for generic three-dimensional positioning in the presence of IRSs with arbitrary configurations. In addition, we consider the problem of optimizing the orientations of IRSs when LOS paths are blocked, and propose an optimal adjustment approach for maximizing the received powers from IRSs based on analytic expressions, which can be solved in closed form or numerically. Since the optimal IRS orientations depend on the actual position of the VLC receiver, an N-step localization algorithm is proposed to perform adjustment of IRS orientations in the absence of any prior knowledge about the position of the VLC receiver. Performance of the proposed approach is evaluated via simulations and compared against the CRLB. It is deduced that although IRSs do no provide critical improvements in positioning accuracy in the presence of LOS signals from a sufficient number of LED transmitters, they can be very important in achieving accurate positioning when all or most of LOS paths are blocked.

Keywords: Visible light positioning (VLP), estimation, localization, malicious LED transmitter, Cramér-Rao lower bound (CRLB), intelligent reflecting surface (IRS), reconfigurable intelligent surface (RIS).

ÖZET

KÖTÜCÜL LED VERİCİLERİ VEYA AKILLI YANSITICI YÜZEYLER VARLIĞINDA GÖRÜNÜR IŞIK KONUMLANDIRMA

Furkan Kökdoğan
Elektronik Mühendisliği, Doktora
Tez Danışmanı: Sinan Gezici
Eylül 2023

Görünür ışık konumlandırma, verici olarak ışık saçan diyotların (LED), alıcı olarak ise ışık detektörlerinin kullanıldığı yeni bir iç ortam konum belirleme çözümüdür. Görünür ışık konumlandırma sistemleri, LED'lerin günümüzde aydınlatma amacıyla geleneksel ampüllere göre belirgin avantajlarından dolayı daha fazla kullanılmasıyla beraber yaygınlaşmıştır. Bu tezde, iki farklı ana senaryo için görünür ışık konumlandırma algoritmaları geliştirilmektedir. İlk senaryoda, sistemin tamamen güvenli olmadığı, LED'lerin güçlerinin, bilinmeyen bir üçüncü parti tarafından konumlandırma doğruluğunu düşürmek amacıyla kontrol edilebildiği varsayılmaktadır. İkinci senaryoda ise sisteme konumlandırma performansını arttırmak amacıyla akıllı yansıtıcı yüzeylerin (AYY'ler) kurulduğu kabul edilmektedir.

İlk olarak, bir alıcının birkaç farklı LED'den yayınlanan sinyalleri alarak konumlandırma yaptığı bir sistem ele alınmaktadır. Her LED vericisi, belirli bir olasılıkla kötücüldür ve bilinmeyen bir güç seviyesinde yayın yapmaktadır. LED vericilerinin kötücül olma olasılıklarının bilgisi kullanılarak en büyük olabilirlik kestiricisi türetilmektedir. Ek olarak, eğitim ölçümleri varlığında LED'lerin kötücüllüklerinin belirlenmesi için karar kuralları tasarlanmakta ve bu karar kurallarının sonuçlarına göre konumlandırma için en yüksek olabilirlik kestiricileri önerilmektedir. Önerilen kestiricilerin performanslarını değerlendirmek için eğitim fazlı ve eğitim fazsız senaryolarda Cramér-Rao alt sınırı (CRLB) türetilmektedir. Ayrıca LED vericilerinin kötücül olma olasılıklarının bilinmediği durumda, bir en büyük olabilirlik kestiricisi türetilmektedir. Önerilen tüm kestiricilerinin performansları sayısal örneklerle değerlendirilmekte ve CRLB ile kıyaslanmaktadır.

İkinci olarak, AYY'lerin varlığında, alınan sinyal gücü tabanlı konumlandırma problemi formüle edilmekte ve incelenmektedir. Önerilen problem formülasyonunda, görünür ışık haberleşme alıcısı birkaç LED'den yayınlanan sinyalleri görüş açısı yolundan veya AYY'lerden yansıyan yollardan alabilmektedir. AYY'lerin varlığında herhangi bir kurulum için üç boyutlu genel bir konumlandırmada CRLB ve en yüksek olabilirlik kestiricisi türetilmektedir. Ek olarak, görüş açısı yollarının engellenmesi durumunda, AYY'lerin yönelimlerinin en uygun hale getirilmesi problemi ele alınmakta ve AYY'lerden alınan sinyal gücünü en yüksek yapan yönelimlerin bulunması için kapalı formda veya nümerik olarak çöözülebilen ifadeler önerilmektedir. En uygun AYY yönelimleri, alıcı konumuna bağlı olduğu için alıcı konumunun ön bilgisinin yokluğunda AYY yönelimlerini ayarlamak için N-adımlı konumlandırma algoritması önerilmektedir. Önerilen yaklaşımın performansı benzetimlerle değerlendirilmekte ve CRLB ile kıyaslanmaktadır. AYY'lerin kullanımının, yeterli sayıda LED vericisinden görüş alanında sinyal alındığı durumlarda konumlandırma doğruluğuna önemli bir iyileştirme sağlamasa da görüş alanı sinyallerinin tamamının veya çoğunun engellendiği durumlarda konumlandırma doğruluğu için oldukça önemli olduğu sonucuna varılmaktadır.

Anahtar sözcükler: Görünür ışık konumlandırma, kestirim, yer bulma, kötücül LED vericisi, Cramér-Rao alt sınırı, akıllı yansıtıcı yüzey (AYY), ayarlanabilir akıllı yüzey.

Acknowledgement

First of all, I would like to present my sincere gratitude to my advisor Prof. Sinan Gezici for his invaluable guidance, support, supervision, and encouragement throughout this work. It is an extraordinary privilege and a great honor for me to work with him as he is an inspiring and very successful yet modest and benevolent academician. I could not wish for a better advisor for my Ph.D. studies. In fact, I truly believe it would not be possible for me to complete this thesis without his encouragement especially even when I was about to lose my belief and give up. I will always feel indebted for his endless support throughout my graduate studies.

I would also like to sincerely thank Prof. Orhan Arıkan and Prof. Berkan Dülek for being a member of thesis monitoring committee and their valuable guidance and supervision throughout my studies. I would like to thank Prof. Tolga Mete Duman and Prof. Umut Orguner for accepting to be a member of my dissertation examination committee.

I would like to thank my dear friend Dr. Onur Yorulmaz for his unrequited help. He is an inspiring person and a fun colleague to work with. I hope to have a chance to work with him again in the future. I would like to thank my dear old friend Fatih Saraydar as well for his supports and companionship through many years. I know I can always trust him to be there for me whenever I need.

I would like to express sincere gratitude to my mother Havva, my father Faruk, my sister Betül and my brother Yasin for their love, encouragement, care, support, and belief in me. I always feel privileged to have them in my life as family.

I would like to specially thank my wife Nagehan for always being there for me. I would not be able to achieve this without her endless support, encouragement, love, and patience. I consider myself lucky to have her as my life companion. She is always the one who cheers me up, she is the joy of my life.

Finally, I would also like to thank The Scientific and Technological Research Council of Turkey (TÜBİTAK) for the financial support through BİDEB 2211-E Scholarship Program during my study.

To my family, with love and gratitude...

Contents

List of Figures

Chapter 1

Introduction

In the last decades, usage of light emitting diodes (LEDs) has been increasingly popular for illumination of indoor environments. Conventional light bulbs are slowly eradicating as the advantages of using LEDs become more apparent in the contexts of illumination efficiency, longevity, environmental friendliness, and functionality [1]. LEDs consume considerably less power, have longer life time, do not contain toxic chemicals, and have dimming and color adjustment capabilities, which make them appealing to prefer over incandescent light bulbs. Besides these advantages, LEDs also have fast switching characteristics allowing data modulation schemes which enables communication and positioning applications through the use of LEDs in indoor environments. In particular, visible light positioning (VLP) has emerged as an attractive approach that provides accurate location information with low implementation complexity, which has attracted significant attention from researchers.

In the literature, various position estimation algorithms are developed and theoretical accuracy limits are investigated for VLP systems thoroughly [2–5] (and references therein). Unlike in radio frequency (RF) systems, position estimation based on received power measurements can achieve high accuracy in VLP systems [6]. Therefore, the received signal strength (RSS) parameter is commonly employed in VLP systems due to its low measurement cost. In [7], closed-form

Cramér-Rao lower bound (CRLB) expressions are derived for location and orientation estimation based on the RSS measurements. In [8], a three-dimensional (3D) positioning approach that utilizes both RSS and angle-of-arrival (AOA) information is introduced for a single-input multiple-output (SIMO) visible light system. The authors in [9] propose a simultaneous position and orientation estimation (SPO) algorithm using RSS measurements in a multi-input multi-output (MIMO) VLP system. The CRLB is also derived to evaluate the performance of the proposed SPO estimator. In [10], deep learning is employed for joint 3D position and orientation estimation of a VLC receiver with random orientation and unknown transmit power based on RSS measurements. In [11], performance analysis of a VLP system, which uses an aperture-based receiver, is conducted. An estimator is proposed by utilizing both RSS and AOA information. Also, the CRLB is derived for assessing the performance of the proposed estimator. In addition to these general references on VLP systems, there exist other studies related to the subject of this thesis, as discussed in the following sections.

1.1 Visible Light Positioning in the Presence of Malicious LED Transmitters

1.1.1 Literature Review

We focus on a VLP system in which a visible light communication (VLC) receiver collects power measurements from signals coming from a number of LED transmitters for the purpose of localization. We also consider that the system is not completely secure and some of the LED transmitters can be malicious (controlled by a third party). Therefore, we aim to develop position estimation algorithms in the presence of malicious LED transmitters. Although various security issues in the physical layer have been investigated for VLC systems [12–21], there exists no such work for VLP systems in the literature. For example, [13] considers the presence of an eavesdropper and proposes a way of securing VLC links via friendly jammers. In addition, a robust beamforming approach is developed to maximize the worst-case secrecy rate in the presence of imperfect knowledge of eavesdropper's channel. In [16], a multiple-input single-output (MISO) VLC system is investigated in the presence of multiple eavesdroppers. The transmit beamformer and jamming precoder are optimized to improve communication secrecy. In [17], simultaneous beamforming and jamming is utilized for MISO VLC systems under the assumption of randomly located eavesdropper in order to enhance the physical layer security. The authors formulate an optimization problem with a focus on the signal-to-interference-plus-noise ratio for the legitimate link and solve it by a heuristic method. In [18], a physical layer security technique is proposed for VLC systems with the utilization of an intelligent mirror array. An achievable secrecy rate maximization problem is formulated for the proposed technique and optimal orientations of the mirrors are found. In addition, the studies in [19] and [20] focus on the calculation of the secrecy capacity for VLC systems in various scenarios. A comprehensive survey on physical layer security for VLC systems can be found in [21]. As an alternative approach, information theoretic learning criteria, such as minimum error entropy (MEE) and maximum correntropy criterion (MCC), can also be employed for parameter estimation in visible light systems. For example, an MEE based channel estimator is proposed in [22] for massive MIMO VLC systems.

In RF systems, position estimation in wireless sensor networks in the presence of malicious nodes has been considered in various studies [23–32]. In [23], independent and collaborative Byzantine attacks are considered and two different schemes are proposed for mitigation of these attacks. In addition, the posterior CRLB is derived to characterize the performance of the wireless sensor network. In [24], an RSS based localization method is proposed in order to mitigate the impacts of Byzantine fault and non-line-of-sight (NLOS) bias on the positioning accuracy. In [25], coding-theory based mitigation approach schemes are discussed in the presence of malicious nodes in sensor networks.

1.1.2 Contributions

The approaches in [23–32] developed for RF systems are not directly applicable to VLP systems which carry significant differences from RF based positioning systems due to distinct propagation characteristics [3]. The main contributions and novelty of this thesis can be summarized as follows:

- Position estimation problems in visible light systems in the presence of malicious LED transmitters are formulated for the first time in the literature.
- A maximum likelihood (ML) estimator is derived based on the knowledge of probabilities that LED transmitters can be malicious.
- In the presence of training measurements, decision rules (namely, generalized likelihood ratio tests) are developed for detection of malicious LED transmitters, and based on detection results, various ML based location estimators are derived.
- CRLB expressions are derived and used as benchmarks for scenarios with and without training measurements.
- An ML estimator is obtained for the case that the probabilities of the LED transmitters being malicious are unknown.

In addition, simulation results are presented to investigate the performance of the proposed algorithms and to compare them against each other and the CRLBs.

1.2 Visible Light Positioning in the Presence of Intelligent Reflecting Surfaces

1.2.1 Literature Review

Recently, emergence of configurable surfaces called intelligent reflecting surfaces (IRSs) has significant drawn attention in the area of RF communications. IRSs consist of a number of low-cost passive elements that can control the phase, amplitude, frequency, and/or polarization of RF signals [33]. The authors in [33] present a detailed overview and historical perspective of the state of the art solutions for usage of IRSs in communication systems. In [34], an algorithm is proposed to minimize the total transmit power by means of jointly optimizing transmit and reflect beamforming via deployment of IRS elements. In [35], it is shown that the use of IRS can help increase the energy efficiency of a wireless communication system by dynamically controlling the reflection coefficients of individual reflecting elements. There are also a number of studies that concerns the usage of IRSs in VLC schemes. Abdelhady et al. propose two types of IRSs for use in VLC systems; namely, metasurfaces and mirror arrays as the adaptation of IRS to the light propagation characteristics in [36]. The authors of [37] propose a solution for joint optimization of time allocation, power control, and phase shift matrix under power constraints to maximize the energy efficiency in a downlink reconfigurable intelligent surface (RIS) aided VLC system. In [38] a low-complexity algorithm is proposed to maximize the achievable sum rate in a VLC system deployed with IRS. It has been shown that IRS can help improve the rate performance and reduce blockage problems of VLC systems. In [39], the role of using IRS is to enhance the link reliability of a VLC system employing non-orthogonal multiple access (NOMA). It is deduced that IRS can significantly improve link reliability especially when the VLC channel is subject to blockage or random device orientation. In [40], the optimal orientation of IRS that maximizes the received power in a wireless communication system is analyzed. It is shown that the achievable rate can significantly be increased by adjusting the orientation of IRSs.

There also exist a number of studies in the literature that investigate the use of IRSs in wireless positioning systems. In [41], it is shown that IRSs can be used to localize a user in the absence of enough transmitters in a wireless network. The authors of [42] propose a device-to-device localization algorithm in an RF system of mmWave frequencies using RISs in the absence of access points. In [43], the use of RISs in a wireless localization system at mmWave frequencies is analyzed. The CRLB is derived and the reflect beamforming is optimized to improve positioning accuracy. In [44], a low complexity fingerprinting based localization algorithm is presented in a wireless communication system using RIS. The authors of [45] propose an angle-of-arrival (AoA) based positioning algorithm in an IRS-aided wireless communication system. In [46], the use of RIS is investigated for replacing the function of a remote cell in the downlink time-difference-of-arrival (DL-TDOA) measurement in 3GPP NR. It is shown that RIS-enabled localization along with a Kalman filter for tracking applications is a cost-effective solution with high accuracy. In [47], a distributed RIS assisted wireless positioning system is considered. A practical structure of indoor positioning is proposed consisting of two modes, namely, quasi-static and dynamic. The authors of [48] investigate the localization and orientation performance of synchronous and asynchronous signalling schemes by deriving the CRLB. In addition, a closed-form RIS phase profile that suits joint communication and localization is proposed. In [49], a general signal model of wideband systems with RISs is presented and the corresponding CRLB is derived to assess the localization performance of RIS-aided wideband systems.

1.2.2 Contributions

Although there are a number of studies focusing on use of IRSs in both wireless RF communication and VLC systems to improve performance and efficiency (and several other studies analyzing the use of IRS in wireless positioning algorithms for RF systems), there exists no studies investigating the deployment of IRSs in VLP systems, to the best of our knowledge. As the light propagation and reflection characteristics are different from those of RF signals, specific analyses are required for VLP systems. In this thesis, we focus on a VLP system in which a VLC receiver equipped with a single photo-detector (PD) aims to estimate its position by utilizing the received power (equivalently, RSS) measurements from a number of LED transmitters by receiving signals from line-of-sight (LOS) paths and/or reflected paths via IRSs [50]. The main contributions of this study to the existing literature can be summarized as follows:

- The problem of received power based position estimation for VLP systems in presence of IRSs is studied for the first time in the literature.
- A CRLB expression is derived for a generic three dimensional VLP system in the presence of IRSs with arbitrary configurations.
- A maximum likelihood (ML) estimator that utilizes the received power measurements from both LOS paths and reflected paths from IRSs is proposed for position estimation.
- The problem of optimizing the orientations of IRSs is considered when LOS paths are blocked, and an optimal adjustment approach is proposed for maximizing the received powers from IRSs based on analytic expressions, which can be solved in closed form or numerically.
- An N-step localization algorithm is proposed to perform adjustment of IRS orientations (hence, to improve localization accuracy) in the absence of any prior knowledge about the position of the VLC receiver.

In addition, extensive simulations are conducted to investigate the effects of IRS parameters (such as reflection and directivity related parameters, and orientation vectors) and the blockage of LOS paths in various scenarios.

1.3 Organization of the Dissertation

The organization of this thesis is as follows. In Chapter 2, we formulate the the VLP problems in the presence of malicious LED transmitters and propose several algorithms for various scenarios. In Chapter 3, we consider a VLP system with deployment of IRS and propose approaches for position estimation and optimal adjustment of IRS orientations. In Chapter 4, the thesis is concluded with final remarks.

Chapter 2

Visible Light Positioning in the Presence of Malicious LED Transmitters

This chapter is organized as follows. The system model for visible light positioning in the presence of malicious LED transmitters is discussed in Section 2.1. In Section 2.2, an ML estimator is derived based on the knowledge of the probabilities of LED transmitters being malicious. In Section 2.3, a training procedure is proposed for the detection of malicious LEDs, and estimators that utilize the training measurements are derived for two different scenarios. In Section 2.4, theoretical limits, namely, the CRLBs, on the positioning accuracy are derived. Simulation results are presented and discussed in Section 2.5. In Section 2.6, an extension is provided for the case of unknown probabilities of LEDs being malicious. Finally, the concluding remarks are presented in Section 2.8.

2.1 System Model

Consider a VLP system with N_{L} LED transmitters at known locations denoted by $\boldsymbol{l}_{\mathrm{T}}^{i}$ for $i \in \{1, \ldots, N_{\mathrm{L}}\}$. The LED transmitters communicate with a VLC receiver, which aims to estimate its unknown location $\boldsymbol{l}_{\mathrm{R}}$ based on signals coming from the LED transmitters. The VLP system is not completely secure and it is possible that some of the LED transmitters can be hijacked by malicious third parties. The VLC receiver does not know which LED transmitters are malicious but it is aware of such a possibility. Namely, it is assumed that the VLC receiver knows the probabilities that the LED transmitters can be malicious. (Extensions to the case of unknown probabilities is provided in Section 2.6.)

The VLC receiver gathers power measurements from the LED transmitters for the purpose of localization, which are expressed as [51]

$$P_{\mathrm{R},i} = R_p \, P_{\mathrm{T},i} \, h_i(\boldsymbol{l}_{\mathrm{R}}) + \eta_i \tag{2.1}$$

for $i = 1, \ldots, N_{\mathrm{L}}$. In (2.1), R_p denotes the responsivity of the photo detector (PD) at the VLC receiver, $P_{\mathrm{T},i}$ is the transmit power of the ith LED transmitter, $h_i(\boldsymbol{l}_{\mathrm{R}})$ represents the channel coefficient between the VLC receiver and the ith LED transmitter, and η_i is zero-mean Gaussian noise with a variance of σ_i^2, which is independent of η_j for all $j \neq i$ [51]. It is assumed that a certain type of multiple access protocol, such as frequency-division or time-division multiple access [52–54], is employed so that the signals coming from different LED transmitters are processed separately and their power levels are measurement individually as in (2.1).

Let γ_i denote the probability that the ith LED transmitter is malicious. Then, the transmit power parameter in (2.1) is given by

$$P_{\mathrm{T},i} = \begin{cases} P_{\mathrm{M},i}\,, & \text{with probability } \gamma_i \\ P_{\mathrm{H},i}\,, & \text{with probability } 1-\gamma_i \end{cases} \tag{2.2}$$

where $P_{\mathrm{M},i}$ denotes the transmit power of the ith LED transmitter if it is malicious (i.e., controlled by a third party) and $P_{\mathrm{H},i}$ represents the transmit power of the ith LED transmitter if it is honest (i.e., not malicious). The parameters $\{P_{\mathrm{H},i}\}_{i=1}^{N_{\mathrm{L}}}$ are known by the VLC receiver since transmit power levels in case of honest LED transmitters are either reported to the VLC receiver or they are set beforehand for localization purposes. On the other hand, when an LED transmitter is malicious, it can change its transmit power level in order to degrade the localization performance of the VLP system. Therefore, $\{P_{\mathrm{M},i}\}_{i=1}^{N_{\mathrm{L}}}$ are modeled as unknown parameters. Also, it is assumed that each LED transmitter can be malicious or honest independently of the other LED transmitters.

Considering a line-of-sight scenario between each LED transmitter and the VLC receiver [3, 55, 56], the channel coefficients in (2.1) can be calculated as

$$h_i(\boldsymbol{l}_{\mathrm{R}}) = \frac{(m_i+1)A_{\mathrm{R}}\left[(\boldsymbol{l}_{\mathrm{R}}-\boldsymbol{l}_{\mathrm{T}}^i)^T\boldsymbol{n}_{\mathrm{T}}^i\right]^{m_i}(\boldsymbol{l}_{\mathrm{T}}^i-\boldsymbol{l}_{\mathrm{R}})^T\boldsymbol{n}_{\mathrm{R}}}{2\pi\left\|\boldsymbol{l}_{\mathrm{R}}-\boldsymbol{l}_{\mathrm{T}}^i\right\|^{m_i+3}} \tag{2.3}$$

where m_i is the Lambertian order for the ith LED transmitter, A_{R} is the area of the PD at the VLC receiver, and $\boldsymbol{n}_{\mathrm{R}}$ and $\boldsymbol{n}_{\mathrm{T}}^i$ represent the orientation vectors of the VLC receiver and the ith LED transmitter, respectively [57]. It is assumed that the VLC receiver knows the parameters A_{R}, R_p, $\boldsymbol{n}_{\mathrm{R}}$, m_i, $\boldsymbol{l}_{\mathrm{T}}^i$, and $\boldsymbol{n}_{\mathrm{T}}^i$, and σ_i^2 [6, 56]. For example, the orientation of the VLC receiver ($\boldsymbol{n}_{\mathrm{R}}$) can be determined by a gyroscope and the LED parameters (m_i, $\boldsymbol{l}_{\mathrm{T}}^i$, and $\boldsymbol{n}_{\mathrm{T}}^i$) can be sent to the receiver via visible light communications [6]. It is noted that the channel coefficient $h_i(\boldsymbol{l}_{\mathrm{R}})$ in (2.3) is a nonlinear function of the parameter of interest, i.e., $\boldsymbol{l}_{\mathrm{R}}$.

Remark 1: As implied from the preceding system model, malicious LED transmitters modify the transmit power levels to degrade the localization performance of the VLP system. Even though a malicious third party can control an LED transmitter, it is not practical for it to change other LED parameters such as $\boldsymbol{l}_{\mathrm{T}}^i$, $\boldsymbol{n}_{\mathrm{T}}^i$, and m_i as their modification requires physical intervention to the system. For example, the modification of $\boldsymbol{l}_{\mathrm{T}}^i$ or $\boldsymbol{n}_{\mathrm{T}}^i$ requires a change in the location or the orientation of the ith LED transmitter. Similarly, the Lambertian order is fixed for a given LED model. On the other hand, the transmit power levels of the LEDs are controlled by the LED drivers (usually via a controller unit). Therefore, without any physical change to the system (such as changing the locations and orientations of the LEDs or replacing the LEDs), a malicious third party can change the transmit power levels by hacking the LED drivers to degrade the positioning accuracy of the VLP system.

Remark 2: The VLP system modeled considered in this work can be practical in the following cases: (i) While the transmit power level is known for a given LED transmitter under normal operating conditions (denoted by $P_{\mathrm{H},i}$ in (2.2)), there can occur situations in which an LED can fail and provide a different (and unknown) power level than the reported one [58]. By considering a more general perspective for being "malicious" and taking into account such failures of LED transmitters, the system model in this section becomes valid. Namely, based on some prior knowledge (such as the LED brand and type, previous operating experience, etc.), the probability of failure can be determined for each LED transmitter, and the model in (2.2) can be applied. In this case, it is reasonable to model that each LED transmitter can fail (i.e., become "malicious") independently of the others. (ii) Consider a hijacking attack in which the malicious third party gets the control of the whole VLP network by accessing the VLP controller. In this case, the malicious third party can randomly select some of the LED transmitters and modify their transmit powers in order not to be detected easily. Hence, the assumption of malicious LED transmitters in this section becomes valid in such a scenario, as well. (iii) Please also see Sections 2.6 and 2.7 for extensions of the system model.

2.2 Position Estimation in the Presence of Malicious LED Transmitters

The aim of the VLC receiver is to estimate its location $\boldsymbol{l}_{\mathrm{R}}$ based on the power measurements in (2.1). Let $\boldsymbol{P}_{\mathrm{R}}$ represent a vector consisting of the power measurements; i.e., $\boldsymbol{P}_{\mathrm{R}} = [P_{\mathrm{R},1} \cdots P_{\mathrm{R},N_{\mathrm{L}}}]^T$. Also, let $\boldsymbol{P}_{\mathrm{M}}$ denote the vector of unknown transmit powers in (2.2); that is, $\boldsymbol{P}_{\mathrm{M}} = [P_{\mathrm{M},1} \cdots P_{\mathrm{M},N_{\mathrm{L}}}]^T$. In practice, upper and lower limits can be imposed on the elements of $\boldsymbol{P}_{\mathrm{M}}$ considering the specifications of the LEDs. Hence, it is assumed that $\boldsymbol{P}_{\mathrm{M}} \in \mathcal{P}$, where $\mathcal{P} = [P_{\min,1}, P_{\max,1}] \times \cdots \times [P_{\min,N_{\mathrm{L}}}, P_{\max,N_{\mathrm{L}}}]$. Similarly, let $\boldsymbol{l}_{\mathrm{R}} \in \mathcal{L}$, where $\mathcal{L}$ denotes the possible locations of the VLC receiver; e.g., all possible locations in a room or factory. It is assumed that there exists no prior statistical information about $\boldsymbol{P}_{\mathrm{M}}$ or $\boldsymbol{l}_{\mathrm{R}}$.

The location of the VLC receiver can be estimated via the ML estimator [59], which is stated as

$$\left(\widehat{\boldsymbol{l}}_{\mathrm{R}}, \widehat{\boldsymbol{P}}_{\mathrm{M}}\right) = \underset{\boldsymbol{l}_{\mathrm{R}} \in \mathcal{L}, \boldsymbol{P}_{\mathrm{M}} \in \mathcal{P}}{\arg\max}\; p(\boldsymbol{P}_{\mathrm{R}} \,|\, \boldsymbol{l}_{\mathrm{R}}, \boldsymbol{P}_{\mathrm{M}}) \tag{2.4}$$

In (2.4), $p(\boldsymbol{P}_{\mathrm{R}} \,|\, \boldsymbol{l}_{\mathrm{R}}, \boldsymbol{P}_{\mathrm{M}})$ denotes the likelihood function, which can be calculated from (2.1) and (2.2) as follows:

$$p(\boldsymbol{P}_{\mathrm{R}} \,|\, \boldsymbol{l}_{\mathrm{R}}, \boldsymbol{P}_{\mathrm{M}}) = \prod_{i=1}^{N_{\mathrm{L}}} \left(\frac{\gamma_i}{\sqrt{2\pi}\sigma_i} e^{-\frac{(P_{\mathrm{R},i} - P_{\mathrm{M},i} R_p h_i(\boldsymbol{l}_{\mathrm{R}}))^2}{2\sigma_i^2}} + \frac{1-\gamma_i}{\sqrt{2\pi}\sigma_i} e^{-\frac{(P_{\mathrm{R},i} - P_{\mathrm{H},i} R_p h_i(\boldsymbol{l}_{\mathrm{R}}))^2}{2\sigma_i^2}} \right) \tag{2.5}$$

From (2.4) and (2.5), it can be shown, after some manipulation, that the ML estimator for the location of the VLC receiver becomes

$$\widehat{\boldsymbol{l}}_{\mathrm{R}} = \underset{\boldsymbol{l}_{\mathrm{R}} \in \mathcal{L}}{\arg\max} \prod_{i=1}^{N_{\mathrm{L}}} \left(\frac{\gamma_i}{\sqrt{2\pi}\sigma_i} e^{-\frac{(P_{\mathrm{R},i} - \widehat{P}_{\mathrm{M},i}(\boldsymbol{l}_{\mathrm{R}}) R_p h_i(\boldsymbol{l}_{\mathrm{R}}))^2}{2\sigma_i^2}} + \frac{1-\gamma_i}{\sqrt{2\pi}\sigma_i} e^{-\frac{(P_{\mathrm{R},i} - P_{\mathrm{H},i} R_p h_i(\boldsymbol{l}_{\mathrm{R}}))^2}{2\sigma_i^2}} \right) \tag{2.6}$$

where $\widehat{P}_{\mathrm{M},i}(\boldsymbol{l}_{\mathrm{R}})$ in (2.6) is given by

$$\widehat{P}_{\mathrm{M},i}(\boldsymbol{l}_{\mathrm{R}}) = \begin{cases} P_{\min,i}, & \text{if } \frac{P_{\mathrm{R},i}}{R_p h_i(\boldsymbol{l}_{\mathrm{R}})} \leq P_{\min,i} \\ P_{\max,i}, & \text{if } \frac{P_{\mathrm{R},i}}{R_p h_i(\boldsymbol{l}_{\mathrm{R}})} \geq P_{\max,i} \\ \frac{P_{\mathrm{R},i}}{R_p h_i(\boldsymbol{l}_{\mathrm{R}})}, & \text{otherwise} \end{cases} \tag{2.7}$$

It is noted that the maximizer of the likelihood function over $P_{\mathrm{M},i}$ is obtained for any given value of $\boldsymbol{l}_{\mathrm{R}}$ as in (2.7), which leads to a significant reduction in computational complexity. Namely, the original formulation of the ML estimator in (2.4), which requires optimization over an $(N_{\mathrm{L}}+3)$-dimensional space is reduced to a three-dimensional search in (2.6).

Remark 3: The ML estimator in (2.6) is in the form of a Gaussian mixture model. In general, the Expectation-Maximization (EM) algorithm can be used to estimate the unknown parameters of Gaussian mixture models and to maximize the likelihood function, examples of which can be found in various studies such as [60–62]. In our case one of the unknown parameters, namely $\boldsymbol{P}_{\mathrm{M}}$, can be expressed in terms of the other one, namely $\boldsymbol{l}_{\mathrm{R}}$, which reduces the unknown parameter set to only the position of the VLC receiver. Therefore, it is possible to directly estimate the unknown location parameter $\boldsymbol{l}_{\mathrm{R}}$ without resorting to EM iterations.

2.3 Position Estimation in the Presence of Malicious LED Transmitters and Training Measurements

In this section, we suppose that power measurements can be taken at known locations in a given environment beforehand for training purposes. Based on those measurements, information related to maliciousness of each LED transmitter can be collected, which can then be used for the location estimation of the VLC receiver.

The power measurements at N_{V} known locations, denoted by $\boldsymbol{l}_{\mathrm{R}}^{(1)}, \ldots, \boldsymbol{l}_{\mathrm{R}}^{(N_{\mathrm{V}})}$, can be expressed as follows:

$$P_{\mathrm{R},i}^{(j)} = R_p\, P_{\mathrm{T},i}^{(j)}\, h_i\big(\boldsymbol{l}_{\mathrm{R}}^{(j)}\big) + \eta_i^{(j)} \tag{2.8}$$

for $i = 1, \ldots, N_{\mathrm{L}}$ and $j = 1, \ldots, N_{\mathrm{V}}$, where $P_{\mathrm{R},i}^{(j)}$ is the power measurement at location $\boldsymbol{l}_{\mathrm{R}}^{(j)}$ due to the signal emitted from the ith LED transmitter, $P_{\mathrm{T},i}^{(j)}$ denotes the transmit power of the ith LED transmitter during the measurement at location $\boldsymbol{l}_{\mathrm{R}}^{(j)}$, and $\eta_i^{(j)}$ is the noise component during the reception of the signal coming from the ith LED transmitter when the VLC receiver is at location $\boldsymbol{l}_{\mathrm{R}}^{(j)}$. The variance of $\eta_i^{(j)}$ is denoted by $\sigma_{i,j}^2$, and $\eta_i^{(j)}$'s are modeled as zero-mean Gaussian random variables that are independent for all i and j.

It is assumed that an LED transmitter is either malicious or honest during the training and estimation stages; i.e., its status does not change over the time interval of interest. In addition, two scenarios, named Scenario 1 and Scenario 2, are considered related to the transmit powers of the malicious LED transmitters.

Scenario 1: Each malicious LED transmitter employs a fixed unknown power level during all the measurements (i.e., during the training and estimation stages). Hence, parameter $P_{\mathrm{T},i}^{(j)}$ in (2.8) is modeled in Scenario 1 as

$$P_{\mathrm{T},i}^{(j)} = \begin{cases} P_{\mathrm{M},i}\,, & \text{with probability } \gamma_i \\ P_{\mathrm{H},i}\,, & \text{with probability } 1-\gamma_i \end{cases} \tag{2.9}$$

for $j \in \{1, \ldots, N_{\mathrm{V}}\}$.

Scenario 2: In this scenario, a malicious LED transmitter is modeled to change its transmit power frequently such that its transmit power can vary for each measurement. Then, $P_{\mathrm{T},i}^{(j)}$ in (2.8) is modeled as

$$P_{\mathrm{T},i}^{(j)} = \begin{cases} P_{\mathrm{M},i}^{(j)}\,, & \text{with probability } \gamma_i \\ P_{\mathrm{H},i}\,, & \text{with probability } 1-\gamma_i \end{cases} \tag{2.10}$$

for $j \in \{1, \ldots, N_{\mathrm{V}}\}$.

Based on the power measurements in (2.8), the aim is to make a decision for each LED transmitter about its status (malicious or honest), and to then perform localization based on a given power measurement vector $\boldsymbol{P}_{\mathrm{R}}$ (see (2.1)) by utilizing those decisions. The preceding two scenarios are investigated in the following.

2.3.1 Detection and Estimation in Scenario 1

In Scenario 1, the following binary hypothesis-testing problem can be formulated for the ith LED transmitter based on the measurements in (2.8):

$$\begin{aligned} \mathcal{H}_i \; &: \; P_{\mathrm{R},i}^{(j)} = R_p\, P_{\mathrm{H},i}\, h_i\big(\boldsymbol{l}_{\mathrm{R}}^{(j)}\big) + \eta_i^{(j)},\; j = 1, \ldots, N_{\mathrm{V}} \\ \mathcal{M}_i \; &: \; P_{\mathrm{R},i}^{(j)} = R_p\, P_{\mathrm{M},i}\, h_i\big(\boldsymbol{l}_{\mathrm{R}}^{(j)}\big) + \eta_i^{(j)},\; j = 1, \ldots, N_{\mathrm{V}} \end{aligned} \tag{2.11}$$

where $\mathcal{H}_i$ and $\mathcal{M}_i$ denote the hypotheses that the ith LED transmitter is honest and malicious, respectively.

As $P_{\mathrm{M},i}$'s are unknown, the hypothesis $\mathcal{M}_i$ is a composite hypothesis and the generalized likelihood ratio test (GLRT) is a well-suited approach for this problem due to the absence of prior distributions of $P_{\mathrm{M},i}$'s [59]. The GLRT for the problem in (2.11) can be stated as

$$\frac{\max\limits_{P_{\mathrm{M},i}\in[P_{\min,i},P_{\max,i}]} \prod_{j=1}^{N_{\mathrm{V}}} \frac{e^{-\frac{\left(P_{\mathrm{R},i}^{(j)}-R_p P_{\mathrm{M},i} h_i\left(\boldsymbol{l}_{\mathrm{R}}^{(j)}\right)\right)^2}{2\sigma_{i,j}^2}}}{\sqrt{2\pi}\sigma_{i,j}}}{\prod_{j=1}^{N_{\mathrm{V}}} \frac{1}{\sqrt{2\pi}\sigma_{i,j}} e^{-\frac{\left(P_{\mathrm{R},i}^{(j)}-R_p P_{\mathrm{H},i} h_i\left(\boldsymbol{l}_{\mathrm{R}}^{(j)}\right)\right)^2}{2\sigma_{i,j}^2}}} \underset{\mathcal{H}_i}{\overset{\mathcal{M}_i}{\gtrless}} \tau_i \tag{2.12}$$

where τ_i denotes the threshold, which can be chosen according to the tradeoff between the conditional probabilities of error [59]. In particular, since the probability distribution under $\mathcal{H}_i$ is completely known, the probability of deciding for $\mathcal{M}_i$ when $\mathcal{H}_i$ is true, i.e., the false alarm probability, can be fixed to a suitable value for setting the threshold.[1] (The effects of the threshold selection on the localization performance are investigated in Section 2.5.) The maximization problem in the numerator of (2.12) yields the following maximizer:

$$\widehat{P}_{\mathrm{M},i} = \begin{cases} P_{\min,i}, & \text{if } g\left(\{P_{\mathrm{R},i}^{(j)}\}_{j=1}^{N_{\mathrm{V}}}\right) \le P_{\min,i} \\ P_{\max,i}, & \text{if } g\left(\{P_{\mathrm{R},i}^{(j)}\}_{j=1}^{N_{\mathrm{V}}}\right) \ge P_{\max,i} \\ g\left(\{P_{\mathrm{R},i}^{(j)}\}_{j=1}^{N_{\mathrm{V}}}\right), & \text{otherwise} \end{cases} \tag{2.13}$$

where

$$g\left(\{P_{\mathrm{R},i}^{(j)}\}_{j=1}^{N_{\mathrm{V}}}\right) \triangleq \frac{\sum_{j=1}^{N_{\mathrm{V}}} P_{\mathrm{R},i}^{(j)} h_i\left(\boldsymbol{l}_{\mathrm{R}}^{(j)}\right)/\sigma_{i,j}^2}{R_p \sum_{j=1}^{N_{\mathrm{V}}} \left(h_i\left(\boldsymbol{l}_{\mathrm{R}}^{(j)}\right)\right)^2/\sigma_{i,j}^2} \tag{2.14}$$

Then, the GLRT in (2.12) can be simplified, after some manipulation, as follows:

$$R_p\left(\widehat{P}_{\mathrm{M},i} - P_{\mathrm{H},i}\right) \sum_{j=1}^{N_{\mathrm{V}}} \frac{P_{\mathrm{R},i}^{(j)} h_i\left(\boldsymbol{l}_{\mathrm{R}}^{(j)}\right)}{\sigma_{i,j}^2} + 0.5R_p^2\left(P_{\mathrm{H},i}^2 - \left(\widehat{P}_{\mathrm{M},i}\right)^2\right) \sum_{j=1}^{N_{\mathrm{V}}} \frac{\left(h_i\left(\boldsymbol{l}_{\mathrm{R}}^{(j)}\right)\right)^2}{\sigma_{i,j}^2} \underset{\mathcal{H}_i}{\overset{\mathcal{M}_i}{\gtrless}} \log(\tau_i) \tag{2.15}$$

[1] In particular, the threshold can be set via Monte-Carlo trials for a given false alarm probability by generating a sufficient number of received power measurements according to the $\mathcal{H}_i$ hypothesis (see (2.11)).

where $\widehat{P}_{\mathrm{M},i}$ is given by (2.13).

Let $\widehat{D}_i$ denote the decision of the GLRT in (2.15), i.e., the decision for the ith LED transmitter, where $i \in \{1, \ldots, N_{\mathrm{L}}\}$. When the power measurements $\boldsymbol{P}_{\mathrm{R}}$ are taken as in (2.1) related to a VLC receiver at an unknown location $\boldsymbol{l}_{\mathrm{R}}$, the problem becomes the estimation of $\boldsymbol{l}_{\mathrm{R}}$ based on $\boldsymbol{P}_{\mathrm{R}}$ and the decisions $\widehat{D}_1, \ldots, \widehat{D}_{N_{\mathrm{L}}}$. In Scenario 1, two approaches are considered as described in the following:

2.3.1.1 Algorithm 1-(a)

In this algorithm, the decisions of the GLRTs in (2.15) and the power estimates in (2.13) are assumed to be perfect, and the probability distribution of $\boldsymbol{P}_{\mathrm{R}}$ is determined accordingly. In particular, let $\widehat{\mathcal{H}}$ and $\widehat{\mathcal{M}}$ denote the sets of honest and malicious LED transmitters according to the decision of the GLRTs in (2.15); that is,

$$\widehat{\mathcal{H}} = \{i \in \{1, \ldots, N_{\mathrm{L}}\} \,|\, \widehat{D}_i = \mathcal{H}_i\} \tag{2.16}$$

$$\widehat{\mathcal{M}} = \{i \in \{1, \ldots, N_{\mathrm{L}}\} \,|\, \widehat{D}_i = \mathcal{M}_i\} \tag{2.17}$$

Then, the likelihood function from this perspective can be expressed as

$$p(\boldsymbol{P}_{\mathrm{R}} \,|\, \boldsymbol{l}_{\mathrm{R}}) = \prod_{i \in \widehat{\mathcal{H}}} \frac{1}{\sqrt{2\pi}\sigma_i} e^{-\frac{(P_{\mathrm{R},i} - P_{\mathrm{H},i} R_p h_i(\boldsymbol{l}_{\mathrm{R}}))^2}{2\sigma_i^2}} \prod_{i \in \widehat{\mathcal{M}}} \frac{1}{\sqrt{2\pi}\sigma_i} e^{-\frac{(P_{\mathrm{R},i} - \widehat{P}_{\mathrm{M},i} R_p h_i(\boldsymbol{l}_{\mathrm{R}}))^2}{2\sigma_i^2}} \tag{2.18}$$

and the resulting ML estimator can be derived as

$$\widehat{\boldsymbol{l}}_{\mathrm{R}} = \arg\min_{\boldsymbol{l}_{\mathrm{R}} \in \mathcal{L}} \sum_{i \in \widehat{\mathcal{H}}} \frac{(P_{\mathrm{R},i} - P_{\mathrm{H},i} R_p h_i(\boldsymbol{l}_{\mathrm{R}}))^2}{2\sigma_i^2} + \sum_{i \in \widehat{\mathcal{M}}} \frac{(P_{\mathrm{R},i} - \widehat{P}_{\mathrm{M},i} R_p h_i(\boldsymbol{l}_{\mathrm{R}}))^2}{2\sigma_i^2} \tag{2.19}$$

where $\widehat{P}_{\mathrm{M},i}$ is as in (2.13) for $i \in \widehat{\mathcal{M}}$.

2.3.1.2 Algorithm 1-(b)

In this algorithm, the estimates in (2.13) are still assumed to be perfect but possible errors in the decisions of the GLRTs in (2.15) are taken into consideration. Specifically, the probability that the ith LED transmitter is malicious is calculated as follows:

$$\widehat{\gamma}_i = \mathrm{P}(\mathcal{M}_i \,|\, \widehat{D}_i) = \frac{\gamma_i \mathrm{P}(\widehat{D}_i \,|\, \mathcal{M}_i)}{\gamma_i \mathrm{P}(\widehat{D}_i \,|\, \mathcal{M}_i) + (1-\gamma_i)\mathrm{P}(\widehat{D}_i \,|\, \mathcal{H}_i)} \tag{2.20}$$

where $\gamma_i = \mathrm{P}(\mathcal{M}_i)$ as defined before. In other words, in Algorithm 1-(b), the probabilities are updated according to the decisions produced by the GLRTs in the training stage. Hence, γ_i and $\widehat{\gamma}_i$ can be regarded, respectively, as the prior and posterior probabilities that the ith LED is malicious. Accordingly, the ML estimator can be obtained as follows:

$$\widehat{\boldsymbol{l}}_{\mathrm{R}} = \arg\max_{\boldsymbol{l}_{\mathrm{R}} \in \mathcal{L}} \prod_{i=1}^{N_{\mathrm{L}}} \left(\frac{\widehat{\gamma}_i}{\sqrt{2\pi}\sigma_i} e^{-\frac{(P_{\mathrm{R},i} - \widehat{P}_{\mathrm{M},i} R_p h_i(\boldsymbol{l}_{\mathrm{R}}))^2}{2\sigma_i^2}} + \frac{1-\widehat{\gamma}_i}{\sqrt{2\pi}\sigma_i} e^{-\frac{(P_{\mathrm{R},i} - P_{\mathrm{H},i} R_p h_i(\boldsymbol{l}_{\mathrm{R}}))^2}{2\sigma_i^2}} \right) \tag{2.21}$$

where $\widehat{\gamma}_i$ is given by (2.20) and $\widehat{P}_{\mathrm{M},i}$ is as in (2.13). It should be noted that $\mathrm{P}(\widehat{D}_i \,|\, \mathcal{M}_i)$ and $\mathrm{P}(\widehat{D}_i \,|\, \mathcal{H}_i)$ can be calculated for the GLRT in (2.15) based on analytical approaches or simply via Monte-Carlo trials.

2.3.2 Detection and Estimation in Scenario 2

In this scenario, the hypothesis-testing problem for the ith LED transmitter can be stated as

$$\begin{aligned} \mathcal{H}_i &: P_{\mathrm{R},i}^{(j)} = R_p\, P_{\mathrm{H},i}\, h_i\big(\boldsymbol{l}_{\mathrm{R}}^{(j)}\big) + \eta_i^{(j)},\ j = 1, \ldots, N_{\mathrm{V}} \\ \mathcal{M}_i &: P_{\mathrm{R},i}^{(j)} = R_p\, P_{\mathrm{M},i}^{(j)}\, h_i\big(\boldsymbol{l}_{\mathrm{R}}^{(j)}\big) + \eta_i^{(j)},\ j = 1, \ldots, N_{\mathrm{V}} \end{aligned} \tag{2.22}$$

Then, the GLRT is given by

$$\frac{\displaystyle\max_{\{P_{\mathrm{M},i}^{(j)}\}_{j=1}^{N_{\mathrm{V}}}} \prod_{j=1}^{N_{\mathrm{V}}} \frac{1}{\sqrt{2\pi}\sigma_{i,j}} e^{-\frac{\left(P_{\mathrm{R},i}^{(j)} - R_p P_{\mathrm{M},i}^{(j)} h_i\left(\boldsymbol{l}_{\mathrm{R}}^{(j)}\right)\right)^2}{2\sigma_{i,j}^2}}}{\displaystyle\prod_{j=1}^{N_{\mathrm{V}}} \frac{1}{\sqrt{2\pi}\sigma_{i,j}} e^{-\frac{\left(P_{\mathrm{R},i}^{(j)} - R_p P_{\mathrm{H},i} h_i\left(\boldsymbol{l}_{\mathrm{R}}^{(j)}\right)\right)^2}{2\sigma_{i,j}^2}}} \underset{\mathcal{H}_i}{\overset{\mathcal{M}_i}{\gtrless}} \kappa_i \tag{2.23}$$

where κ_i denotes the threshold. The maximization problem in the numerator of (2.23) can be solved in closed form, which leads to the following simplified form of the GLRT after some manipulation:

$$\sum_{j=1}^{N_{\rm V}} \frac{1}{\sigma_{i,j}^2}\left(R_p P_{{\rm R},i}^{(j)} h_i\big(\boldsymbol{l}_{\rm R}^{(j)}\big)\big(\widehat{P}_{{\rm M},i}^{(j)} - P_{{\rm H},i}\big) + 0.5R_p^2\big(h_i\big(\boldsymbol{l}_{\rm R}^{(j)}\big)\big)^2\Big(P_{{\rm H},i}^2 - \big(\widehat{P}_{{\rm M},i}^{(j)}\big)^2\Big)\right) \underset{\mathcal{H}_i}{\overset{\mathcal{M}_i}{\gtrless}} \log(\kappa_i) \tag{2.24}$$

where

$$\widehat{P}_{{\rm M},i}^{(j)} = \begin{cases} P_{{\rm min},i}\,, & \text{if } \frac{P_{{\rm R},i}^{(j)}}{R_p h_i\left(\boldsymbol{l}_{\rm R}^{(j)}\right)} \leq P_{{\rm min},i} \\ P_{{\rm max},i}\,, & \text{if } \frac{P_{{\rm R},i}^{(j)}}{R_p h_i\left(\boldsymbol{l}_{\rm R}^{(j)}\right)} \geq P_{{\rm max},i} \\ \frac{P_{{\rm R},i}^{(j)}}{R_p h_i\left(\boldsymbol{l}_{\rm R}^{(j)}\right)}\,, & \text{otherwise} \end{cases} \tag{2.25}$$

Let $\widehat{D}_i$ denote the decision of the GLRT in (2.24) for $i \in \{1, \ldots, N_{\rm L}\}$. When the power measurements $\boldsymbol{P}_{\rm R}$ are taken as in (2.1) related to a VLC receiver at an unknown location $\boldsymbol{l}_{\rm R}$, the estimation of $\boldsymbol{l}_{\rm R}$ can be performed via the following algorithms in Scenario 2:

2.3.2.1 Algorithm 2-(a)

In this algorithm, the decisions of the GLRTs in (2.24) are assumed to be correct and the likelihood function is stated as

$$p(\boldsymbol{P}_{\rm R}\,|\,\boldsymbol{l}_{\rm R}, \boldsymbol{P}_{\rm M}) = \prod_{i\in\widehat{\mathcal{H}}} \frac{1}{\sqrt{2\pi}\sigma_i} e^{-\frac{(P_{{\rm R},i} - P_{{\rm H},i} R_p h_i(\boldsymbol{l}_{\rm R}))^2}{2\sigma_i^2}} \prod_{i\in\widehat{\mathcal{M}}} \frac{1}{\sqrt{2\pi}\sigma_i} e^{-\frac{(P_{{\rm R},i} - P_{{\rm M},i} R_p h_i(\boldsymbol{l}_{\rm R}))^2}{2\sigma_i^2}} \tag{2.26}$$

where $\widehat{\mathcal{H}}$ and $\widehat{\mathcal{M}}$ are as defined in (2.16) and (2.17), respectively, for the GLRTs in (2.24). Then, the corresponding ML estimator is derived as

$$\widehat{\boldsymbol{l}}_{\rm R} = \arg\min_{\boldsymbol{l}_{\rm R}} \sum_{i\in\widehat{\mathcal{H}}} \frac{(P_{{\rm R},i} - P_{{\rm H},i} R_p h_i(\boldsymbol{l}_{\rm R}))^2}{2\sigma_i^2} + \sum_{i\in\widehat{\mathcal{M}}} \frac{(P_{{\rm R},i} - \widehat{P}_{{\rm M},i}(\boldsymbol{l}_{\rm R}) R_p h_i(\boldsymbol{l}_{\rm R}))^2}{2\sigma_i^2} \tag{2.27}$$

where $\widehat{P}_{{\rm M},i}(\boldsymbol{l}_{\rm R})$ is as in (2.7) for $i \in \widehat{\mathcal{M}}$.

2.3.2.2 Algorithm 2-(b)

In this algorithm, possible errors in the decisions of the GLRTs in (2.24) are considered by updating the probabilities that the LED transmitters can be malicious as in (2.20). Then, the ML estimator is designed as in Section 2.2 by replacing γ_i's with $\widehat{\gamma}_i$'s. Consequently, Algorithm 2-(b) can be expressed as in (2.6) and (2.7) by replacing γ_i's in (2.6) with $\widehat{\gamma}_i$'s obtained from (2.20).

Remark 4: It is noted that the estimates obtained in the training stage for the power levels of the malicious LED transmitters in (2.25) are not employed during the estimation stage since the power levels of the malicious LED transmitters vary in Scenario 2 (i.e., they become different in the estimation stage).

Remark 5: It is noted that Algorithm 1-(a) and Algorithm 2-(a) can be implemented without using the probabilities that the LED transmitters can be malicious. However, the knowledge of these probabilities is required for Algorithm 1-(b) and Algorithm 2-(b). In practice, the knowledge of the probabilities that the LED transmitters are malicious can be obtained in various ways: (i) For the case in which an LED transmitter becomes "malicious" due a failure in the LED chip (see Remark 2), the probability that an LED can fail can be learned based on some prior knowledge depending on the LED brand and type or based on previous operating experience. (ii) For the case in which an LED transmitter becomes malicious due to hijacking, the probability of such an event can be estimated based on the history of VLP networks operating in similar environments/conditions.

2.3.3 Alternative Detection Approach for Scenario 1

In Section 2.3.1, the GLRT is obtained as in (2.15) and its threshold is set according to the tradeoff between the conditional probabilities of error, namely, $\mathrm{P}(\widehat{D}_i \,|\, \mathcal{M}_i)$ and $\mathrm{P}(\widehat{D}_i \,|\, \mathcal{H}_i)$. As an alternative approach, the uniformly most powerful (UMP) test can be derived in Scenario 1 if there exists prior information that a malicious LED transmitter does not increase the power level with respect to the power level of an honest LED transmitter; that is, if the following condition is satisfied:

$$P_{\mathrm{M},i} \leq P_{\mathrm{H},i}\,,\ \forall i \tag{2.28}$$

Under this condition, the likelihood ratio test for the hypothesis-testing problem in (2.11) can be expressed as

$$\frac{\exp\left\{\sum_{j=1}^{N_{\mathrm{V}}} \frac{\left(P_{\mathrm{R},i}^{(j)} - R_p P_{\mathrm{H},i} h_i(\boldsymbol{l}_{\mathrm{R}}^{(j)})\right)^2}{2\sigma_{ij}^2}\right\}}{\exp\left\{\sum_{j=1}^{N_{\mathrm{V}}} \frac{\left(P_{\mathrm{R},i}^{(j)} - R_p P_{\mathrm{M},i} h_i(\boldsymbol{l}_{\mathrm{R}}^{(j)})\right)^2}{2\sigma_{ij}^2}\right\}} \underset{\mathcal{H}_i}{\overset{\mathcal{M}_i}{\gtrless}} \eta_i \tag{2.29}$$

where η_i denotes the threshold. Taking the natural logarithm of both sides leads to

$$\sum_{j=1}^{N_{\mathrm{V}}} \frac{R_p h_i(\boldsymbol{l}_{\mathrm{R}}^{(j)}) P_{\mathrm{R},i}^{(j)} (P_{\mathrm{M},i} - P_{\mathrm{H},i})}{\sigma_i^2} + \sum_{j=1}^{N_{\mathrm{V}}} \frac{R_p^2 h_i^2(\boldsymbol{l}_{\mathrm{R}}^{(j)}) \left(P_{\mathrm{H},i}^2 - P_{\mathrm{M},i}^2\right)}{2\sigma_i^2} \underset{\mathcal{H}_i}{\overset{\mathcal{M}_i}{\gtrless}} \log \eta_i \tag{2.30}$$

Based on the condition in (2.28), the expression in (2.30) can be simplified as

$$\sum_{j=1}^{N_{\mathrm{V}}} \frac{P_{\mathrm{R},i}^{(j)} h_i(\boldsymbol{l}_{\mathrm{R}}^{(j)})}{\sigma_{ij}^2} \underset{\mathcal{M}_i}{\overset{\mathcal{H}_i}{\gtrless}} \tilde{\eta}_i \tag{2.31}$$

where $\tilde{\eta}_i$ is defined as $\tilde{\eta}_i \triangleq \left(\log \eta_i - \sum_{j=1}^{N_{\mathrm{V}}} R_p^2 h_i^2(\boldsymbol{l}_{\mathrm{R}}^{(j)})(P_{\mathrm{H},i}^2 - P_{\mathrm{M},i}^2)/(2\sigma_i^2)\right)/(R_p(P_{\mathrm{M},i} - P_{\mathrm{H},i}))$. For the test in (2.31), the false alarm probability can be derived analytically as follows. Under hypothesis $\mathcal{H}_i$ in Scenario 1 (see (2.11)), the received power $P_{\mathrm{R},i}^{(j)}$ follows a Gaussian distribution with mean $R_p P_{\mathrm{H},i} h_i(\boldsymbol{l}_{\mathrm{R}}^{(j)})$ and variance σ_{ij}^2; i.e.,

$$P_{\mathrm{R},i}^{(j)} \sim \mathcal{N}\left(R_p P_{\mathrm{H},i} h_i(\boldsymbol{l}_{\mathrm{R}}^{(j)}), \sigma_{ij}^2\right) \tag{2.32}$$

Since $P_{\mathrm{R},i}^{(j)}$'s are independent for different j's, we get

$$\sum_{j=1}^{N_{\mathrm{V}}} \frac{P_{\mathrm{R},i}^{(j)} h_i(\boldsymbol{l}_{\mathrm{R}}^{(j)})}{\sigma_{ij}^2} \sim \mathcal{N}\left(\sum_{j=1}^{N_{\mathrm{V}}} \frac{R_p P_{\mathrm{H},i} h_i^2(\boldsymbol{l}_{\mathrm{R}}^{(j)})}{\sigma_{ij}^2}, \sum_{j=1}^{N_{\mathrm{V}}} \frac{h_i^2(\boldsymbol{l}_{\mathrm{R}}^{(j)})}{\sigma_{ij}^2}\right) \tag{2.33}$$

Accordingly, setting the false alarm probability to a given level α leads to

$$1 - Q\left(\frac{\tilde{\eta}_i - \sum_{j=1}^{N_{\mathrm{V}}} \frac{R_p P_{\mathrm{H},i} h_i^2(\boldsymbol{l}_{\mathrm{R}}^{(j)})}{\sigma_{ij}^2}}{\sqrt{\sum_{j=1}^{N_{\mathrm{V}}} \frac{h_i^2(\boldsymbol{l}_{\mathrm{R}}^{(j)})}{\sigma_{ij}^2}}}\right) = \alpha \tag{2.34}$$

Then, solving for $\tilde{\eta}_i$ yields the following threshold:

$$\tilde{\eta}_i = \sqrt{\sum_{j=1}^{N_{\rm V}} \frac{h_i^2(\boldsymbol{l}_{\rm R}^{(j)})}{\sigma_{ij}^2}}\, Q^{-1}(1-\alpha) + \sum_{j=1}^{N_{\rm V}} \frac{R_p P_{{\rm H},i} h_i^2(\boldsymbol{l}_{\rm R}^{(j)})}{\sigma_{ij}^2} \tag{2.35}$$

Since the test in (2.31) with the threshold specified by (2.35) is a likelihood ratio test (as it is equivalent to (2.29)) and does change with respect to the unknown parameter $P_{{\rm M},i}$, it is a UMP test for the problem in (2.11) [59]. Hence, when the assumption in (2.28) holds, the UMP test exists for Scenario 1 and can be obtained as described in this section (which can be used instead of the GLRT in (2.15)). It should be noted that if the condition in (2.28) is reversed, i.e., if $P_{{\rm M},i} > P_{{\rm H},i}$, $\forall i$, a UMP test can again be derived based on a similar argument. However, it is more likely for a malicious third party to reduce the transmit powers of the LED transmitters to degrade the positioning accuracy.

2.4 CRLB Derivations

In this section, CRLB expressions are derived for three different cases to establish benchmarks for performance of the proposed algorithms in the absence and presence of training measurements. In the first case, it is assumed that the transmit powers of all the LEDs, i.e., $\{P_{{\rm T},i}\}_{i=1}^{N_{\rm L}}$, are perfectly known. This bound applies to Scenario 1, in which the transmit power of each malicious LED transmitter is fixed and can be estimated via training measurements. In the second case, it is assumed that the transmit power of malicious LED transmitters are unknown but their indices are known. This bound corresponds to Scenario 2, in which there exist training measurements and malicious LED transmitters modify their transmit powers for each measurement. In the third case, the CRLB is derived for the scenario without training measurements, which corresponds to the setting considered in Section 2.2. Overall, via three different CRLB derivations, we take into account various levels of knowledge related to the transmit powers of the malicious LED transmitters and the indices of malicious LEDs.

2.4.1 CRLB for Scenario 1 (Knowledge of Transmit Powers)

In this case, the transmit powers of all the LEDs, i.e., $\{P_{\mathrm{T},i}\}_{i=1}^{N_\mathrm{L}}$, are perfectly known. Therefore, the vector of unknown parameters consists only of the PD location, i.e., $\boldsymbol{l}_\mathrm{R}$. Thus, the likelihood function for $\boldsymbol{l}_\mathrm{R}$ based on the measurements in (2.1) can be expressed as

$$p(\boldsymbol{P}_\mathrm{R}|\boldsymbol{l}_\mathrm{R}) = \left(\prod_{i=1}^{N_\mathrm{L}} \frac{1}{\sqrt{2\pi}\sigma_i}\right) \exp\left\{-\sum_{i=1}^{N_\mathrm{L}} \frac{(P_{\mathrm{R},i} - R_p P_{\mathrm{T},i} h_i(\boldsymbol{l}_\mathrm{R}))^2}{2\sigma_i^2}\right\} \tag{2.36}$$

Then, the Fisher information matrix (FIM) is given by

$$\boldsymbol{J}(\boldsymbol{l}_\mathrm{R}) = \mathbb{E}\{(\nabla_{\boldsymbol{l}_\mathrm{R}} \log p(\boldsymbol{P}_\mathrm{R}|\boldsymbol{l}_\mathrm{R}))(\nabla_{\boldsymbol{l}_\mathrm{R}} \log p(\boldsymbol{P}_\mathrm{R}|\boldsymbol{l}_\mathrm{R}))^T\} \tag{2.37}$$

and the CRLB is expressed as [59]

$$\mathbb{E}\left\{\left\|\widehat{\boldsymbol{l}}_\mathrm{R} - \boldsymbol{l}_\mathrm{R}\right\|^2\right\} \geq \mathrm{trace}\left\{\boldsymbol{J}(\boldsymbol{l}_\mathrm{R})^{-1}\right\} \triangleq CRLB \tag{2.38}$$

After some manipulation, the elements of the FIM in (2.37) can be calculated from (2.36) as follows:

$$[\boldsymbol{J}(\boldsymbol{l}_\mathrm{R})]_{p,q} = R_P^2 \sum_{i=1}^{N_\mathrm{L}} \frac{P_{\mathrm{T},i}^2}{\sigma_i^2} \frac{\partial h_i(\boldsymbol{l}_\mathrm{R})}{\partial \boldsymbol{l}_\mathrm{R}(p)} \frac{\partial h_i(\boldsymbol{l}_\mathrm{R})}{\partial \boldsymbol{l}_\mathrm{R}(q)} \tag{2.39}$$

where $p, q \in \{1, 2, 3\}$ and $\boldsymbol{l}_\mathrm{R}(p)$ denotes the pth element of $\boldsymbol{l}_\mathrm{R}$. In addition, based on (2.3), the partial derivatives of $h_i(\boldsymbol{l}_\mathrm{R})$ with respect to $\boldsymbol{l}_\mathrm{R}(p)$ can be expressed as

$$\frac{\partial h_i(\boldsymbol{l}_\mathrm{R})}{\partial \boldsymbol{l}_\mathrm{R}(p)} = \frac{(m_i+1)A_\mathrm{R}}{2\pi} \frac{[\boldsymbol{g}_{1\mathrm{p}}^i(\boldsymbol{l}_\mathrm{R})\boldsymbol{g}_2^i(\boldsymbol{l}_\mathrm{R}) + \boldsymbol{g}_1^i(\boldsymbol{l}_\mathrm{R})\boldsymbol{g}_{2\mathrm{p}}^i(\boldsymbol{l}_\mathrm{R})]\boldsymbol{g}_3^i(\boldsymbol{l}_\mathrm{R}) - \boldsymbol{g}_1^i(\boldsymbol{l}_\mathrm{R})\boldsymbol{g}_2^i(\boldsymbol{l}_\mathrm{R})\boldsymbol{g}_{3\mathrm{p}}^i(\boldsymbol{l}_\mathrm{R})}{{\boldsymbol{g}_3^i}^2(\boldsymbol{l}_\mathrm{R})} \tag{2.40}$$

where

$$\boldsymbol{g}_1^i(\boldsymbol{l}_\mathrm{R}) = \left[(\boldsymbol{l}_\mathrm{R} - \boldsymbol{l}_\mathrm{T}^i)^T \boldsymbol{n}_\mathrm{T}^i\right]^{m_i} \tag{2.41}$$

$$\boldsymbol{g}_2^i(\boldsymbol{l}_\mathrm{R}) = (\boldsymbol{l}_\mathrm{T}^i - \boldsymbol{l}_\mathrm{R})^T \boldsymbol{n}_\mathrm{R} \tag{2.42}$$

$$\boldsymbol{g}_3^i(\boldsymbol{l}_\mathrm{R}) = \left\|\boldsymbol{l}_\mathrm{R} - \boldsymbol{l}_\mathrm{T}^i\right\|^{m_i+3} \tag{2.43}$$

$$\boldsymbol{g}_{1\mathrm{p}}^i(\boldsymbol{l}_\mathrm{R}) = \frac{\partial \boldsymbol{g}_1^i(\boldsymbol{l}_\mathrm{R})}{\partial \boldsymbol{l}_\mathrm{R}(p)} = m_i \left[(\boldsymbol{l}_\mathrm{R} - \boldsymbol{l}_\mathrm{T}^i)^T \boldsymbol{n}_\mathrm{T}^i\right]^{m_i-1} \boldsymbol{n}_\mathrm{T}^i(p) \tag{2.44}$$

$$\boldsymbol{g}_{2\mathrm{p}}^i(\boldsymbol{l}_\mathrm{R}) = \frac{\partial \boldsymbol{g}_2^i(\boldsymbol{l}_\mathrm{R})}{\partial \boldsymbol{l}_\mathrm{R}(p)} = -\boldsymbol{n}_\mathrm{R}(p) \tag{2.45}$$

$$\boldsymbol{g}_{3\mathrm{p}}^i(\boldsymbol{l}_\mathrm{R}) = \frac{\partial \boldsymbol{g}_3^i(\boldsymbol{l}_\mathrm{R})}{\partial \boldsymbol{l}_\mathrm{R}(p)} = (m_i+3)\left\|\boldsymbol{l}_\mathrm{R} - \boldsymbol{l}_\mathrm{T}^i\right\|^{m_i+1} \left[(\boldsymbol{l}_\mathrm{R}(p) - \boldsymbol{l}_\mathrm{T}^i(p))\right] \tag{2.46}$$

Thus, the CRLB can be obtained from (2.38)–(2.46), yielding a lower bound on mean-squared errors (MSEs) of unbiased estimators for $\boldsymbol{l}_\mathrm{R}$ when the transmit powers of the LEDs are known. Since the malicious LEDs employ fixed transmit powers that can be learned via training measurements in Scenario 1, the CRLB expression in this section applies to Scenario 1; hence, it is referred to as "CRLB - Scen. 1" in Section 2.5.

2.4.2 CRLB for Scenario 2 (Knowledge of Indices of Malicious LEDs)

In this case, it is assumed that the transmit powers of the malicious LEDs are unknown but their indices are known. The set of indices of the malicious LEDs is expressed as

$$\mathcal{M} = \{i \in \{1, \ldots, N_\mathrm{L}\} \,|\, i\text{th LED is malicious}\} \tag{2.47}$$

and the number of elements in $\mathcal{M}$ is denoted by M_L. Then, the vector of unknown parameters is defined as

$$\boldsymbol{\Theta} = \left[\boldsymbol{l}_\mathrm{R}^T \; \boldsymbol{P}_\mathrm{M}^T\right]^T \tag{2.48}$$

where $\boldsymbol{P}_\mathrm{M}$ is the vector consisting of the transmit powers of the malicious LEDs. Accordingly, the likelihood function for $\boldsymbol{\Theta}$ based on the measurements in (2.1) can be expressed as

$$p(\boldsymbol{P}_{\mathrm{R}}|\boldsymbol{\Theta}) = \left(\prod_{i=1}^{N_{\mathrm{L}}} \frac{1}{\sqrt{2\pi}\sigma_i}\right) \exp\left\{-\sum_{i=1}^{N_{\mathrm{L}}} \frac{(P_{\mathrm{R},i} - R_p P_{\mathrm{T},i} h_i(\boldsymbol{l}_{\mathrm{R}}))^2}{2\sigma_i^2}\right\} \tag{2.49}$$

and the FIM is given by

$$\boldsymbol{J}(\boldsymbol{\Theta}) = \mathbb{E}\{(\nabla_{\boldsymbol{\Theta}} \log p(\boldsymbol{P}_{\mathrm{R}}|\boldsymbol{\Theta}))(\nabla_{\boldsymbol{\Theta}} \log p(\boldsymbol{P}_{\mathrm{R}}|\boldsymbol{\Theta}))^T\} \tag{2.50}$$

Based on the FIM, the bound on the estimation error for the location $\boldsymbol{l}_{\mathrm{R}}$ of the VLC receiver can be specified as

$$\mathbb{E}\{\|\widehat{\boldsymbol{l}}_{\mathrm{R}} - \boldsymbol{l}_{\mathrm{R}}\|^2\} \geq \mathrm{trace}\{\boldsymbol{J}(\boldsymbol{\Theta})^{-1}_{1:3,1:3}\} \triangleq CRLB_{\boldsymbol{l}_{\mathrm{R}}} \tag{2.51}$$

where $\widehat{\boldsymbol{l}}_{\mathrm{R}}$ denotes any unbiased estimator of $\boldsymbol{l}_{\mathrm{R}}$. Likewise, the bound on the estimation error for the transmit powers of the malicious LEDs can be stated as

$$\mathbb{E}\{\|\widehat{\boldsymbol{P}}_{\mathrm{M}} - \boldsymbol{P}_{\mathrm{M}}\|^2\} \geq \mathrm{trace}\{\boldsymbol{J}(\boldsymbol{\Theta})^{-1}_{4:M_L+3,4:M_L+3}\} \triangleq CRLB_{\boldsymbol{P}_{\mathrm{M}}} \tag{2.52}$$

where $\widehat{\boldsymbol{P}}_{\mathrm{M}}$ represents any unbiased estimator of $\boldsymbol{P}_{\mathrm{M}}$. After some manipulation, the elements of the FIM in (2.50) can be calculated from (2.49) as

$$[\boldsymbol{J}(\boldsymbol{\Theta})]_{p,q} = R_P^2 \sum_{i=1}^{N_{\mathrm{L}}} \frac{1}{\sigma_i^2} \frac{\partial P_{\mathrm{T},i} h_i(\boldsymbol{l}_{\mathrm{R}})}{\partial \boldsymbol{\Theta}(p)} \frac{\partial P_{\mathrm{T},i} h_i(\boldsymbol{l}_{\mathrm{R}})}{\partial \boldsymbol{\Theta}(q)} \tag{2.53}$$

where $p, q \in \{1, \ldots, M_L + 3\}$ and $\boldsymbol{\Theta}(p)$ denotes the pth element of $\boldsymbol{\Theta}$. As in Section 2.4.1, for $p \in \{1, 2, 3\}$

$$\frac{\partial P_{\mathrm{T},i} h_i(\boldsymbol{l}_{\mathrm{R}})}{\partial \boldsymbol{\Theta}(p)} = P_{\mathrm{T},i} \frac{\partial h_i(\boldsymbol{l}_{\mathrm{R}})}{\partial \boldsymbol{l}_{\mathrm{R}}(p)} \tag{2.54}$$

where $\frac{\partial h_i(\boldsymbol{l}_{\mathrm{R}})}{\partial \boldsymbol{l}_{\mathrm{R}}(p)}$ is as defined in (2.40), and for $p \in \{4, \ldots, M_L + 3\}$

$$\frac{\partial P_{\mathrm{T},i} h_i(\boldsymbol{l}_{\mathrm{R}})}{\partial \boldsymbol{\Theta}(p)} = h_i(\boldsymbol{l}_{\mathrm{R}}) \frac{\partial P_{\mathrm{T},i}}{\partial \boldsymbol{P}_{\mathrm{M}}(p-3)} \tag{2.55}$$

where

$$\frac{\partial P_{\mathrm{T},i}}{\partial \boldsymbol{P}_{\mathrm{M}}(p-3)} = \begin{cases} 1\,, & \text{if } i \in \mathcal{M} \text{ and } i = p-3 \\ 0\,, & \text{otherwise} \end{cases} \tag{2.56}$$

The CRLB expression specified by (2.51) and (2.54)–(2.56) provides a lower bound on position estimation in Scenario 2 since the indices of malicious LED transmitters can be learned via training measurements in that scenario. (However, the transmit powers of malicious LEDs cannot be learned since they change for each measurement in Scenario 2.) Therefore, it is referred to as "CRLB - Scen. 2" in Section 2.5.

2.4.3 CRLB without Training Measurements

In this case, neither the transmit powers nor the indices of the malicious LEDs are known. Therefore, the likelihood function in (2.5) is used to derive the CRLB. The natural logarithm of (2.5) can be expressed as

$$\log p(\boldsymbol{P}_{\mathrm{R}}|\boldsymbol{\Theta}) = \sum_{i=1}^{N_{\mathrm{L}}} \log\left(\gamma_i E_M + (1-\gamma_i)E_H\right) \tag{2.57}$$

where $\boldsymbol{\Theta}$ is as defined in (2.48), and

$$E_M \triangleq \frac{1}{\sqrt{2\pi}\sigma_i} e^{-\frac{(P_{\mathrm{R},i}-P_{\mathrm{M},i}R_p h_i(\boldsymbol{l}_{\mathrm{R}}))^2}{2\sigma_i^2}} \tag{2.58}$$

$$E_H \triangleq \frac{1}{\sqrt{2\pi}\sigma_i} e^{-\frac{(P_{\mathrm{R},i}-P_{\mathrm{H},i}R_p h_i(\boldsymbol{l}_{\mathrm{R}}))^2}{2\sigma_i^2}} \tag{2.59}$$

Based on (2.57), the FIM is constructed as

$$\boldsymbol{J}(\boldsymbol{\Theta}) = \mathbb{E}\{(\nabla_{\boldsymbol{\Theta}} \log p(\boldsymbol{P}_{\mathrm{R}}|\boldsymbol{\Theta}))(\nabla_{\boldsymbol{\Theta}} \log p(\boldsymbol{P}_{\mathrm{R}}|\boldsymbol{\Theta}))^T\} \tag{2.60}$$

The partial derivatives in (2.60) can be expressed as follows:

$$\begin{aligned}\frac{\partial \log p(\boldsymbol{P}_{\mathrm{R}}|\boldsymbol{\Theta})}{\partial \boldsymbol{l}_{\mathrm{R}}(p)} &= \sum_{i=1}^{N_{\mathrm{L}}} \frac{\gamma_i E_M (P_{\mathrm{R},i} - P_{\mathrm{M},i}R_p h_i(\boldsymbol{l}_{\mathrm{R}}))P_{\mathrm{M},i}R_p}{\sigma_i^2 p(\boldsymbol{P}_{\mathrm{R}}|\boldsymbol{\Theta})} \frac{\partial h_i(\boldsymbol{l}_{\mathrm{R}})}{\partial \boldsymbol{l}_{\mathrm{R}}(p)} \\ &+ \sum_{i=1}^{N_{\mathrm{L}}} \frac{(1-\gamma_i) E_H (P_{\mathrm{R},i} - P_{\mathrm{H},i}R_p h_i(\boldsymbol{l}_{\mathrm{R}}))P_{\mathrm{H},i}R_p}{\sigma_i^2 p(\boldsymbol{P}_{\mathrm{R}}|\boldsymbol{\Theta})} \frac{\partial h_i(\boldsymbol{l}_{\mathrm{R}})}{\partial \boldsymbol{l}_{\mathrm{R}}(p)}\end{aligned} \tag{2.61}$$

$$\frac{\partial \log p(\boldsymbol{P}_{\mathrm{R}}|\boldsymbol{\Theta})}{\partial \boldsymbol{P}_{\mathrm{M}}(p)} = \sum_{i=1}^{N_{\mathrm{L}}} \frac{\gamma_i E_M (P_{\mathrm{R},i} - P_{\mathrm{M},i}R_p h_i(\boldsymbol{l}_{\mathrm{R}}))R_p h_i(\boldsymbol{l}_{\mathrm{R}})}{\sigma_i^2 p(\boldsymbol{P}_{\mathrm{R}}|\boldsymbol{\Theta})} \tag{2.62}$$

The partial derivatives $\frac{\partial h_i(\boldsymbol{l}_\mathrm{R})}{\partial \boldsymbol{l}_\mathrm{R}(p)}$ are the same as in (2.40). As the expectation in (2.60) is hard to evaluate analytically, Monte Carlo integration methods can be used to compute the CRLB in a similar fashion to that in [63]. Namely, the FIM in (2.60) can be approximated as follows:

$$\boldsymbol{J}(\boldsymbol{\Theta}) \approx \frac{1}{N_\mathrm{MC}} \sum_{i=1}^{N_\mathrm{MC}} \big(\nabla_{\boldsymbol{\Theta}} \log p\big(\boldsymbol{P}_\mathrm{R}^{(i)}|\boldsymbol{\Theta}\big)\big)\big(\nabla_{\boldsymbol{\Theta}} \log p\big(\boldsymbol{P}_\mathrm{R}^{(i)}|\boldsymbol{\Theta}\big)\big)^T \tag{2.63}$$

where N_MC is the number of Monte-Carlo trials and $\boldsymbol{P}_\mathrm{R}^{(i)}$ is the realization of $\boldsymbol{P}_\mathrm{R}$ in the ith trial. In (2.63), $\nabla_{\boldsymbol{\Theta}} \log p\big(\boldsymbol{P}_\mathrm{R}^{(i)}|\boldsymbol{\Theta}\big)$ is evaluated based on the expressions in (2.61) and (2.62) for the given realization $\boldsymbol{P}_\mathrm{R}^{(i)}$. Hence, a semi-analytic evaluation approach is employed. Finally, the CRLB can be expressed as

$$\mathbb{E}\big\{\big\|\widehat{\boldsymbol{l}}_\mathrm{R} - \boldsymbol{l}_\mathrm{R}\big\|^2\big\} \geq \mathrm{trace}\big\{\boldsymbol{J}(\boldsymbol{\Theta})^{-1}_{1:3,1:3}\big\} \triangleq CRLB_{\boldsymbol{l}_\mathrm{R}} \tag{2.64}$$

This bound is referred to as “CRLB - No Training” in Section 2.5.

2.5 Simulation Results

In this section, simulations are conducted to evaluate the performance of the proposed approaches. A room with dimensions $4 \times 4 \times 3$ meters (width, depth and height, respectively) is considered. The number of LED transmitters is taken as $N_\mathrm{L} = 9$ and they are placed at the following locations: $\{(-1,1,3), (0,1,3), (1,1,3), (-1,0,3), (0,0,3), (1,0,3), (-1,-1,3), (0,-1,3), (1,-1,3)\}$ (all in meters) such that they cover the room in a symmetric manner, where $(0,0,0)$ corresponds to the center of the room floor. The orientation vectors, $\boldsymbol{n}_\mathrm{T}^i$'s, are taken as $[0,0,-1]^T$ $\forall i$ such that all the LEDs face downwards. Also, m_i's are set to 1 $\forall i$. Although the derivations in Section 2.2 and Section 2.3 are generic for any three-dimensional setup, the VLC receiver is considered to be at a fixed height of 0.85 meters in the simulations (i.e., a two-dimensional localization scenario is considered [64]). Moreover, the orientation of the receiver is specified as $\boldsymbol{n}_\mathrm{R} = [0,0,1]^T$, i.e., it faces upwards, the area of the PD is taken as $A_\mathrm{R} = 1\,\mathrm{cm}^2$, and the responsivity of the PD is set to $R_p = 1$. Moreover, the noise variances are assumed to be the same, that

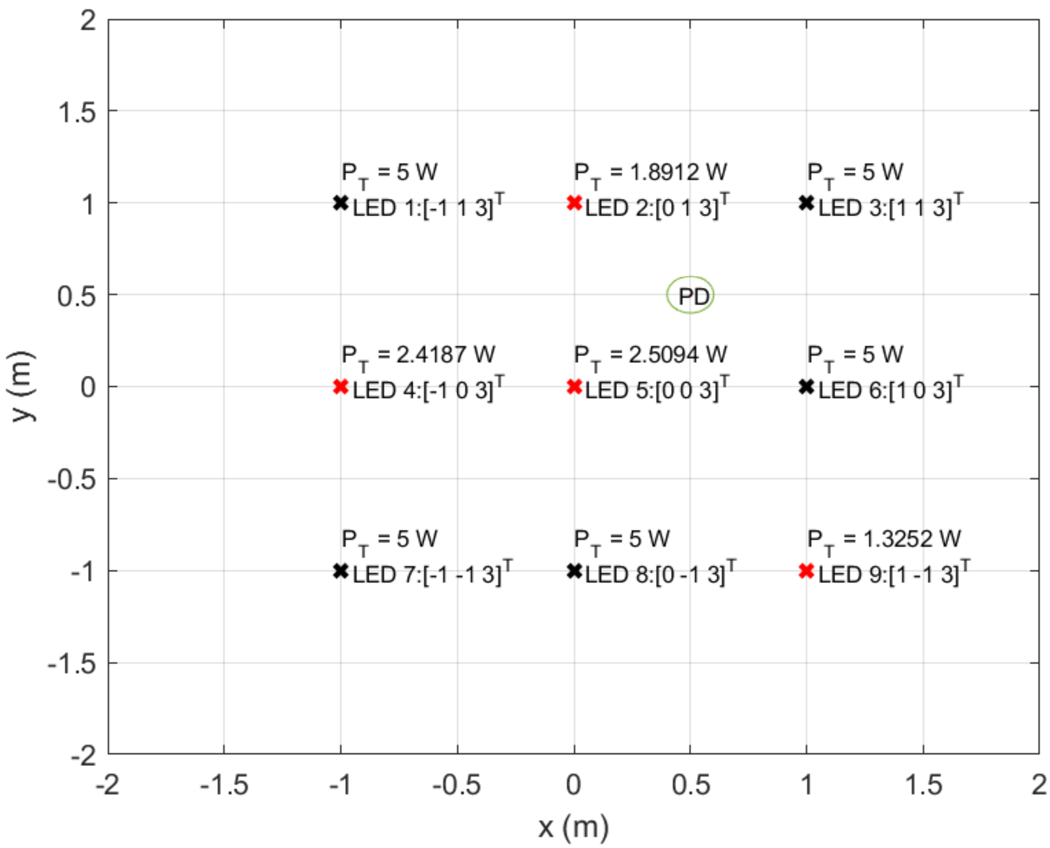

Figure 2.1: Top view of the system setup in an example scenario with 5 honest and 4 malicious LEDs. Black crosses represent honest LEDs and red crosses represent malicious LEDs.

is, $\sigma_i^2 = \sigma^2$ for $i = 1, \ldots, N_{\mathrm{L}}$. A visualization of the system setup is presented in Fig. 2.1 as the top view perspective of the room for an example scenario of malicious LEDs with $\gamma_i = 0.5 \; \forall i$.

Since the localization problem can be ill-posed when the number of honest LED transmitters is below 3, the probabilities that the LED transmitters can be malicious are set as follows:

$$\gamma_i = \begin{cases} 0, & \text{if } i = 1, 6, 7 \\ \gamma, & \text{otherwise} \end{cases} \tag{2.65}$$

Namely, in the simulations, it is guaranteed that there exist at least 3 honest

LED transmitters for any given scenario. It should be noted that the indices of these 3 "always honest" LED transmitters is not known by the VLC receiver and that the other LED transmitters can also be honest with probability $(1-\gamma)$ independently of each other.

To investigate the performance of the proposed ML estimator in (2.6) (which is designed for the scenario without training measurements), the location of the VLC receiver is set to $\boldsymbol{l}_{\mathrm{R}} = [0.5\ 0.5\ 0.85]^T$ meters and various values of γ are considered. For each γ, 10^4 different sets of honest and malicious LED realizations are obtained according to (2.65), and the powers of the malicious LED transmitters, $P_{\mathrm{M},i}$'s, are generated as uniform random variables in the set $[1\,W, 3\,W]$, whereas the honest LED transmit power is set to $5\,W$. In addition, $P_{\mathrm{min},i}$ is set to $1\,W$ and $P_{\mathrm{max},i}$ is set to $10\,W$, which are the estimation parameters used in (2.7), (2.13), and (2.25).

In Fig. 2.2, the root-mean squared error (RMSE) performance of the proposed ML estimator in (2.6) is plotted versus γ for $\sigma^2 = 10^{-11}$. For comparison purposes, we also consider the case in which the VLC receiver is unaware of the security issue and assumes that all the LED transmitters are honest. In this case, the VLC receiver employs the model in (2.1) with $P_{\mathrm{T},i} = P_{\mathrm{H},i}$ for $i = 1, \ldots, N_{\mathrm{L}}$, which results in the following ML estimator: $\widehat{\boldsymbol{l}}_{\mathrm{R}} = \underset{\boldsymbol{l}_{\mathrm{R}} \in \mathcal{L}}{\arg\min} \sum_{i=1}^{N_{\mathrm{L}}} (P_{\mathrm{R},i} - P_{\mathrm{H},i} R_p h_i(\boldsymbol{l}_{\mathrm{R}}))^2/(2\sigma_i^2)$. This ML estimator is labeled as "ML – Unaware" in Fig. 2.2. As another way of comparison, the ML estimator in the presence of perfect knowledge of malicious LED transmitters is considered, which is given by (2.27) when $\widehat{\mathcal{H}}$ and $\widehat{\mathcal{M}}$ are equal to the correct sets of honest and malicious LED transmitters, respectively. This ML estimator is labeled as "ML – Perfect" in Fig. 2.2. The results in the figure show that the proposed estimator in (2.6) provides performance improvements (especially when γ is not small) over the estimator that assumes that all the LED transmitters are honest. Also, the estimator that perfectly knows which LED transmitters are malicious provides a performance lower bound, as expected. In addition, the estimators have higher RMSE values as γ increases due to the increased level of uncertainty about transmission powers. In Fig. 2.2, we also present the CRLB in the absence of training measurements ("CRLB - No

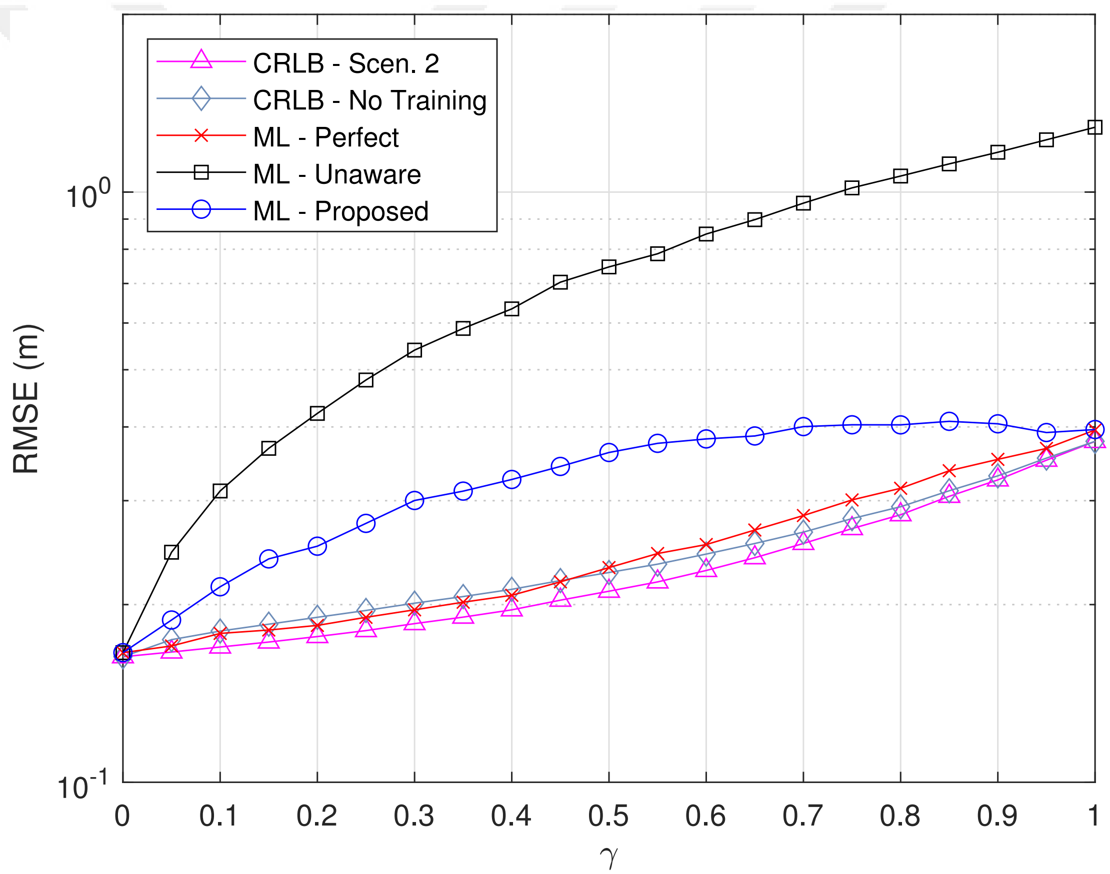

Figure 2.2: RMSE versus γ for $\sigma^2 = 10^{-11}$.

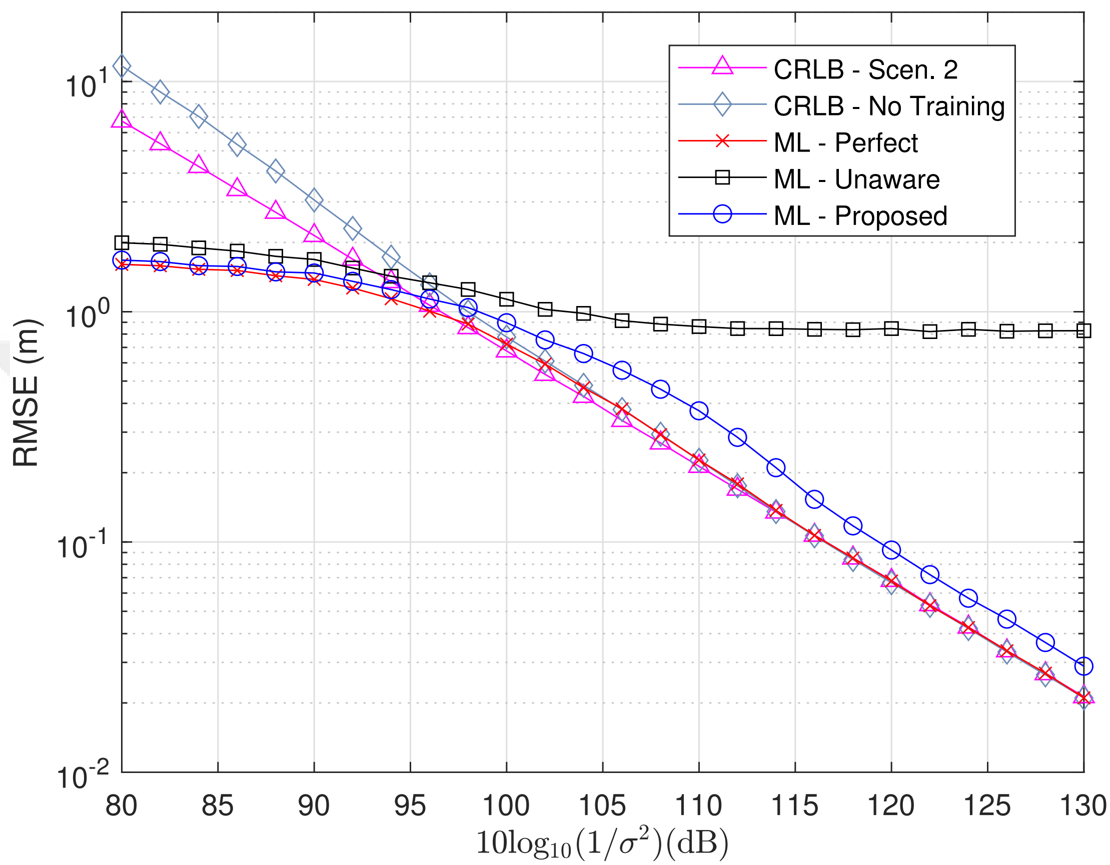

Figure 2.3: RMSE versus $10\log_{10}(1/\sigma^2)$ for $\gamma = 0.5$.

Training") and the CRLB when the indices of malicious LED transmitters are known ("CRLB - Scen. 2"). The CRLB with no training measurements provides a lower bound on the performance of the proposed ML estimator. On the other hand, the CRLB for Scenario 2 presents a performance limit for "ML – Perfect", which is also designed under the assumption of known indices of malicious LED transmitters. It is noted that the CRLB in the absence of training measurements is a tight limit for the RMSE of the proposed ML estimator only when γ is close to zero or one.

In Fig. 2.3, the RMSE performance of the estimators is plotted versus the noise level, $10\log_{10}(1/\sigma^2)$. It is observed that the RMSE of the proposed ML estimator in (2.6) gets close to the CRLB and the RMSE of the "ML – Perfect" as the noise variance decreases. However, the RMSE of "ML – Unaware" estimator does not improve significantly as the noise variance gets lower as it assumes that all the LED transmitters are honest. In addition, it is noticed that for large values of noise variances, the RMSEs of all the estimators are below the CRLBs. This is due to the fact that the possible locations of the VLC receiver in the room are limited to 4×4 meters in two dimensions, and the ML estimators perform the search over this space. On the other hand, the CRLB derivations do not assume any prior information about the location of the VLC receiver; hence, can lead to larger values than RMSEs in very noisy cases.

To evaluate the performance of the algorithms in Section 2.3.1 (Scenario 1), a similar setup is used. The algorithms in this section require a training phase. For this purpose, N_{V} is set to one and the training location is chosen as the center of the room in two dimensions at a height of 0.85 meter, i.e., $(0, 0, 0.85)$ meters. Again, 10^4 different sets of honest and malicious LED realizations are used to obtain average performance results. The same LED transmitter powers as in the previous part are used in both the training and estimation phases since, in Scenario 1, transmit powers of malicious LED transmitters do not change over time. In addition, to set the values of τ_i for the decision rule in (2.15), a Neyman-Pearson type approach is followed. Namely, for each noise variance σ^2, τ_i's are determined so as to set the false alarm probability of each decision rule to a fixed value of $\mathrm{P_F}$ for each LED transmitter. In the simulations, two different values of $\mathrm{P_F}$ are considered, namely, $\mathrm{P_F} = 0.001$ and $\mathrm{P_F} = 0.5$. Based on the obtained thresholds, the conditional error and correct decision probabilities, i.e., $\mathrm{P}(\widehat{D}_i \,|\, \mathcal{M}_i)$ and $\mathrm{P}(\widehat{D}_i \,|\, \mathcal{H}_i)$, are calculated using 10^5 Monte-Carlo trials and employed in Algorithm 1-(b). To provide comparisons, the "ML – Perfect" estimator is also considered, which knows not only the malicious LED transmitters but also their transmit powers in this scenario (Scenario 1).

Fig. 2.4 shows the RMSE performance of the algorithms versus the noise level, $10\log_{10}(1/\sigma^2)$, where $\gamma = 0.5$. It is observed that, for $\mathrm{P_F} = 0.001$, Algorithm 1-(a) has the same performance as the "ML – Unaware" estimator up to around 100 dB and then gets close to "ML – Perfect" at low noise variances. For $\mathrm{P_F} = 0.5$, Algorithm 1-(a) performs worse than "ML – Unaware" up to around 100 dB but afterwards it achieves lower RMSEs than Algorithm 1-(a) with $\mathrm{P_F} = 0.001$ up to

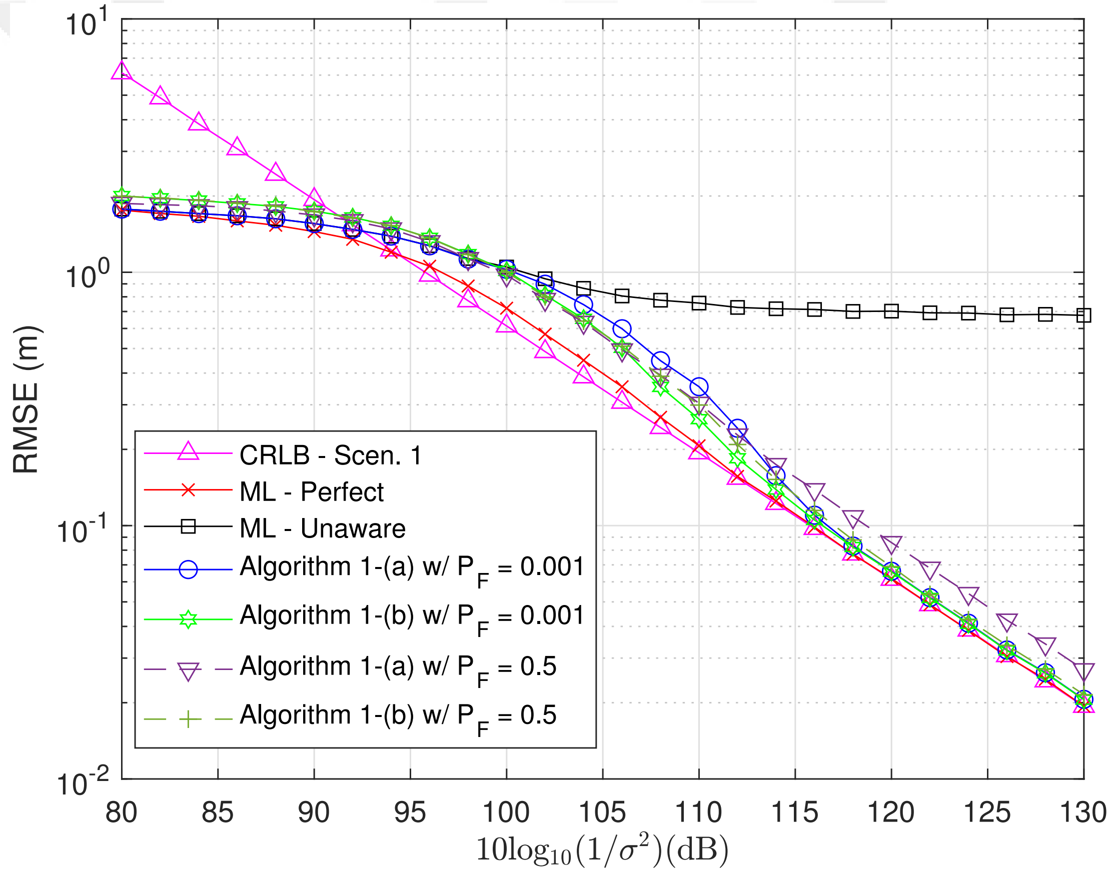

Figure 2.4: RMSE versus $10\log_{10}(1/\sigma^2)$ for Scenario 1 ($\gamma = 0.5$).

around 113 dB. However, for higher values of $10\log_{10}(1/\sigma^2)$, Algorithm 1-(a) with $\mathrm{P_F} = 0.001$ outperforms Algorithm 1-(a) with $\mathrm{P_F} = 0.5$. Moreover, it is noted from Fig. 2.4 that the performance of Algorithm 1-(b) is not affected significantly by the false alarm probability $\mathrm{P_F}$ (equivalently, the thresholds). This is because, in Algorithm 1-(b), the probability that an LED transmitter is malicious, γ, is updated based on the observations (see (2.20)). Thus, Algorithm 1-(b) is robust to changes in the threshold values τ_i as opposed to Algorithm 1-(a), which is a practical advantage.

For performance evaluation of the algorithms in Section 2.3.2 (Scenario 2), 10^4 different sets of honest and malicious LED realizations are employed with a γ value of 0.5. As opposed to Scenario 1, in this scenario, the transmit powers of malicious LEDs are different at each measurement both in the training and estimation phases. Again, N_{V} is chosen as one by considering the same training point as in the previous case. The training is performed according to the decision rule in (2.24). To determine the κ_i values, the same approach as in Scenario 1 is taken by setting $\mathrm{P_F} = 0.001$ and $\mathrm{P_F} = 0.5$. Then, based on the κ_i values, the conditional probabilities $\mathrm{P}(\widehat{D}_i \,|\, \mathcal{M}_i)$ and $\mathrm{P}(\widehat{D}_i \,|\, \mathcal{H}_i)$ are calculated using 10^5 Monte-Carlo trials and employed in Algorithm 2-(b). The results in Fig. 2.5 reveal that for $\mathrm{P_F} = 0.001$, the performance of Algorithm 2-(a) is the same as "ML – Unaware" up to 100 dB and then converges to "ML – Perfect" at low noise variances. However, for $\mathrm{P_F} = 0.5$, Algorithm 2-(a) performs closely to "ML – Perfect" at high noise variances but achieves a significantly inferior performance at low noise variances. In addition, it is observed that the performance of Algorithm 2-(b) is not affected significantly by the false alarm rate $\mathrm{P_F}$ as in Scenario 1. Thus, Algorithm 2-(b) is robust to changes in κ_i values. Based on Fig. 2.4 and Fig. 2.5, it can be noted that if the false alarm probability can be adapted according to the noise variance, the performance of Algorithms 1-(a) and Algorithm 2-(a) can be enhanced. Namely, lower (higher) false alarm rates can be chosen for lower (higher) noise variances.

To observe the effects of the VLC receiver position on the accuracy, the VLC receiver is placed $(0, 0, 0.85)$ meters and moved along the straight line towards the location $(1, 1, 0.85)$ meters, where γ is set to 0.5. The simulations are conducted

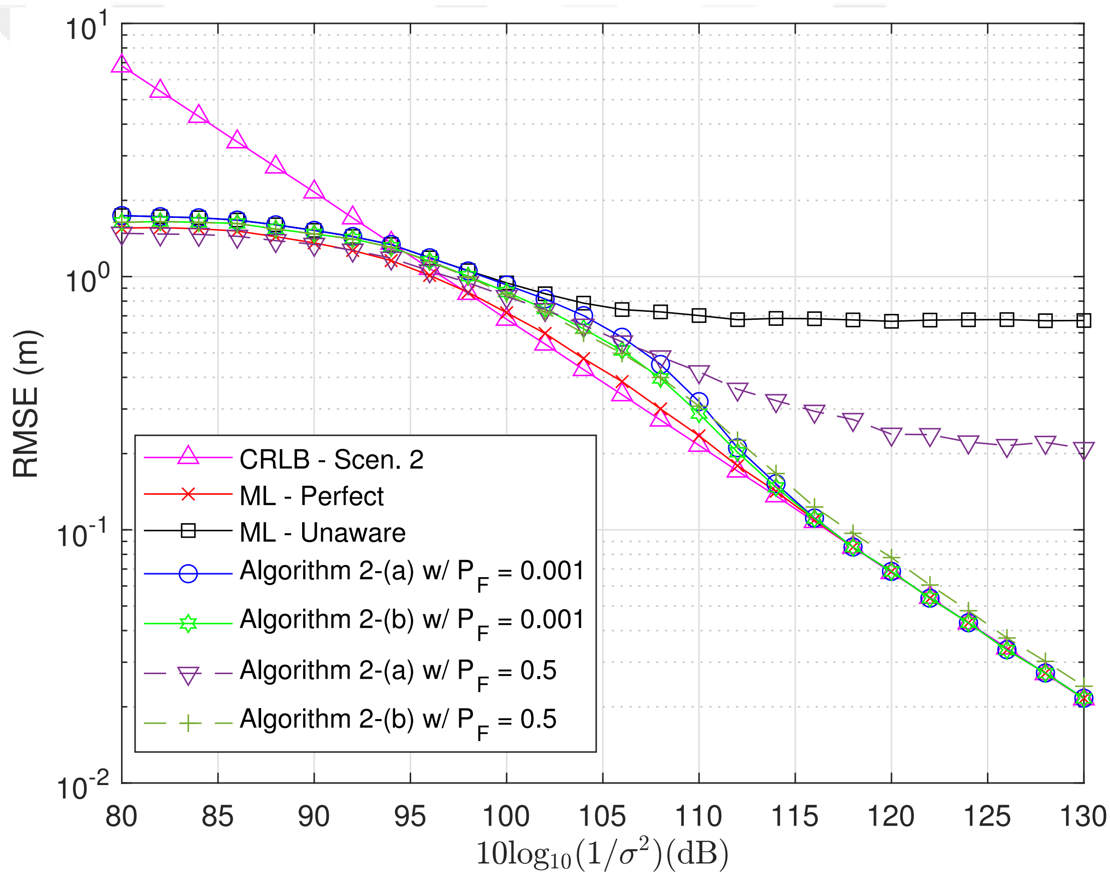

Figure 2.5: RMSE versus $10\log_{10}(1/\sigma^2)$ for Scenario 2 ($\gamma = 0.5$).

for two different values of the noise variance, namely, $\sigma^2 = 10^{-11}$ and $\sigma^2 = 10^{-12}$. In Fig. 2.6-(a), Algorithm 1-(a) achieves lower RMSEs with $\mathrm{P_F} = 0.5$ than with $\mathrm{P_F} = 0.001$. Conversely, in Fig. 2.6-(b), Algorithm 1-(a) with $\mathrm{P_F} = 0.001$ outperforms that with $\mathrm{P_F} = 0.5$. On the other hand, the RMSE performances of Algorithm 1-(b) are very similar at both false alarm probabilities due to its probability update operation, as discussed previously. In addition, it is observed that the RMSEs of the estimators get larger as the VLC receiver moves away from the center. This simulation is repeated for Scenario 2 and the results are presented in Fig. 2.7. In Fig. 2.7-(a), Algorithm 2-(a) with $\mathrm{P_F} = 0.5$ performs better than Algorithm 2-(a) with $\mathrm{P_F} = 0.001$. On the contrary, in Fig. 2.7-(b), Algorithm 2-(a) with $\mathrm{P_F} = 0.5$ performs poorly as the VLC receiver moves away from the center, whereas Algorithm 2-(a) with $\mathrm{P_F} = 0.001$ performs closely to the CRLB. Again, Algorithm 1-(b) achieves very similar RMSEs for both false alarm probabilities and the RMSE values of the estimators and the CRLB tend to increase as the VLC receiver moves away from the center of the room. These results illustrate the robustness of Algorithm 1-(b) and Algorithm 2-(b) against the threshold values used in the detection step. In addition, Algorithm 1-(a) and Algorithm 2-(a) are observed to be sensitive to the threshold values, and it is concluded that lower false alarm probabilities should be used for setting their thresholds as the noise level decreases; i.e., the SNR increases.

Moreover, the UMP test proposed in Section 2.3.3 for Scenario 1 can be investigated as the $P_{\mathrm{M},i}$ values are lower than or equal to $P_{\mathrm{H},i}$, $\forall i$ for the considered setting (namely, $P_{\mathrm{M},i} \in [1\,W, 3\,W]$ and $P_{\mathrm{H},i} = 5\,\mathrm{W}$); hence, the condition in (2.28) is satisfied. The false alarm probability is set to 0.5 in the simulations to highlight the advantage of employing the UMP test. It can be seen from Fig. 2.8 that the UMP test specified by (2.31) and (2.35) achieves higher detection probabilities than the GLRT in (2.15) for the large values of the noise variances while keeping the false alarm probability the same. Thus, the UMP test can lead to improved RMSE performance at high noise levels. In Fig. 2.9, it is observed that Algorithm 1-(a) that utilizes the UMP test, labeled as "Algorithm 1-(a), UMP", outperforms Algorithm 1-(a), which employs the GLRT test. Hence, enhanced localization accuracy can be achieved via the UMP test when the condition in

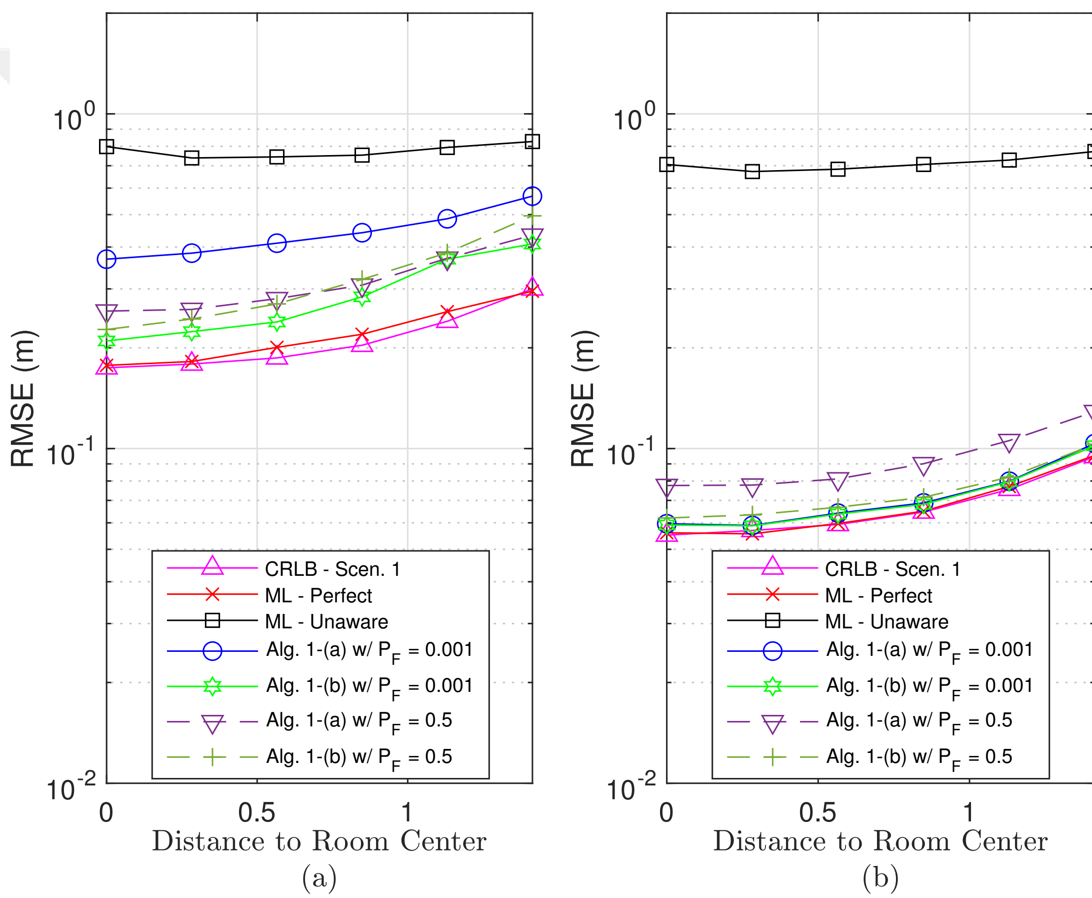

Figure 2.6: For Scenario 1, RMSE versus distance of VLC receiver from location $(0, 0, 0.85)$ m, where $\gamma = 0.5$ and VLC receiver moves on the straight line towards $(1, 1, 0.85)$ m. (a) $\sigma^2 = 10^{-11}$, (b) $\sigma^2 = 10^{-12}$.

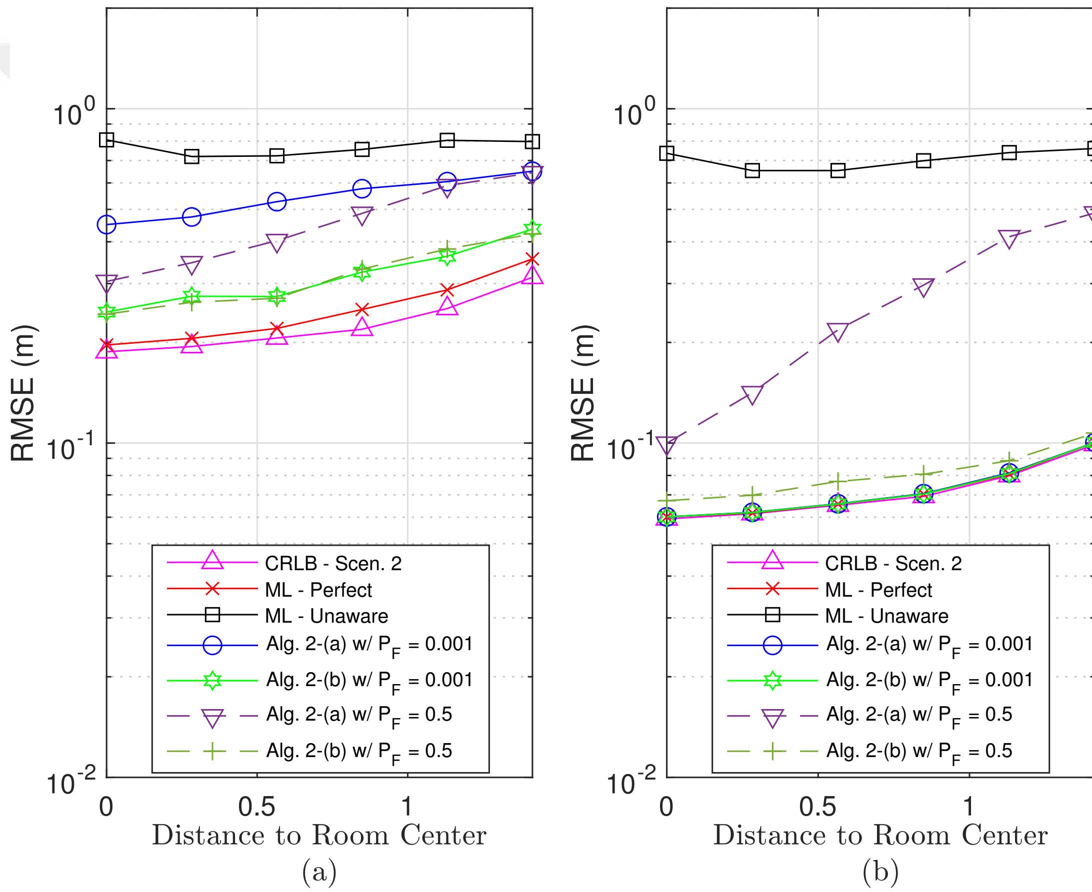

Figure 2.7: For Scenario 2, RMSE versus distance of VLC receiver from location $(0, 0, 0.85)$ m, where $\gamma = 0.5$ and VLC receiver moves on the straight line towards $(1, 1, 0.85)$ m. (a) $\sigma^2 = 10^{-11}$, (b) $\sigma^2 = 10^{-12}$.

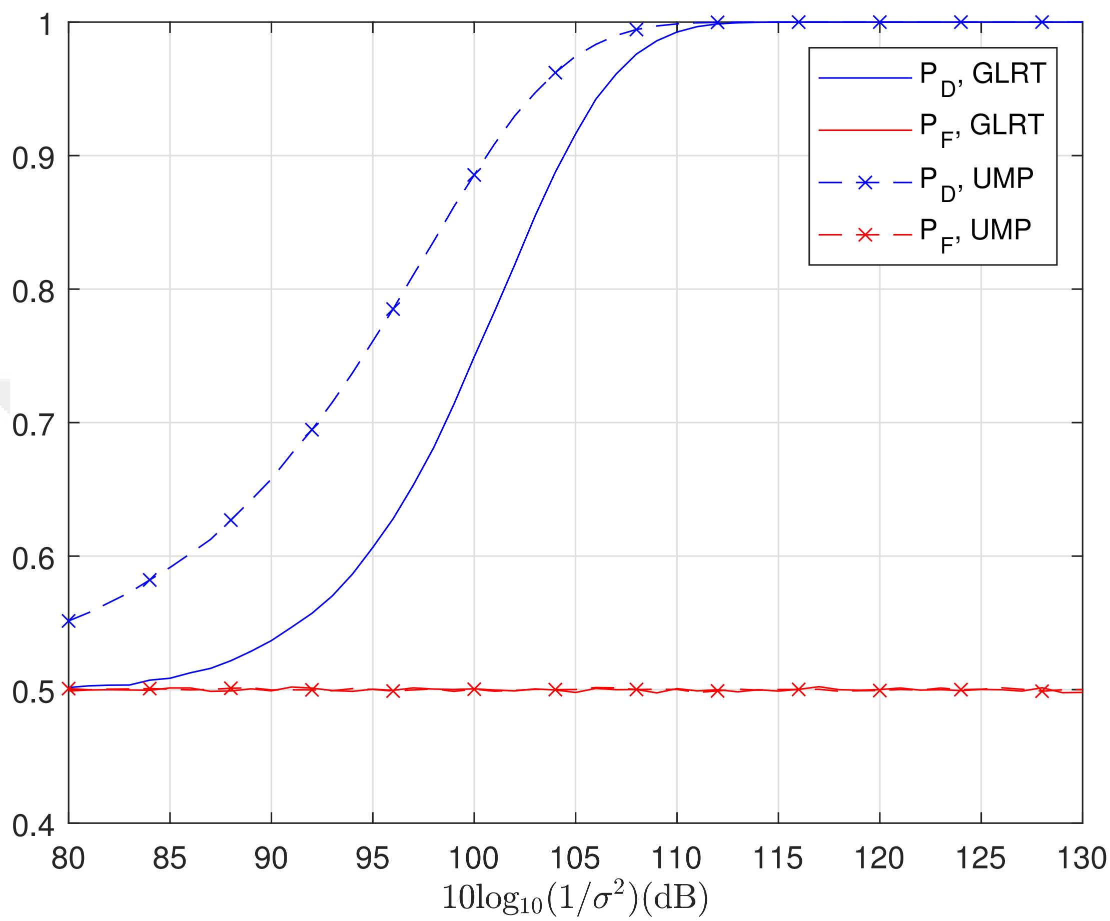

Figure 2.8: Detection and false alarm probabilities of the GLRT and UMP tests versus $10\log_{10}(1/\sigma^2)$ for $P_F = 0.5$.

(2.28) is satisfied. However, Algorithm 1-(b) with the UMP test, labeled as "Algorithm 1-(b), UMP", does not provide significant performance improvements since Algorithm 1-(b) is robust to the changes in the τ_i values.

Furthermore, to investigate the effect of number of training locations, i.e. N_v, used in algorithms in Sec. 2.3 on the positioning accuracy, a simulation is conducted. Noise variance is taken as $\sigma^2 = 10^{-10.5}$ (corresponding to $10\log_{10}(1/\sigma^2) = 105$dB) to highlight the effect of increasing the number of training locations. N_v values are taken from 1 to 16 while keeping the rest of the parameters same. For the choice of training locations, we have used a uniform grid array across the room for each N_v. [2] It can be observed from Fig. 2.10

[2]Obtaining the optimum arrangement of training locations can be considered as an important theoretical problem, which is out of scope of this work.

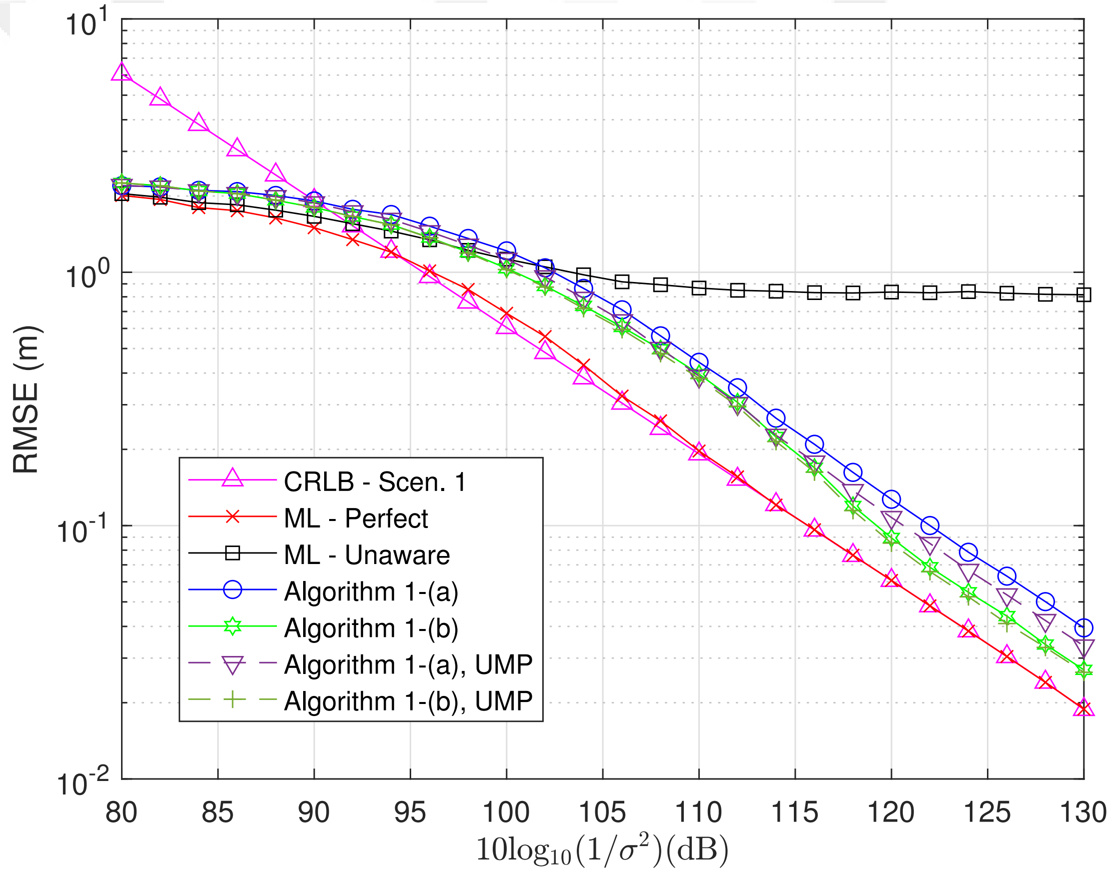

Figure 2.9: RMSE versus $10\log_{10}(1/\sigma^2)$ for Scenario 1 ($\gamma = 0.5$).

that the positioning performance of Algorithm 1-(a) with a false alarm rate of 0.001 converges to the performance of the ML estimator that perfectly knows the transmit powers of the malicious LEDs labeled as "ML – Perfect" as N_v increases. Likewise, the performance of Algorithm 1-(a) with a false alarm rate of 0.5 also enhances as N_v increases, but it is outperformed by Algorithm 1-(a) with 0.001 false alarm rate for the higher values of N_v whereas it performs better for the smaller values of N_v. The performance of Algorithm 1-(b) with a false alarm rate of 0.001 also enhances with increasing N_v but it is outperformed by Algorithm 1-(a) with both false alarm rates for the higher values of N_v. This is because when there are more measurements in the training phase the possible errors in the decisions are getting smaller. Finally, the performance increase for the Algorithm 1-(b) with 0.5 false alarm rate is very limited as N_v increases. It can be argued from Fig. 2.10 that after the value of $N_v = 8$ the performances of all the algorithms do not further enhance. A similar simulation is conducted for Scenario 2 in Sec. 2.3.2 with the same parameters. It can be seen from Fig. 2.11 that the performance of Algorith 2-(a) with a false alarm rate of 0.001 gets closer to the performance of the ML estimator that knows the malicious and honest set of LEDS, $\mathcal{M}$ and $\mathcal{H}$ respectively, labeled as "ML – Perfect" as N_v increases. Algorithm 2-(b) with 0.001 false alarm rate performs better than Algorithm 2-(a) with same false alarm rate for the smaller values of N_v but it performs poorly for the larger values of N_v. This is again because the uncertainty decreases as there are more training measurements. It can be observed that for the false alarm rate 0.5 the performance enhancement is very limited as N_v increases for both Algorithm 2-(a) and Algorithm 2-(b). Similar to Scenario 1 the performances of all the algorithms do not further greatly enhance after the value of $N_v = 12$ also in Scenario 2.

2.6 Extension to the Case of Unknown γ_i's

In this section, we consider the case in which the probabilities of the LED transmitters being malicious, i.e., $\gamma_1, \ldots, \gamma_{N_\mathrm{L}}$, are unknown. Let z_i denote whether

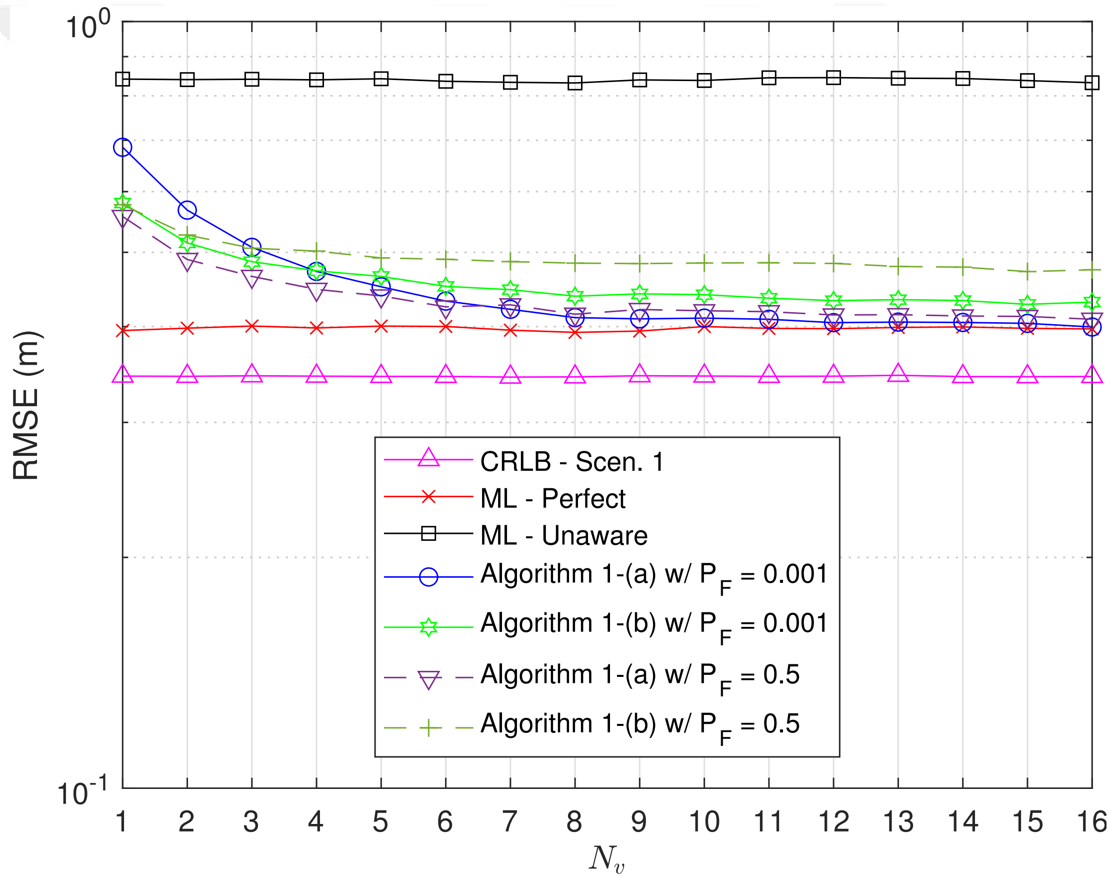

Figure 2.10: RMSE versus N_v for $10\log_{10}(1/\sigma^2) = 105$dB in Scenario 1.

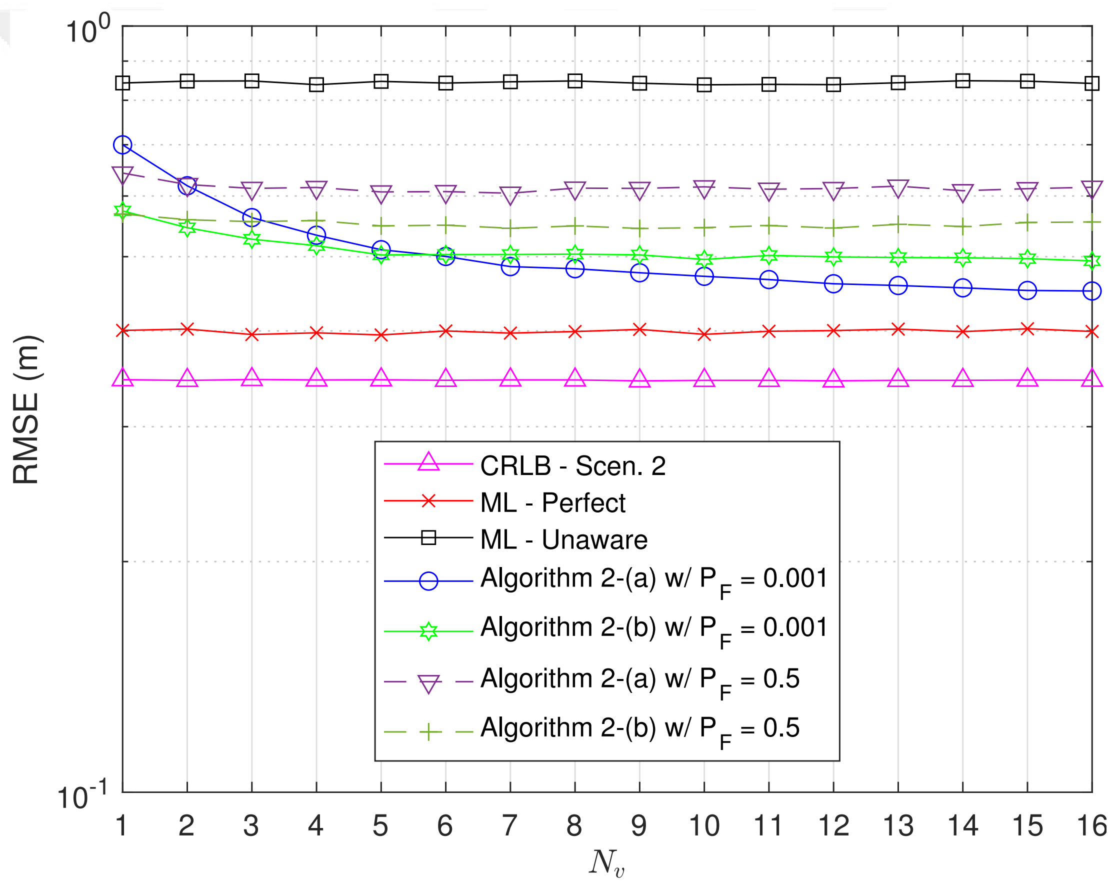

Figure 2.11: RMSE versus N_v for $10\log_{10}(1/\sigma^2) = 105$dB in Scenario 2.

the ith LED transmitter is malicious or not; that is,

$$z_i = \begin{cases} 0\,, & \text{if } i\text{th LED is honest} \\ 1\,, & \text{if } i\text{th LED is malicious} \end{cases} \tag{2.66}$$

which is a Bernoulli random variable with parameter γ_i. Then, using the definition in (2.2), $P_{\mathrm{T},i}$ can be expressed as

$$P_{\mathrm{T},i} = (1 - z_i)P_{\mathrm{H},i} + z_i P_{\mathrm{M},i} \tag{2.67}$$

In this case, the unknown parameters are $\boldsymbol{l}_{\mathrm{R}}$, $\boldsymbol{P}_{\mathrm{M}}$, and $\boldsymbol{z}$, where $\boldsymbol{z}$ denotes the vector of z_i values for $i = 1, \ldots, N_{\mathrm{L}}$. Thus, the likelihood function of $\boldsymbol{P}_{\mathrm{R}}$ given these parameters can be stated as

$$\begin{aligned} p(\boldsymbol{P}_{\mathrm{R}}|\boldsymbol{l}_{\mathrm{R}}, \boldsymbol{P}_{\mathrm{M}}, \boldsymbol{z}) = &\prod_{i\in H_{\boldsymbol{z}}} \frac{1}{\sqrt{2\pi}\sigma_i} \exp\left\{-\frac{(P_{\mathrm{R},i} - P_{\mathrm{H},i}R_p h_i(\boldsymbol{l}_{\mathrm{R}}))^2}{2\sigma_i^2}\right\} \\ &\times \prod_{i\in M_{\boldsymbol{z}}} \frac{1}{\sqrt{2\pi}\sigma_i} \exp\left\{-\frac{(P_{\mathrm{R},i} - P_{\mathrm{M},i}R_p h_i(\boldsymbol{l}_{\mathrm{R}}))^2}{2\sigma_i^2}\right\} \end{aligned} \tag{2.68}$$

where sets $H_{\boldsymbol{z}}$ and $M_{\boldsymbol{z}}$ are defined as

$$H_{\boldsymbol{z}} = \{i \in \{1, \ldots, N_{\mathrm{L}}\} \,|\, z_i = 0\} \tag{2.69}$$

$$M_{\boldsymbol{z}} = \{i \in \{1, \ldots, N_{\mathrm{L}}\} \,|\, z_i = 1\} \tag{2.70}$$

Then, for the estimation without a training phase (as in Section 2.2) in the case of unknown γ_i's, the following ML estimator is derived:

$$(\widehat{\boldsymbol{l}}_{\mathrm{R}}, \widehat{\boldsymbol{P}}_{\mathrm{M}}, \widehat{\boldsymbol{z}}) = \underset{\boldsymbol{l}_{\mathrm{R}},\boldsymbol{P}_{\mathrm{M}},\boldsymbol{z}}{\arg\max}\, p(\boldsymbol{P}_{\mathrm{R}}|\boldsymbol{l}_{\mathrm{R}}, \boldsymbol{P}_{\mathrm{M}}, \boldsymbol{z}) \tag{2.71}$$

$$= \underset{\boldsymbol{l}_{\mathrm{R}},\boldsymbol{z}}{\arg\min} \sum_{i\in H_{\boldsymbol{z}}} \frac{(P_{\mathrm{R},i} - P_{\mathrm{H},i}R_p h_i(\boldsymbol{l}_{\mathrm{R}}))^2}{\sigma_i^2} + \sum_{i\in M_{\boldsymbol{z}}} \frac{(P_{\mathrm{R},i} - \widehat{P}_{\mathrm{M},i}(\boldsymbol{l}_{\mathrm{R}})R_p h_i(\boldsymbol{l}_{\mathrm{R}}))^2}{\sigma_i^2} \tag{2.72}$$

where $\widehat{P}_{\mathrm{M},i}(\boldsymbol{l}_{\mathrm{R}})$ for any $\boldsymbol{z}$ is given by

$$\widehat{P}_{\mathrm{M},i}(\boldsymbol{l}_{\mathrm{R}}) = \begin{cases} P_{\min,i}, & \text{if } \frac{P_{\mathrm{R},i}}{R_p h_i(\boldsymbol{l}_{\mathrm{R}})} \leq P_{\min,i} \\ P_{\max,i}, & \text{if } \frac{P_{\mathrm{R},i}}{R_p h_i(\boldsymbol{l}_{\mathrm{R}})} \geq P_{\max,i} \\ \frac{P_{\mathrm{R},i}}{R_p h_i(\boldsymbol{l}_{\mathrm{R}})}, & \text{otherwise} \end{cases} \tag{2.73}$$

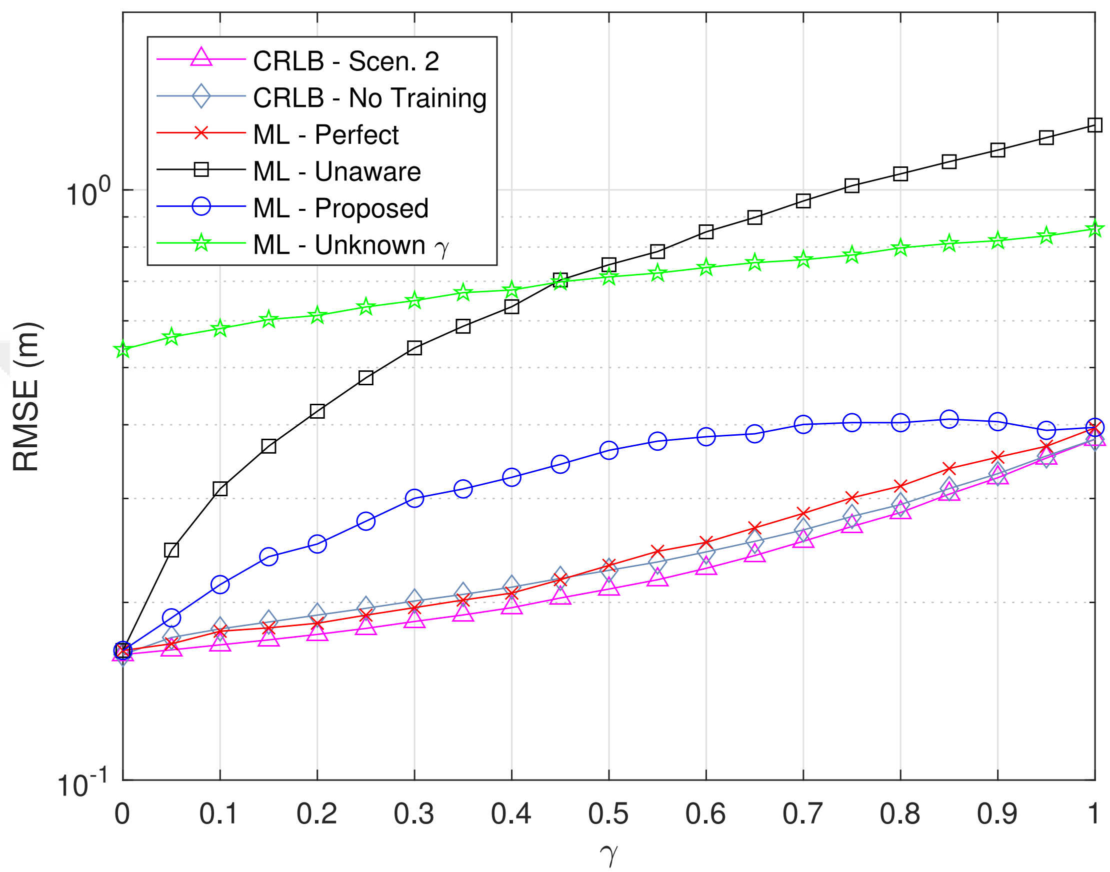

Figure 2.12: RMSE versus γ for $\sigma^2 = 10^{-11}$.

It should be noted that there are 2^{N_L} possible values of $z_1, \ldots, z_{N_{\mathrm{L}}}$. Hence, the ML estimator in (2.72) has high computational complexity for large values of N_{L}.

To evaluate the performance of the proposed ML estimator for the case of unknown γ_i's, simulations are conducted for the setting in Section 2.5 considering no training measurements. The results in Fig. 2.12 illustrate that without the knowledge of γ, the positioning accuracy can degrade significantly for all values of γ compared to the proposed ML estimator in (2.6) for the case of known γ.

2.7 Extension to Cases with All or None of LEDs being Malicious

In this part, we extend the results in Sections 2.2 and 2.3 to cover a different case. Namely, it is assumed that when a hijacking event occurs, the malicious third party accesses the VLP controller and makes all the LED transmitters malicious (i.e., modifies all the power levels). Let the probability of such a hijacking event be denoted by γ. Then, the probability distribution of the received powers from the LED transmitters in (2.1) for given values of the unknown position and malicious power levels can be expressed as follows (cf. (2.5)):

$$p(\boldsymbol{P}_{\mathrm{R}}\,|\,\boldsymbol{l}_{\mathrm{R}},\boldsymbol{P}_{\mathrm{M}}) = \gamma\prod_{i=1}^{N_{\mathrm{L}}}\frac{1}{\sqrt{2\pi}\sigma_i}e^{-\frac{(P_{\mathrm{R},i}-P_{\mathrm{M},i}R_p h_i(\boldsymbol{l}_{\mathrm{R}}))^2}{2\sigma_i^2}} + (1-\gamma)\prod_{i=1}^{N_{\mathrm{L}}}\frac{1}{\sqrt{2\pi}\sigma_i}e^{-\frac{(P_{\mathrm{R},i}-P_{\mathrm{H},i}R_p h_i(\boldsymbol{l}_{\mathrm{R}}))^2}{2\sigma_i^2}} \tag{2.74}$$

Then, the ML estimator for the location of the VLC receiver becomes

$$\widehat{\boldsymbol{l}}_{\mathrm{R}} = \arg\max_{\boldsymbol{l}_{\mathrm{R}}\in\mathcal{L}}\ \gamma\prod_{i=1}^{N_{\mathrm{L}}}\frac{1}{\sqrt{2\pi}\sigma_i}e^{-\frac{(P_{\mathrm{R},i}-\widehat{P}_{\mathrm{M},i}(\boldsymbol{l}_{\mathrm{R}})R_p h_i(\boldsymbol{l}_{\mathrm{R}}))^2}{2\sigma_i^2}} + (1-\gamma)\prod_{i=1}^{N_{\mathrm{L}}}\frac{1}{\sqrt{2\pi}\sigma_i}e^{-\frac{(P_{\mathrm{R},i}-P_{\mathrm{H},i}R_p h_i(\boldsymbol{l}_{\mathrm{R}}))^2}{2\sigma_i^2}}$$

where $\widehat{P}_{\mathrm{M},i}(\boldsymbol{l}_{\mathrm{R}})$ is as in (2.7). In addition, if there exist training measurements, then a single hypothesis-testing problem can be formulated for Scenario 2 (instead of the N_{L} separate problems in (2.22)) as follows:

$$\begin{aligned}\mathcal{H}\ &:\ P_{\mathrm{R},i}^{(j)} = R_p\,P_{\mathrm{H},i}\,h_i\big(\boldsymbol{l}_{\mathrm{R}}^{(j)}\big) + \eta_i^{(j)},\ \ j=1,\ldots,N_{\mathrm{V}},\quad i=1,\ldots N_{\mathrm{L}}\\ \mathcal{M}\ &:\ P_{\mathrm{R},i}^{(j)} = R_p\,P_{\mathrm{M},i}^{(j)}\,h_i\big(\boldsymbol{l}_{\mathrm{R}}^{(j)}\big) + \eta_i^{(j)},\ \ j=1,\ldots,N_{\mathrm{V}},\quad i=1,\ldots N_{\mathrm{L}}\end{aligned} \tag{2.75}$$

where $P_{\mathrm{M},i}^{(j)}$ becomes $P_{\mathrm{M},i}$ in Scenario 1 (cf., the N_{L} separate problems in (2.11)). Then, the GLRT can be formulated as

$$\frac{\max\limits_{\{P_{\mathrm{M},i}^{(j)}\}}\prod_{i=1}^{N_{\mathrm{L}}}\prod_{j=1}^{N_{\mathrm{V}}}\frac{1}{\sqrt{2\pi}\sigma_{i,j}}e^{-\frac{\left(P_{\mathrm{R},i}^{(j)}-R_p P_{\mathrm{M},i}^{(j)}h_i\left(\boldsymbol{l}_{\mathrm{R}}^{(j)}\right)\right)^2}{2\sigma_{i,j}^2}}}{\prod_{i=1}^{N_{\mathrm{L}}}\prod_{j=1}^{N_{\mathrm{V}}}\frac{1}{\sqrt{2\pi}\sigma_{i,j}}e^{-\frac{\left(P_{\mathrm{R},i}^{(j)}-R_p P_{\mathrm{H},i}h_i\left(\boldsymbol{l}_{\mathrm{R}}^{(j)}\right)\right)^2}{2\sigma_{i,j}^2}}} \underset{\mathcal{H}}{\overset{\mathcal{M}}{\gtrless}} \kappa \tag{2.76}$$

which can be simplified into the following rule for Scenario 2 (cf. (2.24)):

$$\sum_{i=1}^{N_{\mathrm{L}}}\sum_{j=1}^{N_{\mathrm{V}}}\frac{1}{\sigma_{i,j}^2}\left(R_p P_{\mathrm{R},i}^{(j)} h_i\big(\boldsymbol{l}_{\mathrm{R}}^{(j)}\big)\big(\widehat{P}_{\mathrm{M},i}^{(j)} - P_{\mathrm{H},i}\big) + 0.5R_p^2\big(h_i\big(\boldsymbol{l}_{\mathrm{R}}^{(j)}\big)\big)^2\Big(P_{\mathrm{H},i}^2 - \big(\widehat{P}_{\mathrm{M},i}^{(j)}\big)^2\Big)\right) \underset{\mathcal{H}}{\overset{\mathcal{M}}{\gtrless}} \log(\kappa)$$

where $\widehat{P}_{\mathrm{M},i}^{(j)}$ is as in (2.25) and κ is the threshold parameter. Also, in Scenario 1, $P_{\mathrm{M},i}^{(j)}$ is set to $P_{\mathrm{M},i}$, and (2.76) is simplified as (cf. (2.15))

$$\sum_{i=1}^{N_{\mathrm{L}}}\left(R_p\big(\widehat{P}_{\mathrm{M},i} - P_{\mathrm{H},i}\big)\sum_{j=1}^{N_{\mathrm{V}}}\frac{P_{\mathrm{R},i}^{(j)} h_i\big(\boldsymbol{l}_{\mathrm{R}}^{(j)}\big)}{\sigma_{i,j}^2} + 0.5R_p^2\Big(P_{\mathrm{H},i}^2 - \big(\widehat{P}_{\mathrm{M},i}\big)^2\Big)\sum_{j=1}^{N_{\mathrm{V}}}\frac{\big(h_i\big(\boldsymbol{l}_{\mathrm{R}}^{(j)}\big)\big)^2}{\sigma_{i,j}^2}\right) \underset{\mathcal{H}}{\overset{\mathcal{M}}{\gtrless}} \log(\kappa)$$

where $\widehat{P}_{\mathrm{M},i}$ is as in (2.13) and (2.14).

In this case, when the decision is hypothesis $\mathcal{M}$, no localization is performed since all the power levels are classified as incorrect (manipulated). This can be regarded as an *outage* event. When the decision is $\mathcal{H}$, localization is performed based on (2.1) with $P_{\mathrm{T},i} = P_{\mathrm{H},i}$ for all $i \in \{1, \ldots, N_{\mathrm{L}}\}$, which leads to the "ML – Unaware" estimator in Section 2.5. Hence, the main ideas in Sections 2.2 and 2.3 can also be employed for the case in which a malicious third party aims to modify the power levels of all the LED transmitters.

2.8 Concluding Remarks

In this chapter, position estimation problems have been formulated for VLP systems in the presence of malicious LED transmitters for the first time in the literature. An ML estimator has been derived based on the knowledge of probabilities that LED transmitters can be malicious. In addition, in the presence of training measurements, GLRTs have been employed for detection of malicious LED transmitters, and based on the decisions of the GLRTs, various ML based location estimators have been developed. Moreover, CRLB expressions have been derived and used as benchmarks to evaluate the performance of the proposed estimators. Finally, an ML estimator has been proposed for the case that the probabilities of the LED transmitters being malicious are unknown.

As possible directions for future work, uncertainties in the knowledge of the probabilities that the LED transmitters are malicious (i.e., γ_i's) can be considered. Also, more general channel models that take into account reflected and/or diffused components (in addition to the line-of-sight component) can be employed. In addition, information theoretic learning criteria such as MEE and MCC can be used for VLP systems in the presence of malicious LED transmitters to develop new approaches. Furthermore, possible ways of dealing with the presence of malicious LED transmitters, such as power allocation, can be developed. Finally, the shot noise component [65], which can be important when the received power levels are high, can be considered to generalize the analyses.

Chapter 3

Visible Light Positioning in the Presence of Intelligent Reflecting Surfaces

This chapter is organized as follows. The system model is described in detail, and the CRLB expression and the ML estimator are derived in Section 3.1. In Section 3.2, the adjustment of IRS orientations is investigated analytically and solutions are derived to maximize the received power at the VLC receiver. Various simulations are conducted to inspect the performance of the proposed algorithms and to observe the effects of critical parameters in Section 3.3. Finally, concluding remarks are presented in Section 3.5.

3.1 VLP with Intelligent Reflecting Surfaces

We consider a VLP system with N_{L} LED transmitters at known locations denoted by $\boldsymbol{l}_1, \ldots, \boldsymbol{l}_{N_{\mathrm{L}}}$ and a VLC receiver at an unknown location represented by $\boldsymbol{x}$. The orientation vectors of the ith LED transmitter and the VLC receiver are assumed to be known and denoted by $\boldsymbol{n}_i$ and $\bar{\boldsymbol{n}}$, respectively, where $i \in \{1, \ldots, N_{\mathrm{L}}\}$.[1] In addition to the VLC receiver and the LED transmitters, there exist intelligent reflecting surfaces in the environment. In particular, there are N_{R} flat surfaces represented by $S_1, \ldots, S_{N_{\mathrm{R}}}$, which are at known locations $\tilde{\boldsymbol{l}}_1, \ldots, \tilde{\boldsymbol{l}}_{N_{\mathrm{R}}}$ and have known orientation vectors $\tilde{\boldsymbol{n}}_1, \ldots, \tilde{\boldsymbol{n}}_{N_{\mathrm{R}}}$. It is assumed that each flat surface causes glossy reflections [67] and the surface reflectance coefficient is the same over each given surface; that is, ρ_k is used to represent the reflectance coefficient for the kth reflecting surface with $k \in \{1, \ldots, N_{\mathrm{R}}\}$. Since the reflective surfaces are considered as a part of the system design, ρ_k and S_k (i.e., the surface equation) are assumed to be known for all $k \in \{1, \ldots, N_{\mathrm{R}}\}$. In this setup, the location $\tilde{\boldsymbol{l}}_k$ of the kth reflecting surface can correspond to any point on the surface (e.g., the center) as the surface equation is already known. The considered system model is illustrated in Fig. 3.1. (Please also see Fig. 3.2 for an example.)[2]

The aim is to estimate the unknown location $\boldsymbol{x}$ of the VLC receiver based on power measurements at the VLC receiver due to the signals emitted by the LED transmitters. Considering a time division multiplexing approach, the VLC receiver can process signals coming from the LED transmitters separately [53,54]. In this scenario, the received power measurement at the VLC receiver due to the signal from the ith LED transmitter can be modeled as follows [68]:[3]

$$P_{\mathrm{RX},i} = P_{\mathrm{TX},i}\, H_i^{\mathrm{LOS}}(\boldsymbol{x}) + P_{\mathrm{TX},i} \sum_{k=1}^{N_{\mathrm{R}}} \int_{S_k} dH_{i,k}^{\mathrm{ref}}\big(\boldsymbol{x}\big) + \eta_i \tag{3.1}$$

for $i = 1, \ldots, N_{\mathrm{L}}$, where $P_{\mathrm{TX},i}$ is the transmit power of the ith LED transmitter, $H_i^{\mathrm{LOS}}(\boldsymbol{x})$ is the channel gain of the LOS path between the ith LED transmitter and the VLC receiver, $dH_{i,k}^{\mathrm{ref}}\big(\boldsymbol{x}\big)$ is the channel gain of the path between the ith LED transmitter and the VLC receiver which makes a single reflection from

[1] For example, $\bar{\boldsymbol{n}}$ can be measured via a gyroscope at the VLC receiver [66].

[2] To keep the configuration of reflecting surfaces in the most generic form, we refer to each surface element as an IRS, which can have arbitrary location and orientation. In practice, a group of surface elements (i.e., "IRSs") are placed together to form a large reflecting surface, as shown in Fig. 3.2.

[3] In practice, the incoming optical signal is converted to an electrical signal by the photo-detector at the VLC receiver, and then the integral of the electrical signal is taken to obtain a measurement that is proportional to the received optical power. Assuming that the responsivity of the photo-detector is known, the received power model in (3.1) can be obtained via scaling.

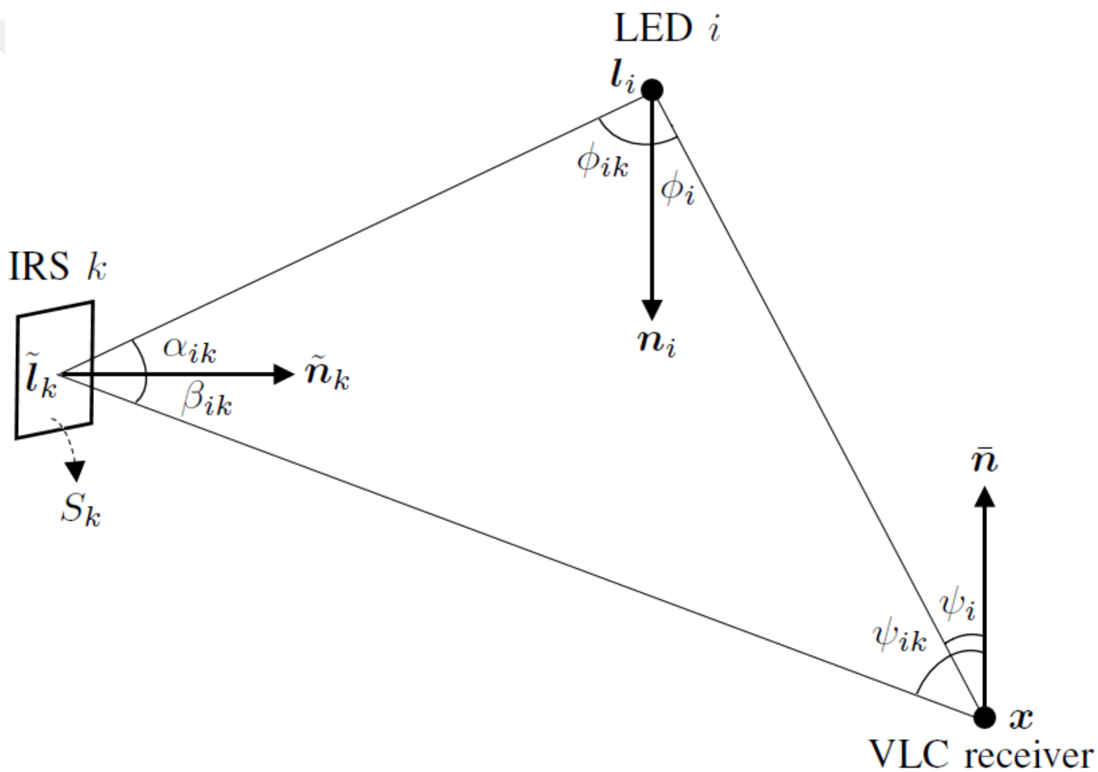

Figure 3.1: A system with N_{L} LED transmitters, N_{R} intelligent reflecting surfaces (IRSs), and a VLC receiver is considered. In the figure, only the ith LED transmitter and the kth IRS are shown. The orientation vectors are denoted by $\bar{\boldsymbol{n}}$, $\boldsymbol{n}_i$, and $\tilde{\boldsymbol{n}}_k$, and the locations are represented by $\boldsymbol{x}$, $\boldsymbol{l}_i$, and $\tilde{\boldsymbol{l}}_k$, all of which are *generic* three dimensional vectors. Also, the irradiance and incidence angles are named as in the figure.

an infinitesimally small area around $\tilde{\boldsymbol{l}}_k$ at the kth reflecting surface (please see Fig. 3.1), and η_i is a zero-mean Gaussian noise component with a variance of σ_i^2, which is independent of η_j for all $j \neq i$ [69].

As in [36], the field-of-view (FOV) of the photo-detector at the VLC receiver is assumed to 90^o by considering the use of a hemispherical lens at the VLC receiver [57]. Then, the channel gains in (3.1) can be calculated as [67][4]

$$H_i^{\mathrm{LOS}}(\boldsymbol{x}) = \frac{(m_i+1)A\,(\cos\phi_i)^{m_i}\,T_s(\psi_i)g(\psi_i)\cos\psi_i}{2\pi\|\boldsymbol{x}-\boldsymbol{l}_i\|^2} \tag{3.2}$$

and

$$\begin{aligned} dH_{i,k}^{\mathrm{ref}}(\boldsymbol{x}) = {} & (m_i+1)A(\cos\phi_{ik})^{m_i}\cos\alpha_{ik}R_k(\alpha_{ik},\beta_{ik}) \\ & \cdot \frac{\cos\psi_{ik}T_s(\psi_{ik})g(\psi_{ik})}{2\pi\|\boldsymbol{l}_i-\tilde{\boldsymbol{l}}_k\|^2\|\boldsymbol{x}-\tilde{\boldsymbol{l}}_k\|^2}\,dS_k \end{aligned} \tag{3.3}$$

with

$$R_k(\alpha_{ik},\beta_{ik}) = \frac{\rho_k}{2\pi}\Big(2r_k\cos\beta_{ik} + (1-r_k)(\mu_k+1)(\cos(\beta_{ik}-\alpha_{ik}))^{\mu_k}\Big) \tag{3.4}$$

where m_i is the Lambertian order for the ith LED transmitter, A is the area of the photo-detector at the VLC receiver, ϕ_i and ψ_i are, respectively, the irradiance angle and the incidence angle for the LOS path between the ith LED transmitter and the VLC receiver, ϕ_{ik} and α_{ik} are, respectively, the irradiance angle and the incidence angle for the direct path between the ith LED transmitter and the reflective point $\tilde{\boldsymbol{l}}_k$ at the kth reflecting surface, β_{ik} and ψ_{ik} are, respectively, the irradiance angle and the incidence angle for the direct path between the reflective point $\tilde{\boldsymbol{l}}_k$ at the kth reflecting surface and the VLC receiver, dS_k represents an infinitesimally small area around $\tilde{\boldsymbol{l}}_k$ at the kth reflecting surface, and $T_s(\psi)$ and $g(\psi)$ are, respectively, the optical filter gain and the optical concentrator gain at the VLC receiver [68]. Commonly, $T_s(\psi)g(\psi)$ is designed to be constant [68]; hence, we set it to one in the remainder of the manuscript to simplify the notation. In (3.4), the first term represents the diffuse component and the second one is related to the specular component, with $r_k \in [0,1]$ specifying the fraction of

[4]As a practical scenario, the VLC receiver is assumed to be at a lower height than the IRSs and the LEDs. In the absence of this assumption, the formulas could be updated by eliminating the signals that would not be in the FOV of the VLC receiver.

diffuse component and μ_k determining the directivity of reflection [67]. (In the special case of $r_k = 1$, only diffuse reflection is considered and the model reduces to that in [68].)

The angles in (3.2) and (3.3) can be specified based on the following geometric relations (cf. Fig. 3.1): $(\boldsymbol{x}-\boldsymbol{l}_i)^T\boldsymbol{n}_i = \|\boldsymbol{x}-\boldsymbol{l}_i\|\cos\phi_i$, $(\boldsymbol{l}_i-\boldsymbol{x})^T\bar{\boldsymbol{n}} = \|\boldsymbol{l}_i-\boldsymbol{x}\|\cos\psi_i$, $(\tilde{\boldsymbol{l}}_k-\boldsymbol{l}_i)^T\boldsymbol{n}_i = \|\tilde{\boldsymbol{l}}_k-\boldsymbol{l}_i\|\cos\phi_{ik}$, $(\tilde{\boldsymbol{l}}_k-\boldsymbol{x})^T\bar{\boldsymbol{n}} = \|\tilde{\boldsymbol{l}}_k-\boldsymbol{x}\|\cos\psi_{ik}$, $(\boldsymbol{l}_i-\tilde{\boldsymbol{l}}_k)^T\tilde{\boldsymbol{n}}_k = \|\boldsymbol{l}_i-\tilde{\boldsymbol{l}}_k\|\cos\alpha_{ik}$, and $(\boldsymbol{x}-\tilde{\boldsymbol{l}}_k)^T\tilde{\boldsymbol{n}}_k = \|\boldsymbol{x}-\tilde{\boldsymbol{l}}_k\|\cos\beta_{ik}$. Then, (3.2) and (3.3) can be expressed via (3.4) as follows:

$$H_i^{\mathrm{LOS}}(\boldsymbol{x}) = \frac{(m_i+1)A\left((\boldsymbol{x}-\boldsymbol{l}_i)^T\boldsymbol{n}_i\right)^{m_i}(\boldsymbol{l}_i-\boldsymbol{x})^T\bar{\boldsymbol{n}}}{2\pi\|\boldsymbol{x}-\boldsymbol{l}_i\|^{m_i+3}} \tag{3.5}$$

$$dH_{i,k}^{\mathrm{ref}}(\boldsymbol{x}) = \frac{(m_i+1)\left((\tilde{\boldsymbol{l}}_k-\boldsymbol{l}_i)^T\boldsymbol{n}_i\right)^{m_i}\left((\boldsymbol{l}_i-\tilde{\boldsymbol{l}}_k)^T\tilde{\boldsymbol{n}}_k\right)}{4\pi^2\|\boldsymbol{l}_i-\tilde{\boldsymbol{l}}_k\|^{m_i+3}\|\boldsymbol{x}-\tilde{\boldsymbol{l}}_k\|^3} A\,\rho_k\left((\tilde{\boldsymbol{l}}_k-\boldsymbol{x})^T\bar{\boldsymbol{n}}\right)dS_k$$
$$\cdot\left\{2r_k\frac{\left((\boldsymbol{x}-\tilde{\boldsymbol{l}}_k)^T\tilde{\boldsymbol{n}}_k\right)}{\|\boldsymbol{x}-\tilde{\boldsymbol{l}}_k\|} + (1-r_k)(\mu_k+1)(\cos(\beta_{ik}-\alpha_{ik}))^{\mu_k}\right\}. \tag{3.6}$$

In addition, $\cos(\beta_{ik}-\alpha_{ik})$ in (3.6) can be calculated as

$$\cos(\beta_{ik}-\alpha_{ik}) = \frac{\left((\boldsymbol{x}-\tilde{\boldsymbol{l}}_k)^T\tilde{\boldsymbol{n}}_k\right)\left((\boldsymbol{l}_i-\tilde{\boldsymbol{l}}_k)^T\tilde{\boldsymbol{n}}_k\right)}{\|\boldsymbol{x}-\tilde{\boldsymbol{l}}_k\|\|\boldsymbol{l}_i-\tilde{\boldsymbol{l}}_k\|} + \frac{\|(\boldsymbol{x}-\tilde{\boldsymbol{l}}_k)\times\tilde{\boldsymbol{n}}_k\|\|(\boldsymbol{l}_i-\tilde{\boldsymbol{l}}_k)\times\tilde{\boldsymbol{n}}_k\|}{\|\boldsymbol{x}-\tilde{\boldsymbol{l}}_k\|\|\boldsymbol{l}_i-\tilde{\boldsymbol{l}}_k\|} \tag{3.7}$$

where $\times$ denotes the cross product.

Remark 1: Only the direct paths among the LED transmitters, the IRSs, and the VLC receiver are considered in the preceding signal model. The main motivations behind omitting the other multipath components can be stated as follows: (i) In general, the received powers due to the direct paths are significantly higher than those due to the other multipath components. (Commonly, IRSs are made of highly reflecting materials for supporting visible light positioning [36]; hence, the direct paths from IRSs are expected to be stronger than the other multipath components, as well.) (ii) By omitting the multipath components, a tractable signal model is obtained, which facilitates theoretical analyses and intuitive explanations, leading to an understanding of the effects of intelligent reflecting surfaces for VLP systems, which have not been investigated previously for the setting considered in this thesis.

Remark 2: We employ a generic model for IRSs by considering the locations, areas, orientations, and reflectance coefficients of the surfaces as generic parameters. Similarly, LED transmitters and VLC receiver can have arbitrary locations and orientation vectors in the three-dimensional space.

Based on the received powers specified by (3.1), the log-likelihood function for the unknown location $\boldsymbol{x}$ of the VLC receiver can be expressed as

$$\log p(\boldsymbol{P}_{\mathrm{RX}} \,|\, \boldsymbol{x}) = \tilde{k} - \sum_{i=1}^{N_{\mathrm{L}}} \frac{1}{2\sigma_i^2} \left(P_{\mathrm{RX},i} - P_{\mathrm{TX},i}\, H_i^{\mathrm{LOS}}(\boldsymbol{x}) - P_{\mathrm{TX},i} \sum_{k=1}^{N_{\mathrm{R}}} \int_{S_k} dH_{i,k}^{\mathrm{ref}}(\boldsymbol{x}) \right)^2 \tag{3.8}$$

where $\tilde{k}$ is a constant independent of $\boldsymbol{x}$. Then, the ML estimator for the location of the VLC receiver can be obtained as follows:

$$\widehat{\boldsymbol{x}}_{\mathrm{ML}} = \arg\min_{\boldsymbol{x}} \sum_{i=1}^{N_{\mathrm{L}}} \frac{1}{\sigma_i^2} \left(P_{\mathrm{RX},i} - P_{\mathrm{TX},i}\, H_i^{\mathrm{LOS}}(\boldsymbol{x}) - P_{\mathrm{TX},i} \sum_{k=1}^{N_{\mathrm{R}}} \int_{S_k} dH_{i,k}^{\mathrm{ref}}(\boldsymbol{x}) \right)^2 \tag{3.9}$$

where H_i^{LOS} and $dH_{i,k}^{\mathrm{ref}}$ are evaluated based on the relations in (3.5)–(3.7).

To derive the CRLB, we first calculate the elements of the Fisher information matrix (FIM) [59], denoted by $\mathbf{I}(\boldsymbol{x})$, from (3.8), as follows:

$$[\mathbf{I}(\boldsymbol{x})]_{\ell_1,\ell_2} = \sum_{i=1}^{N_{\mathrm{L}}} \frac{(P_{\mathrm{TX},i})^2}{\sigma_i^2} \frac{\partial h_i(\boldsymbol{x})}{\partial x_{\ell_1}} \frac{\partial h_i(\boldsymbol{x})}{\partial x_{\ell_2}} \tag{3.10}$$

for $\ell_1, \ell_2 \in \{1, 2, 3\}$, where

$$h_i(\boldsymbol{x}) \triangleq H_i^{\mathrm{LOS}}(\boldsymbol{x}) + \sum_{k=1}^{N_{\mathrm{R}}} \int_{S_k} dH_{i,k}^{\mathrm{ref}}(\boldsymbol{x}). \tag{3.11}$$

The partial derivatives of $h_i(\boldsymbol{x})$ in (3.11) can be stated as

$$\frac{\partial h_i(\boldsymbol{x})}{\partial x_\ell} = \frac{\partial H_i^{\mathrm{LOS}}(\boldsymbol{x})}{\partial x_\ell} + \sum_{k=1}^{N_{\mathrm{R}}} \int_{S_k} \frac{\partial dH_{i,k}^{\mathrm{ref}}(\boldsymbol{x})}{\partial x_\ell} \tag{3.12}$$

for $i \in \{1, \dots, N_{\mathrm{L}}\}$ and $\ell \in \{1, 2, 3\}$. Via (3.12), we can observe the contributions of the LOS path and the reflected paths from the intelligent reflecting surfaces to the FIM in (3.10). Based on the expressions in (3.5)–(3.7), the partial derivatives in (3.12) can be calculated as

$$
\begin{aligned}
\frac{\partial H_i^{\text{LOS}}(\boldsymbol{x})}{\partial x_\ell} &= -\frac{(m_i+1)A}{2\pi\|\boldsymbol{x}-\boldsymbol{l}_i\|^{m_i+3}}\Bigg[\bar{n}_\ell\left((\boldsymbol{x}-\boldsymbol{l}_i)^T\boldsymbol{n}_i\right)^{m_i} \\
&- m_i n_{i,\ell}\left((\boldsymbol{x}-\boldsymbol{l}_i)^T\boldsymbol{n}_i\right)^{m_i-1}(\boldsymbol{l}_i-\boldsymbol{x})^T\bar{\boldsymbol{n}} \\
&+ \frac{(m_i+3)(x_\ell-l_{i,\ell})\left((\boldsymbol{x}-\boldsymbol{l}_i)^T\boldsymbol{n}_i\right)^{m_i}(\boldsymbol{l}_i-\boldsymbol{x})^T\bar{\boldsymbol{n}}}{\|\boldsymbol{x}-\boldsymbol{l}_i\|^2}\Bigg],
\end{aligned} \tag{3.13}
$$

$$
\begin{aligned}
\frac{\partial dH_{i,k}^{\text{ref}}(\boldsymbol{x})}{\partial x_\ell} &= \frac{(m_i+1)A\left((\tilde{\boldsymbol{l}}_k-\boldsymbol{l}_i)^T\boldsymbol{n}_i\right)^{m_i}(\boldsymbol{l}_i-\tilde{\boldsymbol{l}}_k)^T\tilde{\boldsymbol{n}}_k}{4\pi^2\|\boldsymbol{l}_i-\tilde{\boldsymbol{l}}_k\|^{m_i+3}} \\
&\cdot \rho_k dS_k\Bigg\{\Bigg[\left(\tilde{n}_{k,\ell}(\tilde{\boldsymbol{l}}_k-\boldsymbol{x})^T\bar{\boldsymbol{n}}-\bar{n}_\ell((\boldsymbol{x}-\tilde{\boldsymbol{l}}_k)^T\tilde{\boldsymbol{n}}_k\right)\|\boldsymbol{x}-\tilde{\boldsymbol{l}}_k\|^{-4} \\
&- 4\|\boldsymbol{x}-\tilde{\boldsymbol{l}}_k\|^{-6}(x_\ell-\tilde{l}_{k,\ell})(\boldsymbol{x}-\tilde{\boldsymbol{l}}_k)^T\tilde{\boldsymbol{n}}_k(\tilde{\boldsymbol{l}}_k-\boldsymbol{x})^T\bar{\boldsymbol{n}}\Bigg]2r_k \\
&+ (1-r_k)(\mu_k+1)\Bigg[(\cos(\beta_{ik}-\alpha_{ik}))^{\mu_k}\Big(-\bar{n}_\ell\|\boldsymbol{x}-\tilde{\boldsymbol{l}}_k\|^{-3} \\
&- 3(\tilde{\boldsymbol{l}}_k-\boldsymbol{x})^T\bar{\boldsymbol{n}}\|\boldsymbol{x}-\tilde{\boldsymbol{l}}_k\|^{-5}(x_\ell-\tilde{l}_{k,\ell})\Big) \\
&+ \mu_k(\cos(\beta_{ik}-\alpha_{ik}))^{\mu_k-1}\frac{(\tilde{\boldsymbol{l}}_k-\boldsymbol{x})^T\bar{\boldsymbol{n}}}{\|\boldsymbol{x}-\tilde{\boldsymbol{l}}_k\|^3}\frac{\partial\cos(\beta_{ik}-\alpha_{ik})}{\partial x_\ell}\Bigg]\Bigg\}
\end{aligned} \tag{3.14}
$$

with

$$
\begin{aligned}
\frac{\partial\cos(\beta_{ik}-\alpha_{ik})}{\partial x_\ell} &= \cos\alpha_{ik}\Big(\tilde{n}_{k,\ell}\|\boldsymbol{x}-\tilde{\boldsymbol{l}}_k\|^{-1}-(\boldsymbol{x}-\tilde{\boldsymbol{l}}_k)^T\tilde{\boldsymbol{n}}_k\|\boldsymbol{x}-\tilde{\boldsymbol{l}}_k\|^{-3}(x_\ell-\tilde{l}_{k,\ell})\Big) \\
&+ \sin\alpha_{ik}\Big(\big\|(\boldsymbol{x}-\tilde{\boldsymbol{l}}_k)\times\tilde{\boldsymbol{n}}_k\big\|^{-1}\big\{\tilde{n}_{k,f(\ell+1)}\big[(x_\ell-\tilde{l}_{k,\ell})\tilde{l}_{k,f(\ell+1)} \\
&- (x_{f(\ell+1)}-\tilde{l}_{k,f(\ell+1)})\tilde{n}_{k,\ell}\big]-\tilde{n}_{k,f(\ell+2)}\big[(x_{f(\ell+2)}-\tilde{l}_{k,f(\ell+2)})\tilde{n}_{k,\ell} \\
&- (x_\ell-\tilde{l}_{k,\ell})\tilde{n}_{k,f(\ell+2)}\big]\big\}\|\boldsymbol{x}-\tilde{\boldsymbol{l}}_k\|^{-1}-\|\boldsymbol{x}-\tilde{\boldsymbol{l}}_k\|^{-3}(x_\ell-\tilde{l}_{k,l}) \\
&\cdot\big\|(\boldsymbol{x}-\tilde{\boldsymbol{l}}_k)\times\tilde{\boldsymbol{n}}_k\big\|\Big)
\end{aligned} \tag{3.15}
$$

for $\ell \in \{1,2,3\}$, where $\bar{n}_\ell$, $n_{i,\ell}$, x_ℓ, $l_{i,\ell}$, $\tilde{n}_{k,\ell}$, and $\tilde{l}_{k,\ell}$ denote the ℓth components of vectors $\bar{\boldsymbol{n}}$, $\boldsymbol{n}_i$, $\boldsymbol{x}$, $\boldsymbol{l}_i$, $\tilde{\boldsymbol{n}}_k$, and $\tilde{\boldsymbol{l}}_k$, respectively, and $f(\ell)$ is defined as

$$
f(\ell) = \begin{cases} \ell\,, & \text{if } \ell \le 3 \\ \ell-3\,, & \text{otherwise} \end{cases}. \tag{3.16}
$$

As (3.13) is related to the LOS path between the ith LED transmitter and the VLC receiver, it is in the same form as [6, eq. (14)], where visible light positioning in the presence of LOS paths is investigated. However, the expressions in

(3.14) and (3.15) are not available in the literature, which are associated with the additional position related information obtained via the IRSs.

Overall, the CRLB on the mean-squared error (MSE) of any unbiased position estimator $\widehat{\boldsymbol{x}}$ can be specified as $\mathbb{E}\{\|\widehat{\boldsymbol{x}}-\boldsymbol{x}\|^2\} \geq \text{trace}\{\mathbf{I}(\boldsymbol{x})^{-1}\}$ based on the expressions in (3.7), (3.10), and (3.12)–(3.15). The derived CRLB expression is generic since no assumptions are made about the parameters of the IRSs such as their locations, orientations, and shapes. Also, it facilitates evaluation of position estimation accuracy in NLOS scenarios by setting the LOS components to zero. Moreover, via the proposed CRLB expression, desired parameters of IRSs can be optimized in order to enhance localization accuracy, as discussed next.

3.2 Adjustment of IRS Orientations

The locations of the IRSs, $\tilde{\boldsymbol{l}}_k$, are modeled as fixed parameters but it is assumed that their orientations $\tilde{\boldsymbol{n}}_k$ can be adjusted to improve the localization accuracy. For comparison purposes, a default configuration of IRS orientations can be defined such that all the IRSs are perpendicularly oriented to the wall they are located and they face towards the inside of the room. For example, $\tilde{\boldsymbol{n}}_k = [0\ 1\ 0]^T$ for the IRS located on the wall at $y = -2$ and $\tilde{\boldsymbol{n}}_k = [1\ 0\ 0]^T$ for the wall at $x = -2$. (See Fig. 3.2) This configuration will be referred to as "IRS-perpendicular" for the rest of this manuscript. This configuration can be used when the position of the VLC receiver is completely unknown. However, when the position $\boldsymbol{x}$ of the VLC receiver is known even partially, i.e., when a position estimate $\hat{\boldsymbol{x}}$ exists, then the positioning accuracy can be improved by optimizing the orientations of the IRSs. Since the optimization of the CRLB derived in Section 3.1 with respect to the orientation vectors of the all IRSs would be impractically complex, we consider a fundamental approach that aims to increase the received power at the VLC receiver by adjusting the IRS orientations. Therefore, the objective is to find the orientation vectors, $\tilde{\boldsymbol{n}}_{ik}$, such that the $dH_{i,k}^{\text{ref}}$ term in (3.3) is maximized for each LED. As stated before, the VLC receiver can extract the received signal from each LED individually via time division multiplexing. Hence, IRS orientations can be optimized for each LED separately.

The problem of maximizing the received power for the ith LED with respect to the RIS orientations can be expressed as follows:

$$\tilde{\boldsymbol{n}}_{ik}^{*} = \arg\max_{\tilde{\boldsymbol{n}}_k} \; dH_{i,k}^{\text{ref}}\left(\tilde{\boldsymbol{n}}_k\right) \qquad (3.17)$$
$$\text{s.t. } \|\tilde{\boldsymbol{n}}_k\| = 1$$

for $k \in \{1, \ldots, N_{\text{R}}\}$, where $dH_{i,k}^{\text{ref}}$ in (3.3) is considered as a function of the IRS orientation $\tilde{\boldsymbol{n}}_k$, which can be stated as

$$dH_{i,k}^{\text{ref}}\left(\tilde{\boldsymbol{n}}_k\right) = C \cos\alpha_{ik} R_k(\alpha_{ik}, \beta_{ik}) \qquad (3.18)$$

with C representing the terms that do not depend on $\tilde{\boldsymbol{n}}_k$, namely,

$$C \triangleq (m_i + 1) A (\cos\phi_{ik})^{m_i} \frac{\cos\psi_{ik} T_s(\psi_{ik}) g(\psi_{ik})}{2\pi \|\boldsymbol{l}_i - \tilde{\boldsymbol{l}}_k\|^2 \|\boldsymbol{x} - \tilde{\boldsymbol{l}}_k\|^2} \, dS_k. \qquad (3.19)$$

It is noted that since the received power from each IRS is additive as shown in (3.1), the optimal IRS orientation can be found separately for each IRS for a given LED.

Substituting $R_k(\alpha_{ik}, \beta_{ik})$ in (3.4) into (3.18), we obtain

$$dH_{i,k}^{\text{ref}}\left(\tilde{\boldsymbol{n}}_k\right) = C \frac{\rho_k}{2\pi} \cos\alpha_{ik} \Big(2 r_k \cos\beta_{ik} + (1 - r_k)(\mu_k + 1)(\cos(\beta_{ik} - \alpha_{ik}))^{\mu_k} \Big). \qquad (3.20)$$

Considering the system model in Fig. 3.1, it can be noted that the received power decreases when the vectors $(\boldsymbol{l}_i - \tilde{\boldsymbol{l}}_k)$, $(\boldsymbol{x} - \tilde{\boldsymbol{l}}_k)$ and $\tilde{\boldsymbol{n}}_k$ do not lie on the same plane. Therefore, the optimal $\tilde{\boldsymbol{n}}_k$ can be searched over the plane formed by $(\boldsymbol{l}_i - \tilde{\boldsymbol{l}}_k)$ and $(\boldsymbol{x} - \tilde{\boldsymbol{l}}_k)$. In this case, for fixed locations of the LED, the IRS, and the VLC receiver, the sum of α_{ik} and β_{ik} becomes constant, say θ_{ik}; that is, $\alpha_{ik} + \beta_{ik} \triangleq \theta_{ik}$. Accordingly, $dH_{i,k}^{\text{ref}}$ in (3.20) can be stated as

$$dH_{i,k}^{\text{ref}}\left(\tilde{\boldsymbol{n}}_k\right) = \bar{C} \cos\alpha_{ik} \Big(2 r_k \cos(\theta_{ik} - \alpha_{ik}) + (1 - r_k)(\mu_k + 1)(\cos(\theta_{ik} - 2\alpha_{ik}))^{\mu_k} \Big) \qquad (3.21)$$

where $\bar{C} \triangleq C\rho_k/2\pi$. Based on (3.21), the solution of (3.17) can be derived for the cases $r_k = 1$, $r_k = 0$, and $r_k \in (0, 1)$ separately, as discussed below.

3.2.1 Solution for $r_k = 1$

When there is only diffuse reflection, i.e., when $r_k = 1$, $dH_{i,k}^{\text{ref}}$ in (3.21) simplifies to

$$dH_{i,k}^{\text{ref}}(\tilde{\boldsymbol{n}}_k) = 2\bar{C}\cos\alpha_{ik}\cos(\theta_{ik} - \alpha_{ik}). \tag{3.22}$$

The derivative of $dH_{i,k}^{\text{ref}}(\tilde{\boldsymbol{n}}_k)$ with respective to α_{ik} is given by

$$\frac{\partial dH_{i,k}^{\text{ref}}(\tilde{\boldsymbol{n}}_k)}{\partial\alpha_{ik}} = 2\bar{C}\sin(\theta_{ik} - 2\alpha_{ik}). \tag{3.23}$$

Setting the derivative in (3.23) to zero and considering that $\alpha_{ik} + \beta_{ik} = \theta_{ik}$, we obtain

$$\alpha_{ik} = \beta_{ik} = \frac{\theta_{ik}}{2}\,. \tag{3.24}$$

This solution is the maximizer as the second-order derivative can be shown to be negative at this point. This implies that, for the case of $r_k = 1$, the IRS orientation should be at the middle of the angle between the vectors $(\boldsymbol{l}_i - \tilde{\boldsymbol{l}}_k)$ and $(\boldsymbol{x} - \tilde{\boldsymbol{l}}_k)$ (please see Fig. 3.1).

3.2.2 Solution for $r_k = 0$

For $r_k = 0$, $dH_{i,k}^{\text{ref}}$ in (3.21) can be simplified as

$$dH_{i,k}^{\text{ref}}(\tilde{\boldsymbol{n}}_k) = \bar{C}(\mu_k + 1)\cos\alpha_{ik}\cos(\theta_{ik} - 2\alpha_{ik})^{\mu_k}. \tag{3.25}$$

Taking the derivative with respective to α_{ik} yields

$$\begin{aligned}\frac{\partial dH_{i,k}^{\text{ref}}(\tilde{\boldsymbol{n}}_k)}{\partial\alpha_{ik}} &= \bar{C}(\mu_k + 1)\Big(- \sin\alpha_{ik}\cos(\theta_{ik} - 2\alpha_{ik})^{\mu_k} \\ &\quad + 2\mu_k\cos\alpha_{ik}\sin(\theta_{ik} - 2\alpha_{ik}\cos(\theta_{ik} - 2\alpha_{ik})^{\mu_k - 1})\Big).\end{aligned} \tag{3.26}$$

Setting this derivative to zero results in the following condition:

$$\sin\alpha_{ik}\cos(\theta_{ik} - 2\alpha_{ik}) = 2\mu_k\cos\alpha_{ik}\sin(\theta_{ik} - 2\alpha_{ik}). \tag{3.27}$$

As a special case, if $\theta_{ik} = \frac{\pi}{2}$, i.e., if $(\boldsymbol{l}_i - \tilde{\boldsymbol{l}}_k) \perp (\boldsymbol{x} - \tilde{\boldsymbol{l}}_k)$, then (3.27) becomes

$$\sin\alpha_{ik}\sin(2\alpha_{ik}) = 2\mu_k\cos\alpha_{ik}\cos(2\alpha_{ik}) \tag{3.28}$$

which leads to the following relations:

$$\tan\alpha_{ik}\tan(2\alpha_{ik}) = 2\mu_k \tag{3.29}$$

$$\frac{2\tan^2\alpha_{ik}}{1-\tan^2\alpha_{ik}} = 2\mu_k \tag{3.30}$$

$$\alpha_{ik} = \tan^{-1}\left(\sqrt{\frac{\mu_k}{\mu_k+1}}\right) \tag{3.31}$$

It should be noted that there exist two α_{ik} values that satisfy (3.31). The positive value of α_{ik} must be chosen since the reflected light would be out of the FOV of the photo-detector at the VLC receiver for the negative value of α_{ik}.

If $\theta_{ik} \neq \dfrac{\pi}{2}$, then (3.27) becomes

$$\tan\alpha_{ik} = 2\mu_k\tan(\theta_{ik} - 2\alpha_{ik}). \tag{3.32}$$

After some manipulation, (3.32) results in the following equation:

$$\tan^3\alpha_{ik} + (-2\mu_k\tan\theta_{ik} - 2\tan\theta_{ik})\tan^2\alpha_{ik} + (-4\mu_k - 1)\tan\alpha_{ik} + 2\mu_k\tan\theta_{ik} = 0 \tag{3.33}$$

which is in the form of a cubic equation. The roots of this cubic equation can be obtained as follows:

$$\alpha_{ik,w} = \tan^{-1}\left(-\frac{1}{3a}\left(b + \zeta^w D + \frac{\Delta_0}{\zeta^w D}\right)\right) \tag{3.34}$$

for $w \in \{0, 1, 2\}$, where

$$\begin{aligned}
a &= 1 \\
b &= -2\mu_k \tan\theta_{ik} - 2\tan\theta_{ik} \\
c &= -4\mu_k - 1 \\
d &= 2\mu_k \tan\theta_{ik} \\
\Delta_0 &= b^2 - 3ac \\
\Delta_1 &= 2b^3 - 9ac + 27a^2 d \\
D &= \sqrt[3]{\frac{\Delta_1 + \sqrt{\Delta_1^2 - 4\Delta_0^3}}{2}} \\
\zeta &= \frac{-1 + \sqrt{-3}}{2}
\end{aligned} \tag{3.35}$$

Out of the three roots of the cubic equation given by (3.34) and (3.35), the root that satisfies $0 \leq \alpha_{ik,w} \leq \theta_{ik}$ must be chosen since the reflected light would be out of the FOV of the photo-detector at the VLC receiver otherwise.

Based on the preceding closed-form expressions, the optimal value of α_{ik} can be calculated, which also yields the optimal value of β_{ik} since $\alpha_{ik} + \beta_{ik} = \theta_{ik}$.

3.2.3 Solution for $r_k \in (0, 1)$

For $r_k \in (0, 1)$, the generic expression in (3.21) is used without any simplification, the derivative of which is obtained as follows:

$$\begin{aligned}
\frac{\partial dH_{i,k}^{\text{ref}}(\tilde{\boldsymbol{n}}_k)}{\partial \alpha_{ik}} = \bar{C}\Bigg(& 2r_k\Big(-\sin\alpha_{ik}\cos(\theta_{ik} - \alpha_{ik}) + \cos\alpha_{ik}\sin(\theta_{ik} - \alpha_{ik})\Big) \\
&+ (1 - r_k)(\mu_k + 1)\Big(-\sin\alpha_{ik}\cos(\theta_{ik} - 2\alpha_{ik})^{\mu_k} \\
&+ 2\mu_k\cos\alpha_{ik}\cos(\theta_{ik} - 2\alpha_{ik})^{\mu_k - 1}\Big)\Bigg)
\end{aligned} \tag{3.36}$$

Setting this derivative to zero yields the following equation:

$$\begin{aligned}
&\frac{2r_k \sin(\theta_{ik} - 2\alpha_{ik})}{(1 - r_k)(\mu_k + 1)} + \cos(\theta_{ik} - 2\alpha_{ik})^{\mu_k - 1}\big(-\sin\alpha_{ik} \\
&\cos(\theta_{ik} - 2\alpha_{ik}) + 2\mu_k\cos\alpha_{ik}\sin(\theta_{ik} - 2\alpha_{ik})\big) = 0
\end{aligned} \tag{3.37}$$

From (3.37), α_{ik} cannot be expressed in closed form. However, it can be numerically solved to find the optimal values of α_{ik} and β_{ik} rapidly, e.g., the bisection method can be applied.

For all the cases in Sections 3.2.1, 3.2.2, and 3.2.3, $\tilde{\boldsymbol{n}}_k$ can be expressed based on the obtained values of α_{ik} and β_{ik}. Let $\boldsymbol{u}_{ik} \triangleq \frac{(\boldsymbol{l}_i-\tilde{\boldsymbol{l}}_k)}{\|\boldsymbol{l}_i-\tilde{\boldsymbol{l}}_k\|}$ and $\boldsymbol{v}_{ik} \triangleq \frac{(\boldsymbol{x}-\tilde{\boldsymbol{l}}_k)}{\|\boldsymbol{x}-\tilde{\boldsymbol{l}}_k\|}$. By geometry, we have (see Fig. 3.1)

$$\begin{aligned} \boldsymbol{u}_{ik}^T\tilde{\boldsymbol{n}}_k &= \cos\alpha_{ik} \\ \boldsymbol{v}_{ik}^T\tilde{\boldsymbol{n}}_k &= \cos\beta_{ik} \end{aligned} \tag{3.38}$$

It is noted that $\tilde{\boldsymbol{n}}_k$ can be expressed as a linear combination of $\boldsymbol{u}_{ik}$ and $\boldsymbol{v}_{ik}$ since all these vectors lie on the same plane. Letting $\tilde{\boldsymbol{n}}_k \triangleq p\boldsymbol{u}_{ik}+q\boldsymbol{v}_{ik}$ and substituting this into (3.38), we obtain

$$\begin{aligned} \boldsymbol{u}_{ik}^T(p\boldsymbol{u}_{ik}+q\boldsymbol{v}_{ik}) &= \cos\alpha_{ik} \\ \boldsymbol{v}_{ik}^T(p\boldsymbol{u}_{ik}+q\boldsymbol{v}_{ik}) &= \cos\beta_{ik} \end{aligned} \tag{3.39}$$

By noting that $\|\boldsymbol{u}_{ik}\|=\|\boldsymbol{v}_{ik}\|=1$, (3.39) leads to the following relations:

$$\begin{aligned} p+q\boldsymbol{u}_{ik}^T\boldsymbol{v}_{ik} &= \cos\alpha_{ik} \\ p\boldsymbol{u}_{ik}^T\boldsymbol{v}_{ik}+q &= \cos\beta_{ik} \end{aligned} \tag{3.40}$$

Solving this system of equations for p and q yields

$$\begin{aligned} p &= \frac{\cos\alpha_{ik}-\boldsymbol{u}_{ik}^T\boldsymbol{v}_{ik}\cos\beta_{ik}}{1-(\boldsymbol{u}_{ik}^T\boldsymbol{v}_{ik})^2} \\ q &= \frac{\boldsymbol{u}_{ik}^T\boldsymbol{v}_{ik}\cos\alpha_{ik}-\cos\beta_{ik}}{(\boldsymbol{u}_{ik}^T\boldsymbol{v}_{ik})^2-1} \end{aligned} \tag{3.41}$$

Hence, the orientation vector $\tilde{\boldsymbol{n}}_k$ that maximizes $dH_{i,k}^{\mathrm{ref}}$ can be expressed, based on the obtained values of α_{ik} and β_{ik} in Sections 3.2.1, 3.2.2, and 3.2.3, as follows:

$$\begin{aligned} \tilde{\boldsymbol{n}}_{ik}^* = &\frac{\cos\alpha_{ik}-\boldsymbol{u}_{ik}^T\boldsymbol{v}_{ik}\cos\beta_{ik}}{1-(\boldsymbol{u}_{ik}^T\boldsymbol{v}_{ik})^2}\boldsymbol{u}_{ik} \\ &+\frac{\boldsymbol{u}_{ik}^T\boldsymbol{v}_{ik}\cos\alpha_{ik}-\cos\beta_{ik}}{(\boldsymbol{u}_{ik}^T\boldsymbol{v}_{ik})^2-1}\boldsymbol{v}_{ik} \end{aligned} \tag{3.42}$$

for $k \in \{1,\ldots,N_{\mathrm{R}}\}$ and $i \in \{1,\ldots,N_{\mathrm{L}}\}$.

3.2.4 N-Step Localization Algorithm

For calculating the optimal orientation vectors obtained in Section 3.2, the position of the VLC receiver should be known. At the beginning of the localization process and when there exists no prior information about the VLC position, optimal IRS orientations cannot be calculated. In that case, we start with the "IRS-perpendicular" configuration (described at the beginning of Section 3.2), and perform position estimation based on this configuration. Then using the resulting position estimate, the IRS orientations can be optimized and the resulting configuration is called "IRS-focused", which can lead to more accurate localization. This procedure can be repeated a number of times to improve adjustment of IRS orientations and consequently, the positioning accuracy. Algorithm 1 below, which is called "N-Step Localization Algorithm", defines a procedure to improve the positioning accuracy with multiples usage of "IRS-focused" configurations.

It should be emphasized that in tracking applications, the position estimate of the VLC receiver at the previous time step can be used as a rough position estimate to determine IRS orientations. In such cases, it may not be necessary to start the N-step localization algorithm with the "IRS-perpendicular" configuration.

Algorithm 1 N-Step Localization Algorithm

1: Estimate position of VLC receiver as $\hat{\boldsymbol{x}}$ using "IRS-perpendicular" configuration
2: **for** $i = 1 \rightarrow \mathrm{N} - 1$ **do**
3: Based on $\hat{\boldsymbol{x}}$, calculate $\tilde{\boldsymbol{n}}_{ik}^{*}$ as in Section 3.2 to obtain "IRS-focused" configuration
4: Estimate position of VLC receiver as $\hat{\boldsymbol{x}}$ using "IRS-focused" configuration
5: **end for**

Remark 3: As discussed in Section 3.3, the received signals from the IRSs become crucial for localization when the LOS paths between the LEDs and the VLC receiver are blocked. Therefore, optimization of IRS orientations is important for NLOS scenarios. On the other hand, when LOS paths exist between the LEDs and the VLC receiver, it is not critical to adjust the orientation vectors of the IRSs.

3.3 Simulation Results

In this section, simulations are conducted to evaluate the performance of the proposed positioning approach with intelligent reflecting surfaces. A room with dimensions $4 \times 4 \times 3$ meters (width, depth and height, respectively) is considered. The number of LED transmitters is taken as $N_{\mathrm{L}} = 4$ and they are placed at the following locations: $\{(-1,1,3),(1,1,3),(1,-1,3),(-1,-1,3)\}$ (all in meters) such that the room is covered symmetrically, where $(0,0,0)$ corresponds to the center of the room floor. The orientation vectors, $\boldsymbol{n}_i$'s, are taken as $[0,0,-1]^T$ $\forall i$ meaning that all the LEDs face downwards. The transmit powers of the LEDs, $P_{\mathrm{TX},i}$, are set to 5W, and m_i's are taken as 1 $\forall i$. Also, the orientation of the receiver is specified as $\bar{\boldsymbol{n}} = [0,0,1]^T$, i.e., it faces upwards. Moreover, the noise variances are assumed to be the same, that is, $\sigma_i^2 = \sigma^2$ for $i = 1,\ldots,N_{\mathrm{L}}$. On each wall, $N_{\mathrm{R}}/4$ IRSs are used, which are placed as a $\sqrt{N_{\mathrm{R}}/4} \times \sqrt{N_{\mathrm{R}}/4}$ array. N_{R} is taken as 1764 in the simulations; hence, there are 21×21 IRSs on each wall, as shown in Fig. 3.2. The width and the height of each rectangular IRS is set to $w_u = 4$ cm and $h_u = 2$ cm, respectively. Thus, the area of each IRS, S_k, is set to 8 cm^2 $\forall k$. The IRSs are separated from each other with $w_d = 2$ cm horizontally and $h_d = 1$ cm vertically to prevent the inter-element blockage as shown in detail in Fig. 3.3. IRSs are located to cover the center of the wall both horizontally and vertically for each wall, meaning that the center of the two-dimensional IRS array is the center point of the wall. As the default configuration, the normal vectors of each IRS is chosen such that the IRSs are perpendicular to the wall. Finally, the reflectance coefficient of IRS elements is set to $\rho_k = 0.95$ $\forall k$. A visualization of the overall configuration of the simulation environment can be seen in Fig. 3.2.

The fraction of diffuse component r_k, the directivity of reflection μ_k, and the orientation of IRSs $\tilde{n}_k$ are significant parameters that affect the positioning accuracy. To investigate the effects of these parameters on the positioning accuracy, three sets of (r_k, μ_k) pair are chosen as $\{(1,-),(0.5,5),(0,5)\}$.[5] Also, the orientation vectors of the IRSs are designed for two different configurations. The

[5]When the value of r_k is 1, the received power is independent of the value of μ_k (see (3.4)). Therefore this pair is stated as $(r_k, \mu_k) = (1,-)$.

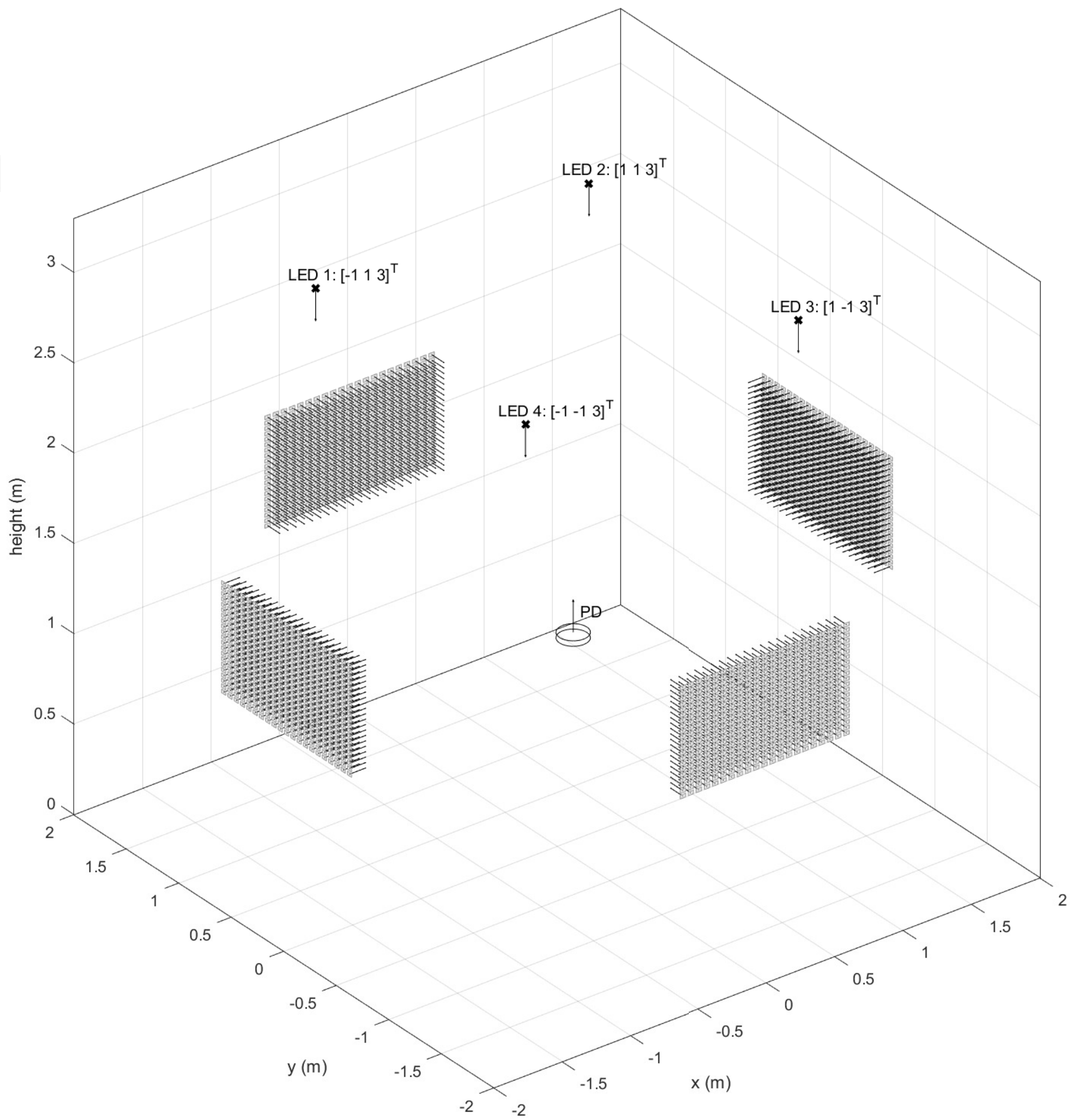

Figure 3.2: Visualization of the room setup used in the simulations. Gray rectangles on the walls represent IRSs and small black arrows represent their normal vectors.

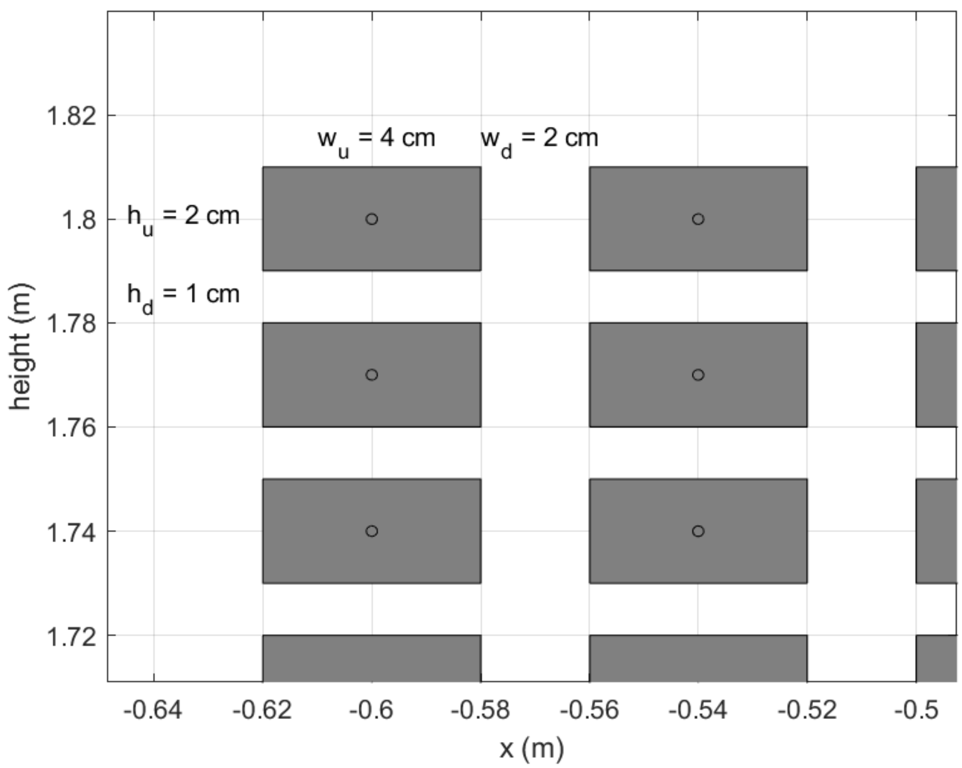

Figure 3.3: A zoomed view of configuration of IRSs on the wall at $y = -2$.

first configuration is "IRS-perpendicular" in which all the IRSs are oriented as perpendicular to the wall and face inside. The second configuration is "IRS-focused" in which the orientations of the IRSs are optimized as in Section 3.2 to maximize the received power at the VLC receiver. The actual position of the VLC receiver is used when optimizing the orientation vectors to provide a benchmark. (When the position of the VLC receiver is unknown, the IRS orientations will be adjusted during the implementation of the N-step localization algorithm.) As an example, we illustrate in Fig. 3.4 the optimal orientations of the IRSs to maximize the received power at the VLC receiver from each LED transmitter. (The top view of the room is displayed for ease of interpretation.) In the simulations, the receiver unit is located at $(0.5, 0.5, 0.85)$ meters and the CRLB derived in Section 3.1 is calculated as a benchmark for three dimensional localization accuracy with different values of the noise variance σ^2. It is assumed that the LOS path is not available and the VLC receiver only utilizes the reflections from the IRSs for position estimation. The ML estimator defined in (3.9) is used to estimate the position of the VLC receiver. For each noise variance value, the simulation is repeated for 1000 times and the root mean squared error (RMSE) is calculated. The simulations are repeated for each (r_k, μ_k) pair for both IRS-perpendicular and IRS-focused configurations to see the effects of these parameters on the positioning accuracy.

In Fig. 3.5, the RMSEs of the ML estimators and the CRLBs are plotted versus the noise variance for different parameter sets and IRS configurations. It is observed that the RMSE of the ML estimator for the IRS-perpendicular configuration with $r_k = 1$ achieves an accuracy of 27.5 cm for the lowest noise variance (i.e., the highest signal-to-noise ratio (SNR)) in the figure.[6] For the parameter set $(r_k, \mu_k) = (0.5, 5)$, the RMSE reduces to 23.5 cm, whereas for $(r_k, \mu_k) = (0, 5)$, the RMSE becomes 21.5 cm. Thus, it can be argued that when the LOS paths

[6]It is noticed that for large values of noise variances (low SNR values), the RMSEs of the estimators for all configurations are below the CRLBs. This is due to the fact that the possible locations of the VLC receiver in the room are limited to $4 \times 4 \times 3$ meters in three dimensions, and the ML estimators perform the search over this space. On the other hand, the CRLB derivations do not assume any prior information about the location of the VLC receiver; hence, can lead to larger values than RMSEs in very noisy cases.

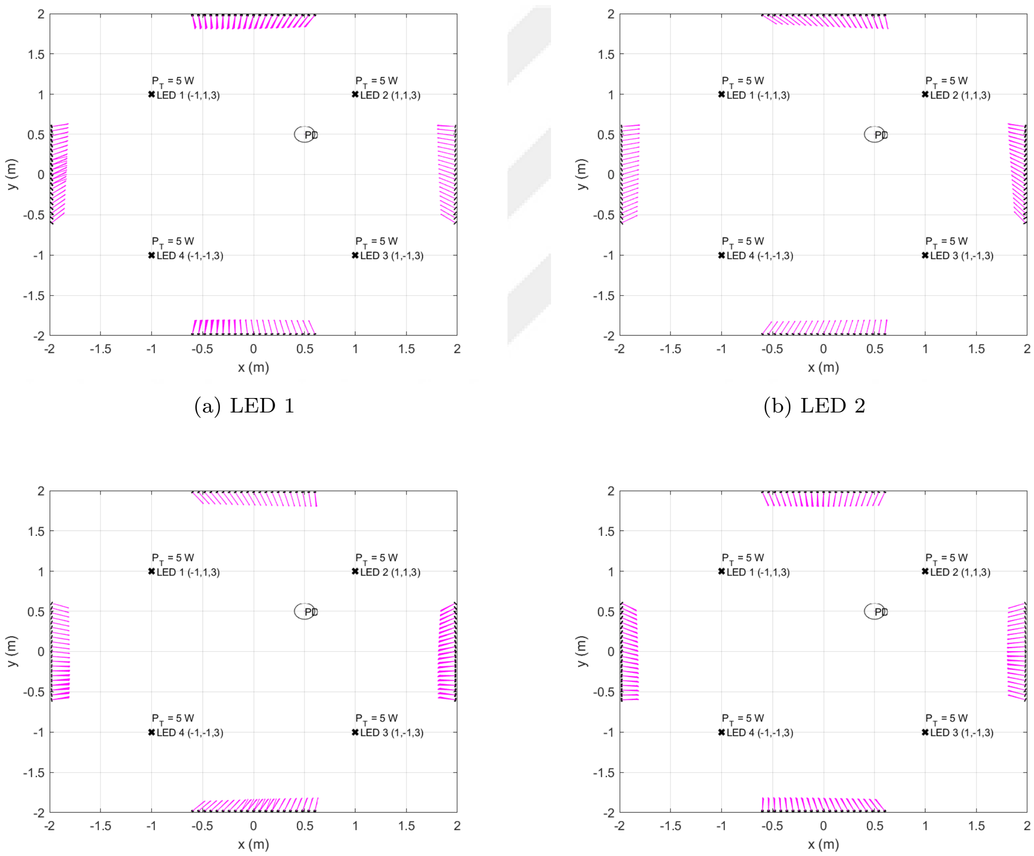

(a) LED 1

(b) LED 2

(c) LED 3

(d) LED 4

Figure 3.4: Top view of the room illustrating the optimized orientations of IRSs for each LED.

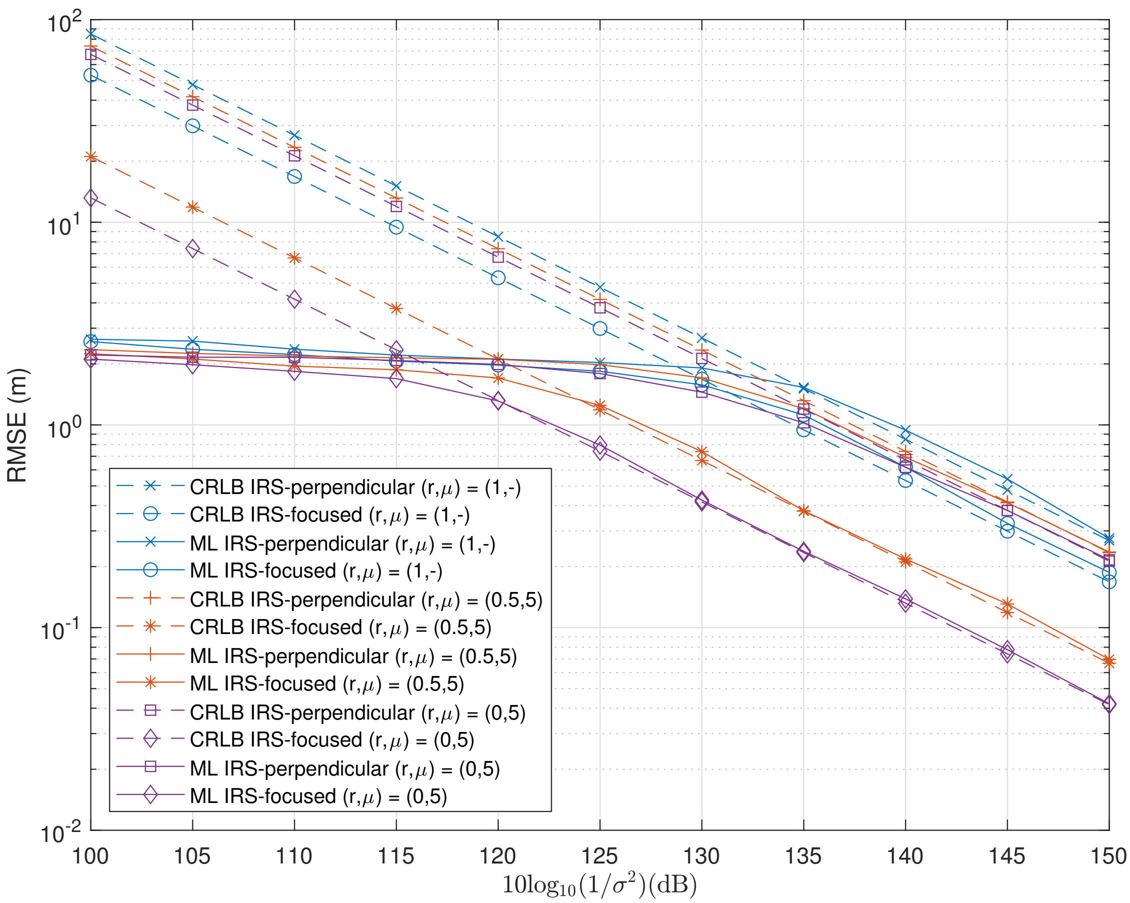

Figure 3.5: RMSE versus $10\log_{10}(1/\sigma^2)$ for various settings in NLOS scenario.

are not available, increasing the directivity of the reflected paths, i.e., μ_k, improves the positioning accuracy. For the focused IRS configuration, it is seem from Fig. 3.5 that adjusting the orientations of the IRSs such that the received power at the VLC receiver is maximized improves the positioning accuracy significantly. When the IRSs are focused to the location of the VLC receiver, the RMSEs of the ML estimators reduce to 16.8 cm, 6.6 cm, and 4.2 cm for the parameter sets $(r_k, \mu_k) = (1, -)$, $(r_k, \mu_k) = (0.5, 5)$, and $(r_k, \mu_k) = (0, 5)$, respectively. This means that the performance of the IRS-perpendicular configuration can be achieved with 5 dB, 10 dB and 15 dB lower SNR by using the IRS-focused configurations, respectively for these (r_k, μ_k) pairs. It should be noted that the resulting accuracy improvement is asymptotic since the perfect knowledge of the receiver location is assumed in these scenarios. Thus, this constitutes a lower bound on the achievable RMSE when optimizing the IRS orientations. (The achievability of this bound in practical situations is illustrated next.)

To investigate the performance of the N-step localization algorithm, simulations are conducted with $\mathrm{N} = \{2, 3\}$, which are repeated for each (r_k, μ_k) pair considered in the previous scenario. In this case, the VLC receiver is assumed to have an unknown position initially, and the IRS-perpendicular configuration is used in the first step. Then, the IRS orientations are focused in the next step(s) as described in Algorithm 1. It can be seen from Fig. 3.6 that for $10\log_{10}(1/\sigma^2) = 125\,\mathrm{dB}$, 2-Step and 3-Step localization algorithms improve the positioning accuracy significantly compared to the IRS-perpendicular configuration but cannot achieve the CRLB, which is obtained based on the perfect knowledge of the receiver position. For $10\log_{10}(1/\sigma^2) = 130\,\mathrm{dB}$, the 3-step localization algorithm gets very close to the CRLB. For lower noise variance, both the 2-step and 3-step localization algorithms converge to the CRLB. Therefore, the positioning accuracy can be significantly improved for $(r_k, \mu_k) = (0, 5)$ even though the VLC receiver has an unknown position initially. From Fig. 3.7, which is obtained for $(r_k, \mu_k) = (0.5, 5)$, it is observed that the positioning accuracy improvement is reduced but still both algorithms converge to the CRLB, which assumes the perfect knowledge of the receiver position for optimizing IRS orientations, when $10\log_{10}(1/\sigma^2)$ is higher than 140 dB. In addition, Fig. 3.8 suggests

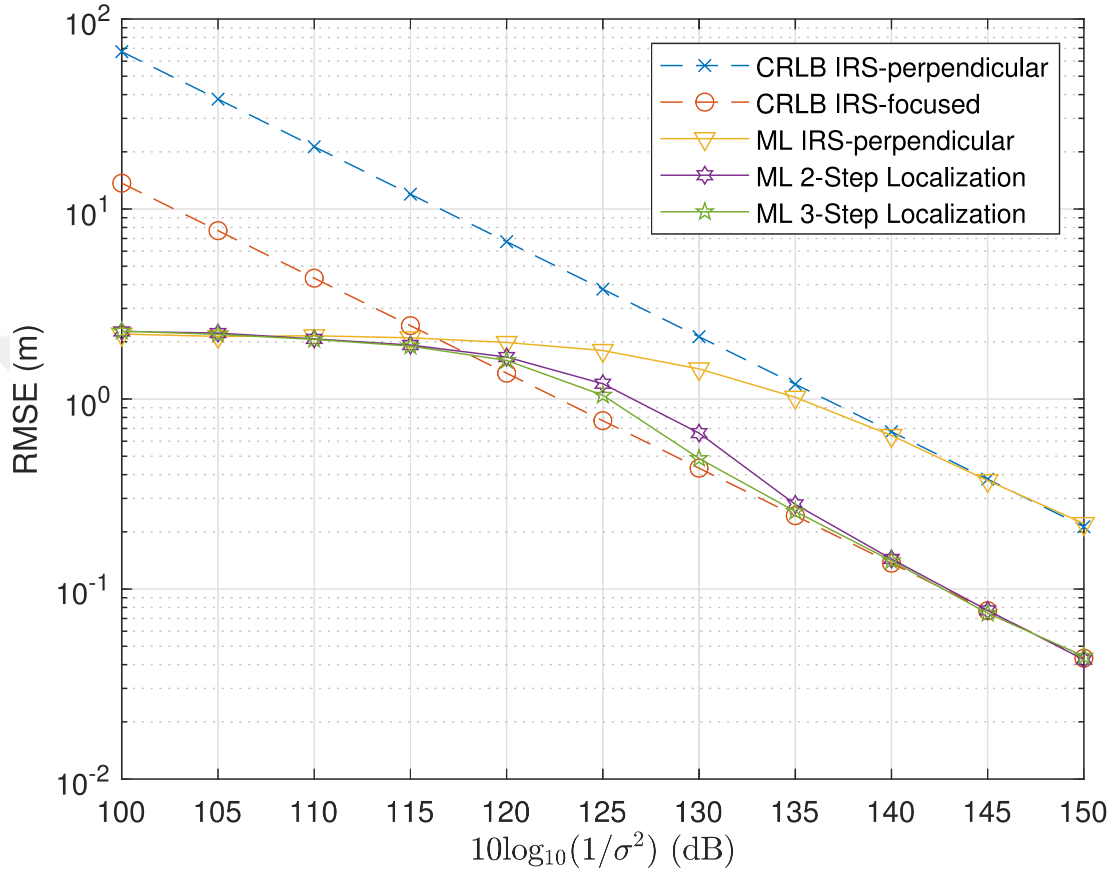

Figure 3.6: RMSE versus $10\log_{10}(1/\sigma^2)$ for $(r_k, \mu_k) = (0, 5)$.

that the improvement in accuracy is limited for $(r_k, \mu_k) = (1, -)$ and a lower value of σ^2 is needed for convergence to the CRLB. This means that when the IRSs perform only diffuse reflection, IRS focusing becomes less effective.

In addition to the preceding simulations conducted for NLOS environments, we also consider scenarios in which the received power from LOS and IRS paths are utilized together. We calculate the CRLBs for those scenarios to investigate the effects of the received power from the IRS elements when a subset of LOS components is present. The first scenario is that the VLC receiver gets signals from only the LOS paths between itself and all the LEDs, i.e., the IRSs are not present. This scenario is referred to as “4 LOS + 0 IRS”. In the second scenario, the VLC receiver obtains power measurements from both the LOS and IRS paths

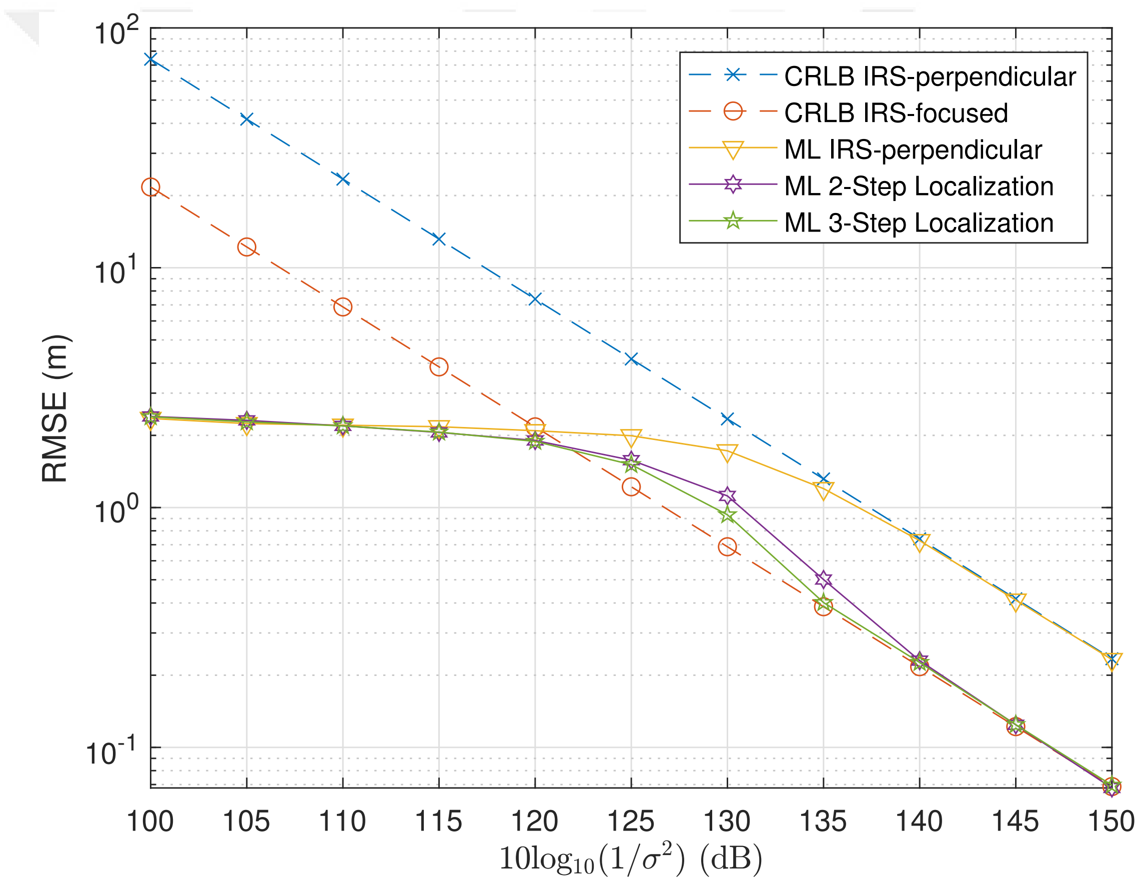

Figure 3.7: RMSE versus $10\log_{10}(1/\sigma^2)$ for $(r_k, \mu_k) = (0.5, 5)$.

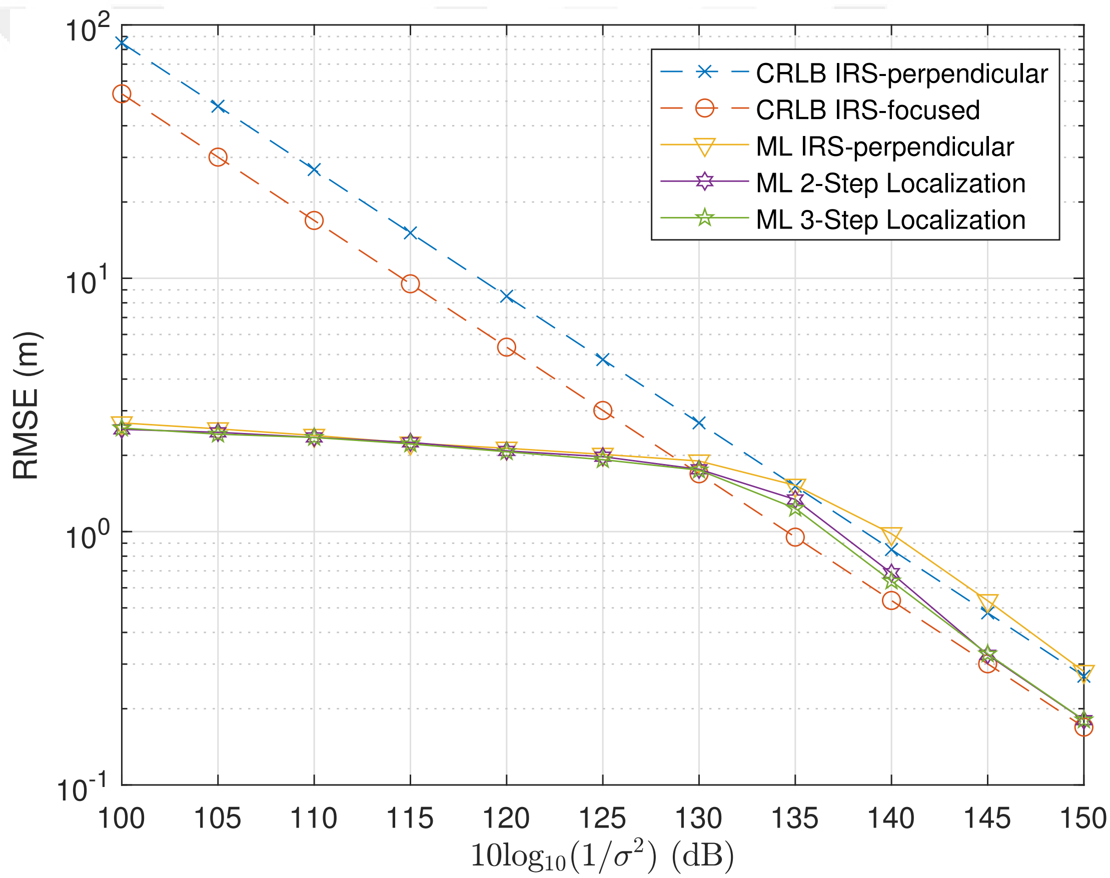

Figure 3.8: RMSE versus $10\log_{10}(1/\sigma^2)$ for $(r_k, \mu_k) = (1, -)$.

for all the LEDs (be referred to as "4 LOS + 4 IRS"). In the third scenario, it is assumed that the LOS path from one of the randomly chosen LED is unavailable, hence, the VLC receiver utilizes only the LOS signals from the remaining LEDs while the IRS elements are not present (referred to as "3 LOS + 0 IRS"). In the fourth scenario, on top of the LOS signals from these three LEDs (as specified in the third scenario), there also exist IRSs which reflect the signals from all the LEDs (referred to as "3 LOS + 4 IRS"). In other words, only the LOS path of one randomly chosen LED is not present in this scenario. As the fifth scenario, the LOS paths from two randomly chosen LEDs are assumed to be unavailable; however, all of the reflected paths are present from the IRSs for all the LEDs (referred to as "2 LOS + 4 IRS"). In the sixth scenario, only one LOS path from a randomly chosen LED is available and all the IRS reflections are present (referred to as "1 LOS + 4 IRS"). In the seventh and final scenario, no LOS paths are available and the positioning is performed based only on the components from the IRSs (referred to as "0 LOS + 4 IRS"). For the scenarios involving a blockage of LOS path(s) from a subset of LEDs, the CRLB is calculated and averaged out based on 1000 random selections of LEDs to remove the effects of the choice of blocked LEDs. In addition, the IRS-perpendicular configuration is used in all of the scenarios described above involving the use of IRSs.

Fig. 3.9 illustrates the CRLBs for the seven scenarios described in the previous paragraph. From the figure, it is seen that the scenario with "0 LOS + 4 IRS" (Scenario 7) has the lowest performance (highest CRLB), as expected. When an LOS LED is present (Scenario 6), the accuracy improves slightly. The scenario with "2 LOS + 4 IRS" has notable improvement in accuracy compared to Scenarios 6 and 7. In addition, the scenarios with 3 and 4 LOS LEDs significantly outperform the remaining three scenarios since information from 3 or 4 LOS signals can provide accurate position information. As expected, the case with 4 LOS LEDs has the best performance. It is also observed that using the powers obtained via IRSs does not improve the positioning accuracy when 3 or 4 LOS LEDs are present; on the contrary, the positioning accuracy is slightly decreased. The reason for this interesting situation is that an increase in total received power does not always result in improved localization performance. This

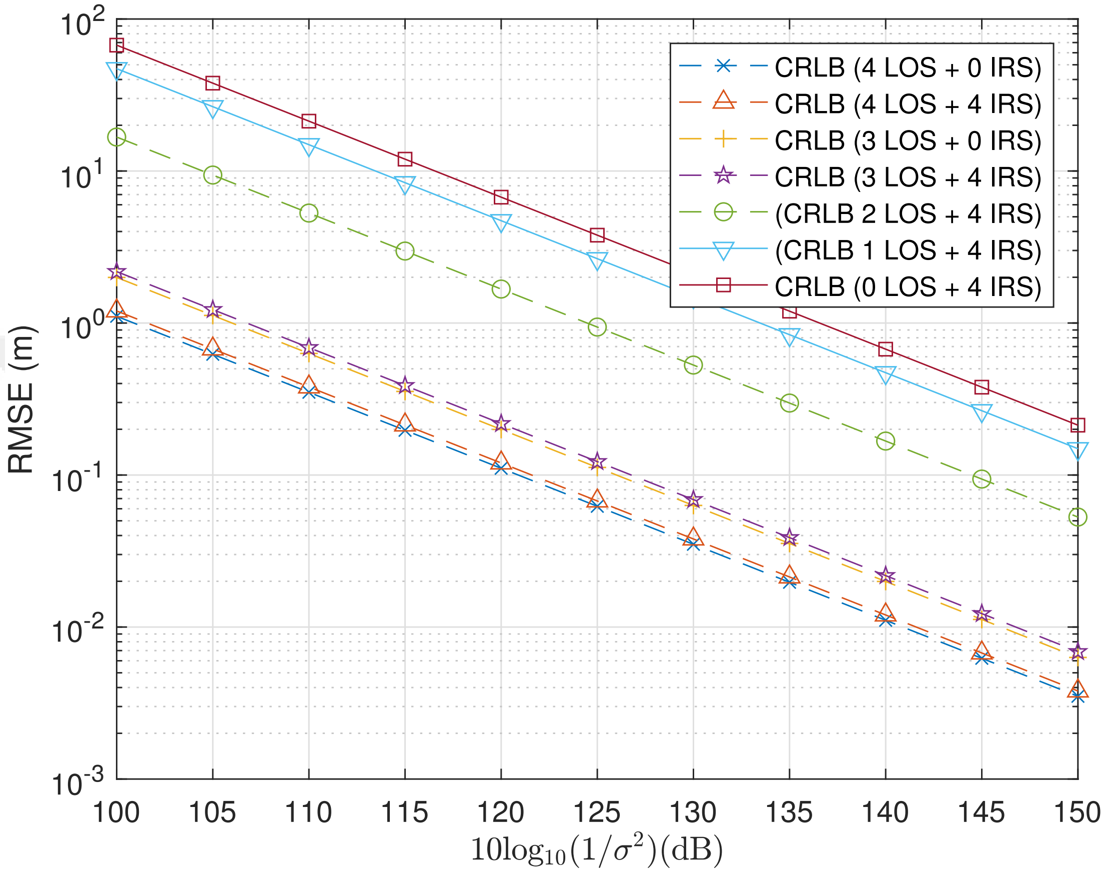

Figure 3.9: CRLB versus $10\log_{10}(1/\sigma^2)$ for various IRS aided scenarios when the VLC receiver is placed at $\boldsymbol{x} = [0.5\ 0.5\ 0.85]^T$ meters.

is because the partial derivatives with respect to the components of the unknown position vector $\boldsymbol{x}$ can have opposite signs for LOS and IRS paths depending on the position of the VLC receiver (please see (3.10) and (3.12)). To observe this, the receiver is moved to another location, namely, $(1.5, 1.5, 0.85)$ meters and the CRLB calculations are repeated, as depicted in Fig. 3.10. It is noted that the scenario with "4 LOS + 4 IRS" has the best performance in this case. For this position of the VLC receiver, the partial derivatives in (3.12) have the same sign, hence, the CRLB decreases. Using the reflected signals from the IRSs slightly increases the positioning performance in this case. (The improvement is slight since the LOS paths are significantly stronger.) As another remark, it is observed that the scenario with "0 LOS + 4 IRS" outperforms the scenario with "1 LOS + 4 IRS". This is due to the fact that the presence of a LOS component from a

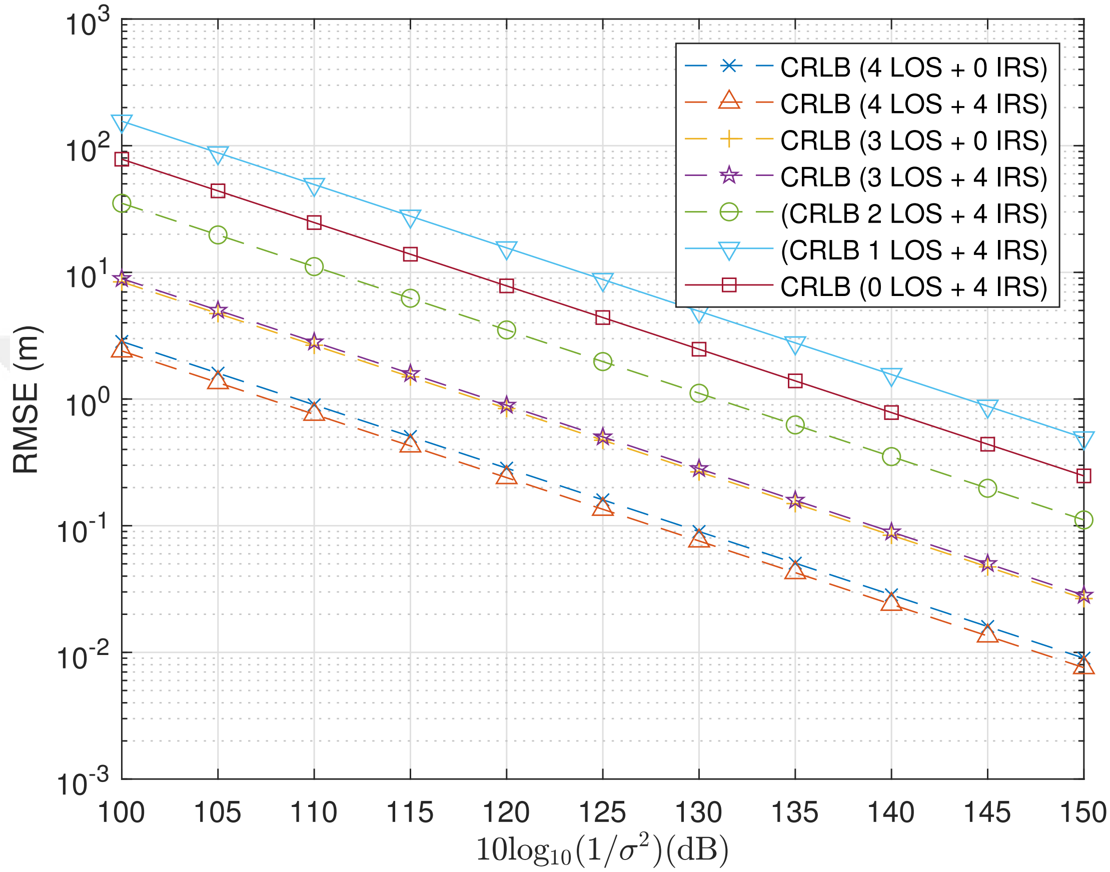

Figure 3.10: CRLB versus $10\log_{10}(1/\sigma^2)$ for various IRS aided scenarios when the VLC receiver is placed at $\boldsymbol{x} = [1.5\ 1.5\ 0.85]^T$ meters.

single LED affects the positioning accuracy negatively for the given position of the VLC receiver.

We also perform additional simulations to have a better understanding of effects of utilizing the IRSs on positioning accuracy in the presence of LOS paths for all the LEDs. For this purpose, the VLC receiver is moved across the room horizontally by fixing its height to 0.85 meter and the corresponding CRLB values are calculated for the three-dimensional localization problem. Since the aim is to investigate the contribution of reflected signals from the IRSs on the positioning accuracy, the VLC receiver is assumed to get LOS signals from all the LEDs. At each position of the VLC receiver, the CRLB is first obtained without the presence of IRS paths. Then, the CRLB calculation is repeated using the

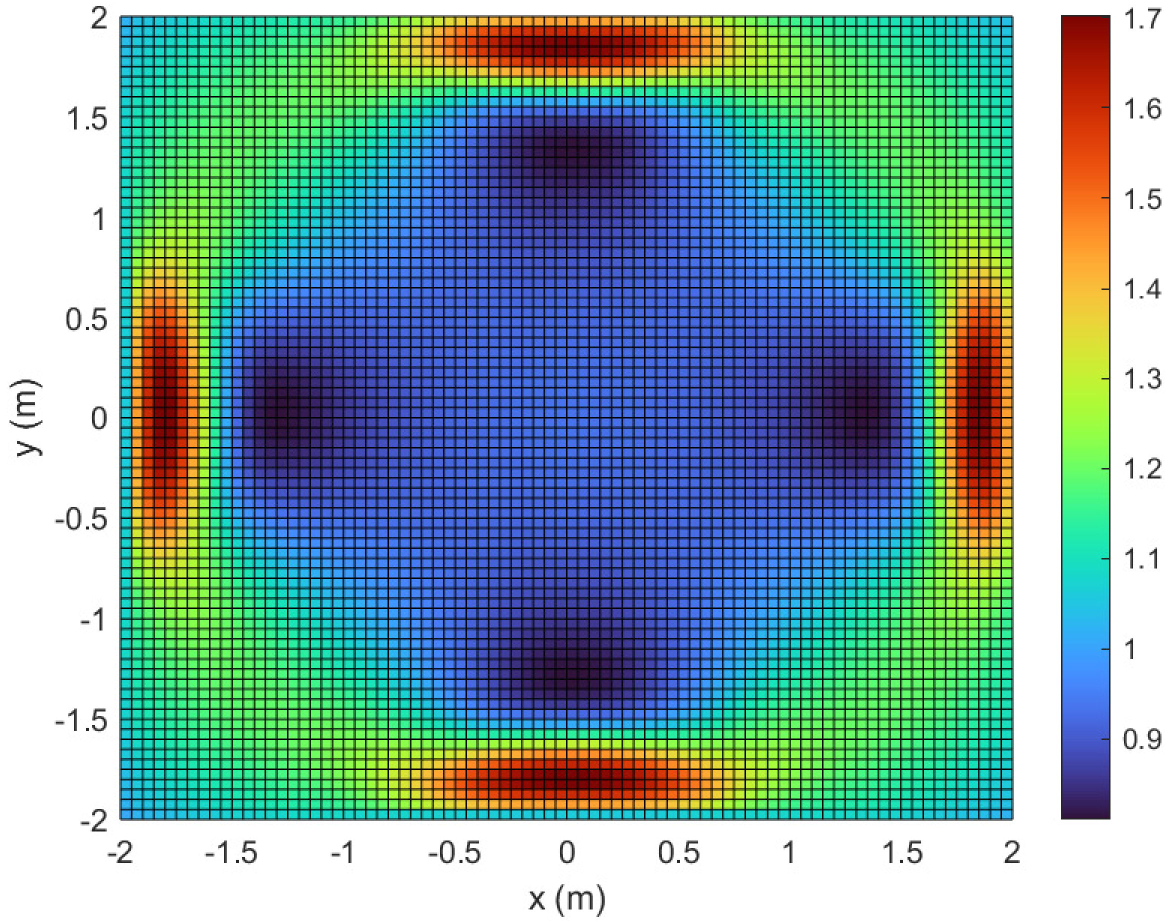

Figure 3.11: Ratio between the CRLB using only LOS components and the CRLB using both LOS and IRS components.

IRS-perpendicular configuration and utilizing both the LOS and IRS components.

In order to have a clear interpretation, the ratio of the CRLB values, namely, the CRLB based only on the LOS paths divided by the CRLB based on both the LOS and IRS paths, is plotted in Fig. 3.11. It can be seen that the contribution of the IRSs to the positioning accuracy becomes significant when the VLC receiver is away from the center of the room especially when it is close to the center of a wall. Conversely, when the VLC receiver is closer to the room center, the contribution of the IRSs to the accuracy is very small or even slightly negative in some areas.

Overall, it is concluded that when LOS signals are available at the VLC receiver from a sufficiently high number of LED transmitters, utilization of signals from IRSs may not provide significant improvements in position estimation based on received power measurements and can even degrade localization accuracy in some cases (see Figs. .3.9 and 3.11). However, IRSs facilitate position estimation even in the absence of LOS signals from the LED transmitters or even when most of the LOS paths between the LED transmitters and the VLC receiver are blocked (Figs. 3.9 and 3.10). Therefore, IRSs are useful for VLP systems based on received power measurements particularly for NLOS environments. As illustrated in Figs. 3.5–3.8, the proposed adjustment technique for IRS orientations can also be employed to provide significant enhancements to localization accuracy of VLP systems in NLOS scenarios.

3.4 An Alternative Approach for Adjustments of IRS Orientations

In Section 3.2, it has been assumed that the VLC receiver can gather information from LEDs at different time intervals, i.e., time division multiplexing is employed. This facilitates the optimal adjustment of IRS orientations for each LED, therefore it is possible to maximize the received power at the VLC receiver from the reflected path from kth IRS unit for each LED separately. However, this requires the modification of IRS orientations N_{L} times to perform a single position estimation, which introduces a latency. To avoid this delay, an alternative approach is to adjust the IRS orientations such that the sum of the received powers of the all signals emitted from the LEDs and reflected from kth IRS unit is maximized [7]. This optimization problem can be formulated as follows:

$$\tilde{\boldsymbol{n}}_k^* = \arg\max_{\tilde{\boldsymbol{n}}_k} \sum_{i=1}^{N_{\mathrm{L}}} dH_{i,k}^{\mathrm{ref}}\left(\tilde{\boldsymbol{n}}_k\right) \qquad (3.43)$$
$$\text{s.t. } \|\tilde{\boldsymbol{n}}_k\| = 1.$$

[7]FDMA or CDMA schemes can be employed in this case for the VLC receiver to utilize the signals from different LEDs at the same time.

As an approach to solve this optimization problem, the optimal orientation vectors $\tilde{\boldsymbol{n}}_k^*$ can be regarded as rotated versions of the vectors in the IRS-perpendicular configuration. As an example, the IRS units at wall $x = -2$ have the orientation vector $\tilde{\boldsymbol{n}}_k = [1\ 0\ 0]^{\mathrm{T}}\ \forall k$. All the possible orientations that face inside the room can be obtained via rotating this vector around y and z axes. Likewise for the IRS units located on the wall at $y = -2$, the orientation vector $\tilde{\boldsymbol{n}}_k = [0\ 1\ 0]^{\mathrm{T}}\ \forall k$ can be rotated around x and z axes to obtain an arbitrary orientation facing inside the room. Thus, the optimal orientation vector $\tilde{\boldsymbol{n}}_k^*$ can be expressed as follows:

$$\tilde{\boldsymbol{n}}_k^* = \boldsymbol{R}(\omega_{x,k}, \omega_{y,k}, \omega_{z,k})\tilde{\boldsymbol{n}}_k \tag{3.44}$$

where $\boldsymbol{R}(\omega_{x,k}, \omega_{y,k}, \omega_{z,k})$ is the 3D rotation matrix and $\omega_{x,k}$, $\omega_{y,k}$ and $\omega_{z,k}$ are the angles of rotation around x, y and z axes respectively for the k^{th} IRS unit, which can be expressed as follows:

$$\boldsymbol{R}(\omega_{x,k}, \omega_{y,k}, \omega_{z,k}) = \boldsymbol{R}(\omega_{x,k})\boldsymbol{R}(\omega_{y,k})\boldsymbol{R}(\omega_{z,k}) \tag{3.45}$$

with,

$$\boldsymbol{R}(\omega_{x,k}) = \begin{bmatrix} 1 & 0 & 0 \\ 0 & \cos\omega_{x,k} & -\sin\omega_{x,k} \\ 0 & \sin\omega_{x,k} & \cos\omega_{x,k} \end{bmatrix} \tag{3.46}$$

$$\boldsymbol{R}(\omega_{y,k}) = \begin{bmatrix} \cos\omega_{y,k} & 0 & \sin\omega_{y,k} \\ 0 & 1 & 0 \\ -\sin\omega_{y,k} & 0 & \cos\omega_{y,k} \end{bmatrix} \tag{3.47}$$

$$\boldsymbol{R}(\omega_{z,k}) = \begin{bmatrix} \cos\omega_{z,k} & -\sin\omega_{z,k} & 0 \\ \sin\omega_{z,k} & \cos\omega_{z,k} & 0 \\ 0 & 0 & 1 \end{bmatrix} \tag{3.48}$$

Rotation around x axis is not needed for the IRS units located on the walls at $x = -2$ and $x = 2$, i.e., $\alpha_x = 0$. The problem is reduced to finding the angles $\omega_{y,k}$ and $\omega_{z,k}$ for k^{th} IRS unit in this case as follows:

$$(\omega_{y,k}^*, \omega_{z,k}^*) = \arg\max_{\omega_{y,k},\omega_{z,k}} \sum_{i=1}^{N_L} dH_{i,k}^{\mathrm{ref}}\left(\boldsymbol{R}(0, \omega_{y,k}, \omega_{z,k})\tilde{\boldsymbol{n}}_k\right) \tag{3.49}$$

where $\tilde{\boldsymbol{n}}_k = [1\ 0\ 0]^{\mathrm{T}}\ \forall k$ for the wall at $x = -2$ and $\tilde{\boldsymbol{n}}_k = [-1\ 0\ 0]^{\mathrm{T}}\ \forall k$ for the wall at $x = 2$. Likewise, rotation around y axis is not needed for the IRS units located on the walls at $y = -2$ and $y = 2$, i.e., $\beta_y = 0$. The problem is reduced to finding the angles $\omega_{x,k}$ and $\omega_{z,k}$ in this case as follows:

$$(\alpha^*_{x,k}, \gamma^*_{z,k}) = \arg \max_{\alpha_{x,k}, \gamma_{z,k}} \sum_{i=1}^{N_L} dH^{\mathrm{ref}}_{i,k} \left(\boldsymbol{R}(\alpha_{x,k}, 0, \gamma_{z,k}) \tilde{\boldsymbol{n}}_k \right) \tag{3.50}$$

where $\tilde{\boldsymbol{n}}_k = [0\ 1\ 0]^{\mathrm{T}}\ \forall k$ for the wall at $y = -2$ and $\tilde{\boldsymbol{n}}_k = [0\ -1\ 0]^{\mathrm{T}}\ \forall k$ for the wall at $y = 2$. Based on the formulations (3.49) and (3.50), the optimal adjustments of IRS units can be found by using a numerical optimization method.

Further simulations are conducted in order to evaluate the performance of this alternative IRS adjustment approach. Optimal orientation vectors are obtained via Particle Swarm Optimization (PSO) using the actual position of the VLC receiver and the resulting IRS configuration is referred to as "IRS-avg.focused". The value of (r_k, μ_k) pair is taken as $(0, 5)$. From Fig. 3.12 it can be observed that the performance of the IRS-avg.focused configuration is significantly better than IRS-perpendicular configuration yet slightly worse than the IRS-focused configuration. This is because a single optimized IRS configuration is used for all the LEDs at once instead of optimizing the orientations for each LED separately. However, this approach has the advantage of using the same configuration for all N_{L} LEDs which does not introduce a latency and easier to implement in practical scenarios as it does not require time division multiplexing while improving the positioning accuracy compared to the IRS-perpendicular configuration.

3.5 Concluding Remarks

In this manuscript, we have formulated the received power based position estimation problem in a VLP system with IRS deployment. An ML estimator utilizing signals from both LOS and IRS components has been presented. Optimal adjustment of IRS orientations that maximizes the received power has been derived analytically. An algorithm has been proposed to improve positioning accuracy in

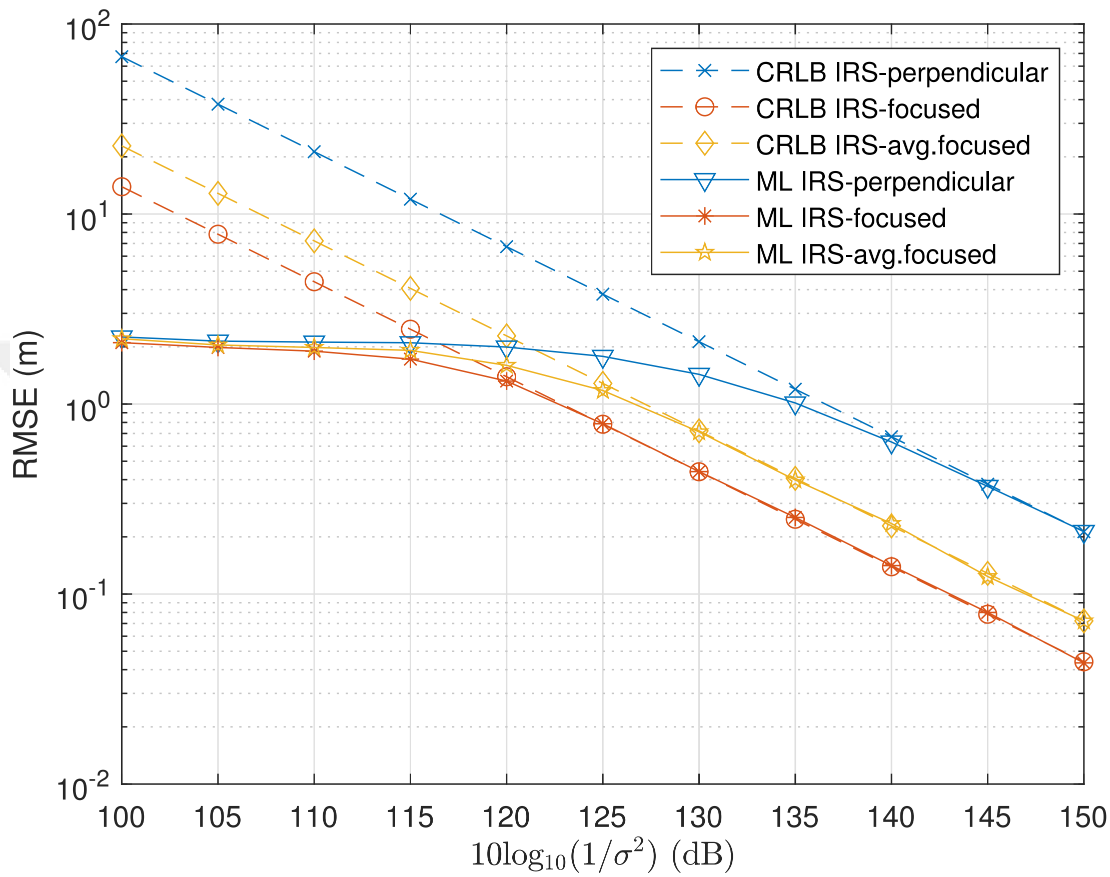

Figure 3.12: RMSE versus $10\log_{10}(1/\sigma^2)$ for alternative IRS configuration in NLOS scenario.

the absence of LOS signals. A generic CRLB expression has been derived and employed as a benchmark for evaluating the performance of the proposed algorithm. Various simulations have been conducted to verify the analytical results and to investigate the performance of the proposed positioning approach. We have also analyzed the impacts of IRS parameters, namely the fraction of the diffuse component and the directivity, on the positioning accuracy. Finally, the effects of using IRSs in the presence of LOS paths on the positioning accuracy have further been investigated for various positions of the VLC receiver. It has been concluded that although IRSs do no provide critical improvements in positioning accuracy in the presence of LOS signals from a sufficient number of LED transmitters, they can be very important in achieving accurate positioning when all or most of LOS paths are blocked.

Chapter 4

Conclusions and Future Work

In this thesis, VLP algorithms in the presence of malicious LED transmitters or IRSs have been developed. In Chapter 2, we have considered a VLP system in which a VLC receiver collects power from a number of LED transmitters and performs position estimation. Unlike the common scenarios in existing studies, we have assumed that the VLP system is not completely secure meaning that a subset of the LED transmitters might be in control of an unknown third party, i.e., hijacked or hacked, with the purpose of degrading the positioning accuracy. It is assumed that each LED transmitter is malicious with a certain probability and transmits signals at an unknown power level. We have derived an ML estimator based on the knowledge of probabilities of LEDs being malicious in such a scenario. Additionally, we have proposed a training phase for the detection of malicious LEDs and estimation of their transmit powers in the scenario that the transmit power is constant. We have designed decision rules based on training phase measurements and we have proposed various ML estimators for several scenarios. Moreover, the CRLB has been derived for the scenarios with and without a training phase. Numerical examples have been presented to evaluate the performance of the proposed estimators and CRLBs are used as benchmark. It has been shown that the proposed algorithms provide significant improvements to the positioning accuracy compared to an algorithm that is unaware of the potential security problems and the performance of these algorithms are very close to the corresponding CRLBs at high SNR values.

As possible future studies of this problem, the uncertainties in γ_i values, i.e. probability of ith LED being malicious, can be considered. Robustness of the proposed algorithms to the deviations in γ_i values can be investigated.

In Chapter 3, we have considered a VLP system with deployment of IRSs. It has been assumed that the VLC receiver can collect signals from LOS paths and/or reflected paths from IRSs. We have derived CRLB expressions and proposed an ML estimator in a generic three-dimensional positioning scheme for arbitrary IRS configurations. Additionally, we have considered the optimization of orientations of IRSs when the LOS paths are blocked. We have derived analytic expressions for this problem which can be solved in closed form or numerically. As this analysis requires the knowledge of the receiver position, we have proposed an N-step localization algorithm to jointly find the optimized IRS orientations and the receiver location in the absence of prior knowledge on the position of the VLC receiver. Performance of this algorithm has been evaluated via numerical examples and compared against the CRLB. We have shown that the proposed algorithm achieves the lower bound for high SNRs. Moreover, we have investigated the effects of using IRSs on the positioning accuracy for several scenarios in which the LOS signals from a subset of LED transmitters are blocked. We have deduced that while use of IRS is not critical in the presence of LOS paths from all the LEDs, it can become substantially important in case all or most of the LOS paths are blocked.

As future work, use of IRSs can be investigated further for VLP systems based on power measurements. In particular, various IRS configurations can be designed to develop fingerprinting approaches for VLP in the presence of IRSs. Machine learning techniques such as neural networks or nearest neighbor algorithms can then be used to locate the VLC receiver based on fingerprint measurements for different IRS configurations. Furthermore, a noise reduction approach can be taken similar to the studies in [70, 71] in the presence of IRSs via the use of neural networks.

Bibliography

[1] M. Yoshino, S. Haruyama, and M. Nakagawa, "High-accuracy positioning system using visible LED lights and image sensor," in *2008 IEEE Radio and Wireless Symposium*, pp. 439–442, 2008.

[2] J. Luo, L. Fan, and H. Li, "Indoor positioning systems based on visible light communication: State of the art," *IEEE Communications Surveys & Tutorials*, vol. 19, pp. 2871–2893, 4th Quart. 2017.

[3] M. F. Keskin, A. D. Sezer, and S. Gezici, "Localization via visible light systems," *Proceedings of the IEEE*, vol. 106, pp. 1063–1088, June 2018.

[4] J. Armstrong, Y. A. Sekercioglu, and A. Neild, "Visible light positioning: a roadmap for international standardization," *IEEE Communications Magazine*, vol. 51, no. 12, pp. 68–73, 2013.

[5] H. Steendam, T. Q. Wang, and J. Armstrong, "Cramer-Rao bound for AOA-based VLP with an aperture-based receiver," in *2017 IEEE International Conference on Communications (ICC)*, pp. 1–6, 2017.

[6] M. F. Keskin, S. Gezici, and O. Arikan, "Direct and two-step positioning in visible light systems," *IEEE Transactions on Communications*, vol. 66, pp. 239–254, Jan. 2018.

[7] B. Zhou, A. Liu, and V. Lau, "On the fundamental performance limit of visible light-based positioning," in *2019 13th International Conference on Signal Processing and Communication Systems (ICSPCS)*, pp. 1–6, 2019.

[8] S.-H. Yang, H.-S. Kim, Y.-H. Son, and S.-K. Han, “Three-dimensional visible light indoor localization using AOA and RSS with multiple optical receivers,” *Journal of Lightwave Technology*, vol. 32, pp. 2480–2485, July 2014.

[9] S. Shen, S. Li, and H. Steendam, “Simultaneous position and orientation estimation for visible light systems with multiple LEDs and multiple PDs,” *IEEE Journal on Selected Areas in Communications*, vol. 38, no. 8, pp. 1866–1879, 2020.

[10] M. A. Arfaoui, M. D. Soltani, I. Tavakkolnia, A. Ghrayeb, C. M. Assi, M. Safari, and H. Haas, “Invoking deep learning for joint estimation of indoor LiFi user position and orientation,” *IEEE Journal on Selected Areas in Communications*, vol. 39, no. 9, pp. 2890–2905, 2021.

[11] H. Steendam, T. Q. Wang, and J. Armstrong, “Theoretical lower bound for indoor visible light positioning using received signal strength measurements and an aperture-based receiver,” *Journal of Lightwave Technology*, vol. 35, no. 2, pp. 309–319, 2017.

[12] G. Blinowski, “Security of visible light communication systems-A survey,” *Physical Communication*, vol. 34, pp. 246–260, June 2019.

[13] A. Mostafa and L. Lampe, “Securing visible light communications via friendly jamming,” in *IEEE Globecom Workshops (GC Wkshps)*, pp. 524–529, 2014.

[14] S. Cho, G. Chen, and J. P. Coon, “Securing visible light communications with spatial jamming,” in *IEEE International Conference on Communications (ICC)*, pp. 1–6, 2019.

[15] F. Wang, C. Liu, Q. Wang, J. Zhang, R. Zhang, L. Yang, and L. Hanzo, “Optical jamming enhances the secrecy performance of the generalized space-shift-keying-aided visible-light downlink,” *IEEE Transactions on Communications*, vol. 66, pp. 4087–4102, Sep. 2018.

[16] H. Shen, Y. Deng, W. Xu, and C. Zhao, “Secrecy-oriented transmitter optimization for visible light communication systems,” *IEEE Photonics Journal*, vol. 8, no. 5, pp. 1–14, 2016.

[17] S. Cho, G. Chen, and J. P. Coon, "Enhancement of physical layer security with simultaneous beamforming and jamming for visible light communication systems," *IEEE Transactions on Information Forensics and Security*, vol. 14, no. 10, pp. 2633–2648, 2019.

[18] L. Qian, X. Chi, L. Zhao, and A. Chaaban, "Secure visible light communications via intelligent reflecting surfaces," in *ICC 2021 - IEEE International Conference on Communications*, pp. 1–6, 2021.

[19] M. A. Arfaoui, Z. Rezki, A. Ghrayeb, and M. S. Alouini, "On the secrecy capacity of MISO visible light communication channels," in *IEEE Global Communications Conference*, pp. 1–7, 2016.

[20] H. Abumarshoud, M. D. Soltani, M. Safari, and H. Haas, "Secrecy capacity of LiFi systems," in *Emerging Imaging and Sensing Technologies for Security and Defence V; and Advanced Manufacturing Technologies for Micro- and Nanosystems in Security and Defence III* (G. S. Buller, R. C. Hollins, R. A. Lamb, M. Laurenzis, A. Camposeo, M. Farsari, L. Persano, and L. E. Busse, eds.), vol. 11540, pp. 127–137, International Society for Optics and Photonics, SPIE, 2020.

[21] M. A. Arfaoui, M. D. Soltani, I. Tavakkolnia, A. Ghrayeb, M. Safari, C. M. Assi, and H. Haas, "Physical layer security for visible light communication systems: A survey," *IEEE Communications Surveys & Tutorials*, vol. 22, no. 3, pp. 1887–1908, 2020.

[22] R. Mitra and V. Bhatia, "Minimum error entropy criterion based channel estimation for massive-MIMO in VLC," *IEEE Transactions on Vehicular Technology*, vol. 68, no. 1, pp. 1014–1018, 2019.

[23] A. Vempaty, O. Ozdemir, K. Agrawal, H. Chen, and P. K. Varshney, "Localization in wireless sensor networks: Byzantines and mitigation techniques," *IEEE Transactions on Signal Processing*, vol. 61, no. 6, pp. 1495–1508, 2013.

[24] X. Mei, H. Wu, J. Xian, and B. Chen, "RSS-based Byzantine fault-tolerant localization algorithm under NLOS environment," *IEEE Communications Letters*, vol. 25, no. 2, pp. 474–478, 2021.

[25] R. Niu, A. Vempaty, and P. K. Varshney, "Received-signal-strength-based localization in wireless sensor networks," *Proceedings of the IEEE*, vol. 106, no. 7, pp. 1166–1182, 2018.

[26] A. Vempaty, Y. S. Han, and P. K. Varshney, "Byzantine tolerant target localization in wireless sensor networks over non-ideal channels," in *2013 13th International Symposium on Communications and Information Technologies (ISCIT)*, pp. 407–411, 2013.

[27] A. Vempaty, Y. S. Han, and P. K. Varshney, "Target localization in wireless sensor networks using error correcting codes," *IEEE Transactions on Information Theory*, vol. 60, no. 1, pp. 697–712, 2014.

[28] S. K. Saini and P. Singh, "Analysis and detection of Byzantine attack in wireless sensor network," in *2016 3rd International Conference on Computing for Sustainable Global Development (INDIACom)*, pp. 3189–3191, 2016.

[29] A. Vempaty, O. Ozdemir, and P. K. Varshney, "Target tracking in wireless sensor networks in the presence of Byzantines," in *Proceedings of the 16th International Conference on Information Fusion*, pp. 968–973, 2013.

[30] Q. Yu, H. Chen, and L. Xie, "A modified distributed target localization scheme in the presence of Byzantine attack," in *2015 International Conference on Wireless Communications Signal Processing (WCSP)*, pp. 1–5, 2015.

[31] P. Zhang, S. G. Nagarajan, and I. Nevat, "Secure location of things (SLOT): Mitigating localization spoofing attacks in the internet of things," *IEEE Internet of Things Journal*, vol. 4, no. 6, pp. 2199–2206, 2017.

[32] M. Prakruthi and M. Varalatchoumy., "Detecting malicious beacon nodes for secure localization in distributed wireless networks," in *3rd International Conference on Advances in Recent Technologies in Communication and Computing (ARTCom 2011)*, pp. 206–208, 2011.

[33] E. Basar, M. Di Renzo, J. De Rosny, M. Debbah, M.-S. Alouini, and R. Zhang, "Wireless communications through reconfigurable intelligent surfaces," *IEEE Access*, vol. 7, pp. 116753–116773, 2019.

[34] Q. Wu and R. Zhang, "Intelligent reflecting surface enhanced wireless network via joint active and passive beamforming," *IEEE Transactions on Wireless Communications*, vol. 18, no. 11, pp. 5394–5409, 2019.

[35] Z. Yang, M. Chen, W. Saad, W. Xu, M. Shikh-Bahaei, H. V. Poor, and S. Cui, "Energy-efficient wireless communications with distributed reconfigurable intelligent surfaces," *IEEE Transactions on Wireless Communications*, vol. 21, no. 1, pp. 665–679, 2022.

[36] A. M. Abdelhady, A. K. S. Salem, O. Amin, B. Shihada, and M.-S. Alouini, "Visible light communications via intelligent reflecting surfaces: Metasurfaces vs mirror arrays," *IEEE Open Journal of the Communications Society*, vol. 2, pp. 1–20, 2021.

[37] B. Cao, M. Chen, Z. Yang, M. Zhang, J. Zhao, and M. Chen, "Reflecting the light: Energy efficient visible light communication with reconfigurable intelligent surface," in *2020 IEEE 92nd Vehicular Technology Conference (VTC2020-Fall)*, pp. 1–5, 2020.

[38] S. Sun, F. Yang, and J. Song, "Sum rate maximization for intelligent reflecting surface-aided visible light communications," *IEEE Communications Letters*, vol. 25, no. 11, pp. 3619–3623, 2021.

[39] H. Abumarshoud, B. Selim, M. Tatipamula, and H. Haas, "Intelligent reflecting surfaces for enhanced noma-based visible light communications," in *ICC 2022 - IEEE International Conference on Communications*, pp. 571–576, 2022.

[40] K. Prabhath, S. K. Jayaweera, and S. A. Lane, "Intelligent reflecting surface orientation optimization to enhance the performance of wireless communications systems," in *2022 International Workshop on Antenna Technology (iWAT)*, pp. 231–234, 2022.

[41] A. Nasri, A. H. A. Bafghi, and M. Nasiri-Kenari, "Wireless localization in the presence of intelligent reflecting surface," *IEEE Wireless Communications Letters*, vol. 11, no. 7, pp. 1315–1319, 2022.

[42] M. Ammous and S. Valaee, “Cooperative positioning with the aid of reconfigurable intelligent surfaces and zero access points,” in *2022 IEEE 96th Vehicular Technology Conference (VTC2022-Fall)*, pp. 1–5, 2022.

[43] Y. Liu, E. Liu, R. Wang, and Y. Geng, “Reconfigurable intelligent surface aided wireless localization,” in *ICC 2021 - IEEE International Conference on Communications*, pp. 1–6, 2021.

[44] N. Afzali, M. J. Omidi, K. Navaie, and N. S. Moayedian, “Low complexity multi-user indoor localization using reconfigurable intelligent surface,” in *2022 30th International Conference on Electrical Engineering (ICEE)*, pp. 731–736, 2022.

[45] T. Zhou, K. Xu, Z. Shen, W. Xie, D. Zhang, and J. Xu, “Aoa-based positioning for aerial intelligent reflecting surface-aided wireless communications: An angle-domain approach,” *IEEE Wireless Communications Letters*, vol. 11, no. 4, pp. 761–765, 2022.

[46] M. Ammous and S. Valaee, “Positioning and tracking using reconfigurable intelligent surfaces and extended kalman filter,” in *2022 IEEE 95th Vehicular Technology Conference: (VTC2022-Spring)*, pp. 1–6, 2022.

[47] T. Ma, Y. Xiao, X. Lei, W. Xiong, and M. Xiao, “Distributed reconfigurable intelligent surfaces assisted indoor positioning,” *IEEE Transactions on Wireless Communications*, vol. 22, no. 1, pp. 47–58, 2023.

[48] A. Elzanaty, A. Guerra, F. Guidi, and M.-S. Alouini, “Reconfigurable intelligent surfaces for localization: Position and orientation error bounds,” *IEEE Transactions on Signal Processing*, vol. 69, pp. 5386–5402, 2021.

[49] Z. Wang, Z. Liu, Y. Shen, A. Conti, and M. Z. Win, “Wideband localization with reconfigurable intelligent surfaces,” in *2022 IEEE 95th Vehicular Technology Conference: (VTC2022-Spring)*, pp. 1–6, 2022.

[50] F. Kokdogan and S. Gezici, “Intelligent reflecting surfaces for visible light positioning based on received power measurements,” *submitted to IEEE Transactions on Vehicular Technology*, 2023.

[51] E. Gonendik and S. Gezici, "Fundamental limits on rss based range estimation in visible light positioning systems," *IEEE Communications Letters*, 2015.

[52] M. F. Keskin, A. D. Sezer, and S. Gezici, "Optimal and robust power allocation for visible light positioning systems under illumination constraints," 2018.

[53] D. Karunatilaka, F. Zafar, V. Kalavally, and R. Parthiban, "LED based indoor visible light communications: State of the art," *IEEE Communications Surveys & Tutorials*, vol. 17, pp. 1649–1678, 3rd Quart. 2015.

[54] S. D. Lausnay, L. D. Strycker, J. P. Goemaere, B. Nauwelaers, and N. Stevens, "A survey on multiple access visible light positioning," in *IEEE International Conference on Emerging Technologies and Innovative Business Practices for the Transformation of Societies (EmergiTech)*, pp. 38–42, Aug. 2016.

[55] T. Wang, Y. Sekercioglu, A. Neild, and J. Armstrong, "Position accuracy of time-of-arrival based ranging using visible light with application in indoor localization systems," *Journal of Lightwave Technology*, vol. 31, pp. 3302–3308, Oct. 2013.

[56] A. Sahin, Y. S. Eroglu, I. Guvenc, N. Pala, and M. Yuksel, "Hybrid 3-D localization for visible light communication systems," *Journal of Lightwave Technology*, vol. 33, pp. 4589–4599, Nov. 2015.

[57] J. M. Kahn and J. R. Barry, "Wireless infrared communications," *Proceedings of the IEEE*, vol. 85, pp. 265–298, Feb. 1997.

[58] D. Plets, S. Bastiaens, L. Martens, W. Joseph, and N. Stevens, "On the impact of LED power uncertainty on the accuracy of 2D and 3D visible light positioning," *Optik*, vol. 195, p. 163027, 2019.

[59] H. V. Poor, *An Introduction to Signal Detection and Estimation.* New York: Springer-Verlag, 1994.

[60] W. Meng, W. Xiao, and L. Xie, “An efficient em algorithm for energy-based multisource localization in wireless sensor networks,” *IEEE Transactions on Instrumentation and Measurement*, vol. 60, no. 3, pp. 1017–1027, 2011.

[61] W. Yuan, N. Wu, T. Cheng, H. Wang, and J. Kuang, “Expectation maximization-based passive localization in asynchronous wireless networks,” in *2015 IEEE/CIC International Conference on Communications in China (ICCC)*, pp. 1–5, 2015.

[62] H. Wang, “Bayesian radio map learning for robust indoor positioning,” in *2011 International Conference on Indoor Positioning and Indoor Navigation*, pp. 1–6, 2011.

[63] C. Robert and G. Casella, *Monte Carlo statistical methods*. Springer Verlag, 2004.

[64] M. F. Keskin and S. Gezici, “Comparative theoretical analysis of distance estimation in visible light positioning systems,” *Journal of Lightwave Technology*, vol. 34, pp. 854–865, Feb. 2016.

[65] X. Liu, D. Zou, N. Huang, and S. Zhang, “A comprehensive accuracy analysis of visible light positioning under shot noise,” in *2020 IEEE/CIC International Conference on Communications in China (ICCC Workshops)*, pp. 167–172, 2020.

[66] M. F. Keskin, A. D. Sezer, and S. Gezici, “Optimal and robust power allocation for visible light positioning systems under illumination constraints,” *IEEE Transactions on Communications*, vol. 67, no. 1, pp. 527–542, 2019.

[67] O. Gonzalez, S. Rodriguez, R. Perez-Jimenez, B. Mendoza, and A. Ayala, “Error analysis of the simulated impulse response on indoor wireless optical channels using a Monte Carlo-based ray-tracing algorithm,” *IEEE Transactions on Communications*, vol. 53, no. 1, pp. 124–130, 2005.

[68] T. Komine and M. Nakagawa, “Fundamental analysis for visible-light communication system using LED lights,” *IEEE Transactions on Consumer Electronics*, vol. 50, pp. 100–107, Feb. 2004.

[69] E. Gonendik and S. Gezici, “Fundamental limits on RSS based range estimation in visible light positioning systems,” *IEEE Communications Letters*, vol. 19, pp. 2138–2141, Dec. 2015.

[70] M. Yan, F. Xu, S. Bai, and Q. Wan, “A noise reduction fingerprint feature for indoor localization,” in *2018 10th International Conference on Wireless Communications and Signal Processing (WCSP)*, pp. 1–6, 2018.

[71] S.-H. Fang and T.-N. Lin, “Robust wireless lan location fingerprinting by svd-based noise reduction,” in *2008 3rd International Symposium on Communications, Control and Signal Processing*, pp. 295–298, 2008.